Chemical composition of diesel particulate matter and its control

Article *in* Catalysis Reviews · June 2019

DOI: 10.1080/01614940.2019.1617607

7 authors, including:

Rohini Khobragade
National Institute of Chemistry
14 PUBLICATIONS **361** CITATIONS
SEE PROFILE

Sunit Kumar Singh
CSIR-National Environmental Engineering Research Institute, Nagpur, India
32 PUBLICATIONS **764** CITATIONS
SEE PROFILE

Tarun Gupta
Indian Institute of Technology Kanpur
346 PUBLICATIONS **24,330** CITATIONS
SEE PROFILE

Ahmed Alfatesh
King Saud University
261 PUBLICATIONS **5,521** CITATIONS
SEE PROFILE

Taylor & Francis
Taylor & Francis Group

Catalysis Reviews
Science and Engineering

ISSN: 0161-4940 (Print) 1520-5703 (Online) Journal homepage: https://www.tandfonline.com/loi/lctr20

Chemical composition of diesel particulate matter and its control

Rohini Khobragade, Sunit Kumar Singh, Pravesh Chandra Shukla, Tarun Gupta, Ahmed S. Al-Fatesh, Avinash Kumar Agarwal & Nitin K. Labhasetwar

To cite this article: Rohini Khobragade, Sunit Kumar Singh, Pravesh Chandra Shukla, Tarun Gupta, Ahmed S. Al-Fatesh, Avinash Kumar Agarwal & Nitin K. Labhasetwar (2019): Chemical composition of diesel particulate matter and its control, Catalysis Reviews, DOI: 10.1080/01614940.2019.1617607

To link to this article: https://doi.org/10.1080/01614940.2019.1617607

CATALYSIS REVIEWS
https://doi.org/10.1080/01614940.2019.1617607

Taylor & Francis
Taylor & Francis Group

Chemical composition of diesel particulate matter and its control

Rohini Khobragade[a,b], Sunit Kumar Singh[a], Pravesh Chandra Shukla[c], Tarun Gupta[c], Ahmed S. Al-Fatesh[d], Avinash Kumar Agarwal[e], and Nitin K. Labhasetwar[a,b]

[a]Energy and Resource Management Division, CSIR-National Environmental Engineering Research Institute, Nagpur, India; [b]Academy of Scientific and Innovative Research (AcSIR), CSIR-National Environmental Engineering Research Institute (CSIR-NEERI), Nagpur, India; [c]Department of Civil Engineering, Indian Institute of Technology Kanpur, Kanpur, India; [d]Chemical Engineering Department, College of Engineering, King Saud University, Riyadh, Saudi Arabia; [e]Department of Mechanical Engineering, Indian Institute of Technology Kanpur, Kanpur, India

ABSTRACT

In this review, we have systematically discussed diesel particulate composition and its formation, understanding of which is essential to design the effective catalyst compositions. The most commonly used after treatment strategies such as diesel oxidation catalysts, diesel particulate filters, and partial flow filters are described followed by chronological and category-wise discussions on various groups of reported soot oxidation catalysts. A detailed review is also presented on mechanistic and kinetics aspects of non-catalytic direct particulate matter (PM) or soot oxidation in air/O_2 and NO_2. Recent progress in catalyst development with a focus on the low-cost catalyst for diesel PM oxidation has been given more emphasis considering their renewed importance.

ARTICLE HISTORY
Received 23 July 2018
Revised 01 May 2019
Accepted 06 May 2019

KEYWORDS
Particulate matter; diesel oxidation catalyst (DOC); diesel particulate filter (DPF); catalysts

1. Introduction

Diesel engine being an internal combustion engine ignites the fuel injected due to high temperature achieved by great adiabatic compression and hence is also known as compression-ignition (CI) engine. This is contrary to gasoline/gas engines, which require spark plugs to ignite an air–fuel mixture, also called spark-ignition engines.[1] Diesel engines, since last few decades, have been observed to have increased demands in passenger cars, road transport, diesel locomotives in railways, and non-road diesel engine applications. The reasons for these demands are high fuel efficiency with higher load carrying capacity, very high expansion ratio, and inherent lean burn enabling heat dissipation by excess air. This lean combustion enables diesel engines to emit

CONTACT Rohini Khobragade rohini295@gmail.com; Nitin Labhsetwar nk_labhsetwar@neeri.res.in Energy and Resource Management Division, CSIR-National Environmental Engineering Research Institute, Nagpur 440020, India
Present affiliation for Dr Pravesh Chandra Shukla is Department of Mechanical Engineering, Indian Institute of Technology Bhilai.
Color versions of one or more of the figures in the article can be found online at www.tandfonline.com/lctr.

lower carbon monoxide (CO) in exhaust gases.[2] Besides, the possibility of using nonfossil fuels such as long-chained fatty acid methyl esters/biodiesel blends with diesel is the attractive advantage of diesel engines for environmental protection thus lowering carbon footprint.[3–6]

Fuel is injected as fine droplets in the combustion chamber of the diesel engine. Incomplete combustion of inadequately vaporized droplets leads to the formation of soot, which is ultrafine particulate matter (PM). It is caused by oxygen-deficient region around droplets and generation of local cold spots near combustion chamber walls. It also leads to the formation of precursor molecules like acetylene followed by nucleation and particle growth by reacting with other gaseous components and consequent carbonization.[7–9] Increasing engine speeds enhance this phenomenon by increasing oxygen deficiencies.[10] Normally, 0.2%–0.5% of fuel (by mass) is emitted as particulates (PM) from the combustion chamber of a typical diesel engine.[11] The fine PMs have been categorized as PM10 (with a diameter less than 10 μm), PM2.5 (with a diameter less than 2.5 μm), and PM0.1 (with a diameter less than 0.1 μm).[9]

PMs create numerous health hazards such as hypersensitivity and allergic effects due to adsorbed chemicals and intake of toxic metals such as Pb, Cd, Zn into the blood via respiratory pathways. It can also cause bacterial and fungal infections from live organisms, cancer, lung fibrosis, and irritation of mucous membranes.[12] PM, in the atmosphere as a pollutant, also disturbs the atmospheric radiative balance (of about 1.1 W/m^2) thus contributing to global warming effects.[13,14] PMs can absorb incoming and outgoing radiation both and hence more prominently contributes to global warming as compared several greenhouse gases, which only absorbs the outgoing radiations. PM deposition on ice glaciers and snow adversely affects their reflectivity thus increasing absorption of radiations. This increased radiation absorption leads to their accelerated melting. Additional adverse effects include modification in distribution and properties of clouds, reduction of their reflectivity, lifetime, and precipitation.[15]

2. Diesel particulate composition and its formation

2.1. *Particulate composition*

Diesel exhaust particulates are mainly composed of nonvolatile (insoluble) and volatile (soluble) fractions. Volatile compounds are constituted by organic carbon, sulfate, and nitrate compounds while nonvolatile fraction consists of carbonaceous (soot) fraction and ash content.[16] Toxicity of diesel particulate is dependent on the particle composition and its size. Figures 1 and 2[16,17] show typical composition of diesel particulates.

Volatile fractions in PM are considered for imparting toxicity including potential carcinogenicity. Volatile fraction may be found in the gas phase; it

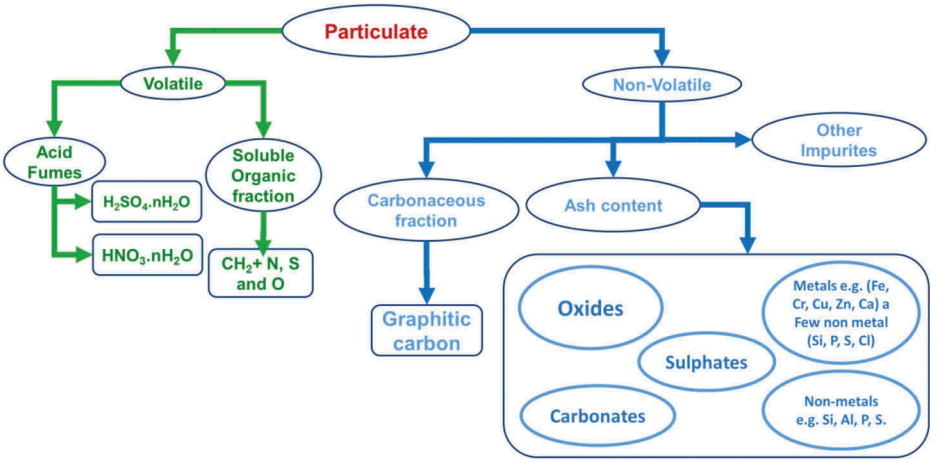

Figure 1. Conceptual model of particulate composition, terminating in five distinct groups, or fractions: sulfates, nitrates, organics, carbonaceous, and ash (reproduced with permission from Ref. [16]).

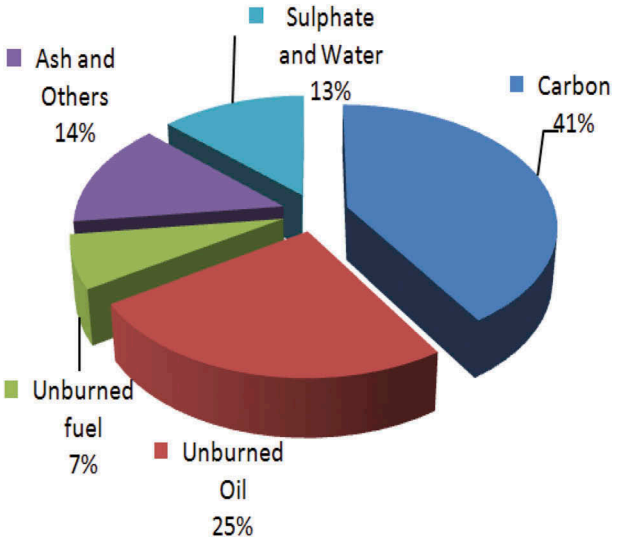

Figure 2. Typical particle composition for a heavy-duty diesel engine tested in a heavy-duty transient cycle (reproduced with permission from Ref. [17]).[17]

can condense on the surface of the solid particle or may nucleate to form the particles. Exhaust sample also consists of secondary particles which form during the sampling process in the particulate sampling system. Some losses of primary particulate may occur during the particulate collection.

Primary particles, which are generally 15–40 nm in diameter, formed during the combustion agglomerates and form relatively bigger particles. It is sometimes observed that the particle microscopic morphology for the particulate emitted from a modern diesel engine equipped with Common Rail Direct

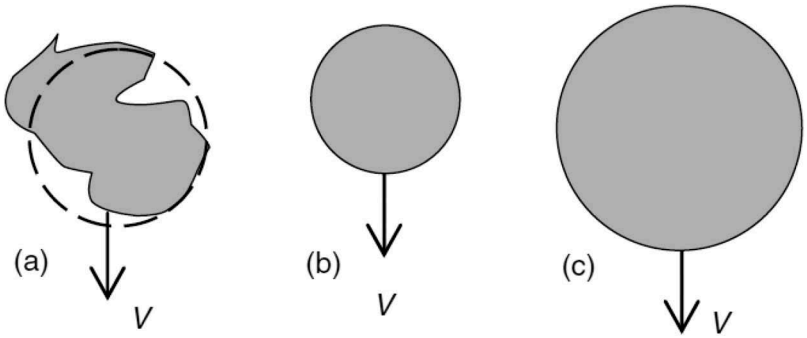

Figure 3. Various concepts of "diameter": (a) an irregularly shaped particle, and, superimposed, the volume equivalent sphere; (b) a Stokes-equivalent sphere (same density as (a)); (c) an aerodynamic-equivalent sphere (unit density). The irregular particle, Stokes-equivalent sphere, and aerodynamic-equivalent sphere all have the same settling velocity (reproduced with permission from Ref. [18]).[18]

Injection (CRDI) injection system is different as compare to older diesel engines. Modern diesel engines emit relatively small-sized particles in greater number and lower total particulate mass as compare to the older engines. The structures of particulate from modern diesel engines are of cage-like structures (fullerene) and graphitic for the particulates emitted from older engines. Diesel particulates are mainly characterized by the particle diameter (Figure 3). Due to the complex morphological structure, diameter of diesel particulates cannot be characterized simply by measuring its geometrical dimensions under the microscope. Irregular shapes with non-sphericity of the diesel particulates are one of the most important characteristics. Certain PM measurement instruments can charge the diesel particulates and these charged particles can respond to the electric field produced by the instrument. Since, the diameter of the particles is measured by evaluating the effect of electric field on charged particles, it is called electric mobility diameter. Electrical mobility diameter, the velocity with which particles move in an applied electrical field, is generally used to express the size of the diesel particulates.

Figure 4 shows some typical particles likely to be emitted by an internal combustion engine.[16] The most important aspect about the particulate size is its trimodality; nucleation mode, agglomeration mode, and coarse mode particles. Particulate emission from diesel vehicles also exhibits these characteristics. Particle sizes are independent of the engine operating conditions and all the three particle modes are found in the diesel exhaust. Nucleation mode particles mainly consist of volatile materials, which are very small particles and less studied. Researchers have reported that these are made up of volatile materials mostly but some researches claimed that it also include solid materials. Accumulation mode particles are those which form due to the accumulation of smaller primary particles.

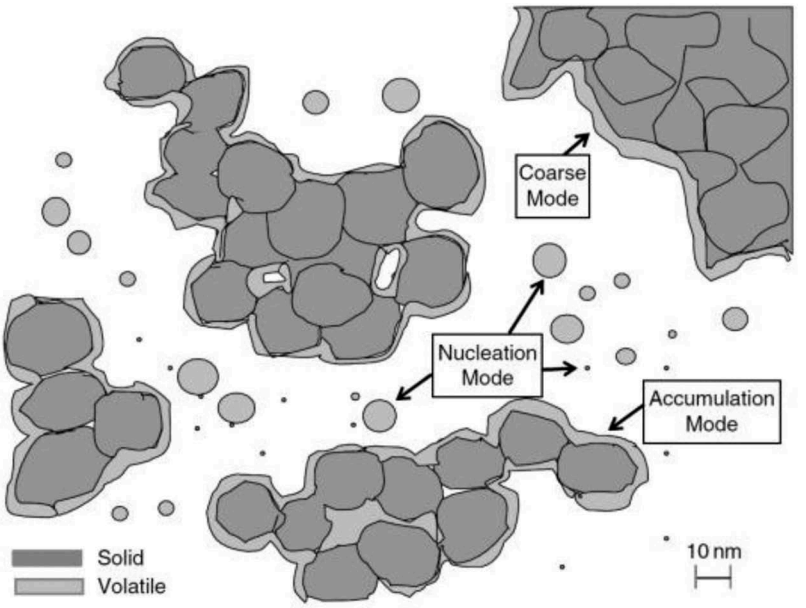

Figure 4. Some typical particles likely to be emitted by an internal combustion engine, depicted schematically: coarse mode (largest, shown in part), nucleation mode (smallest), accumulation mode (middling) (reproduced with permission from Ref. [16]).

These primary particles are also known as spherules.[16] Spherules are the small primary particles in definite narrow size range, which are not spherical in shape but very close to this shape. The size range for these particles vary between 20 and 50 nm. The size of the accumulation mode particles may vary depending upon the number spherules in the particle. Spherules are building blocks and form the backbone for the accumulation particles.[16] The surface of the agglomerated particle from spherules may be coated with the volatile substances in the exhaust stream. This coating of volatile material leads to the formation of the wet particulates. By heating the wet particulates, solid carbonaceous core remains as particulate, which is called dry particulates.

2.2. *Particulate Formation*

In diesel engines, injection of fuel is attained at high temperature and pressure as fuel atomization and spray penetration are better at high temperature and pressure leading to better mixing of fuel and air. It improves the homogeneity of combustion. At high injection pressure, fuel in the combustion chamber is converted into small droplets. Due to nonuniform dispersion of these droplets, the excess air ratio value (λ) varies at every location of the combustion chamber and is very low at droplet surface and thereby increases with distance from the droplet surface. It should be noted that λ is the ratio of inducted air mass to the theoretical air requirement. This results in heterogeneity in fuel–air mixture. Local excess air

ratio is very low near the droplet which indicates the deficiency of oxygen results in incomplete combustion. Alternatively, λ value is high at distance from the droplet with excess availability of oxygen leading to complete combustion of fuel vapors. Incomplete combustion is mainly responsible for PM formation. The deficiency of oxygen results in the occurrence of pyrolytic reactions which produces paralyzed compounds. One of the main products of these pyrolytic reactions is acetylene. The acetylene is the main precursor molecule for the formation of polycyclic structure molecules. Number of acetylene molecules can make ring-like structure to form polycyclic compounds. These kind of reactions are mainly responsible for the production of very small primary particles called "spherules" in large numbers which are the main building blocks of the agglomerated particles. This chain of particle formation is almost same for all forms of combustion or there may be little difference in the steps.

Figures 5 and 6 show schematic of PM formation. Particulate formation mainly takes place in five following steps: pyrolysis, nucleation, surface growth, agglomeration, and oxidation. Diesel fuel molecules mostly contain 12–22 carbon atoms and almost double the hydrogen molecules in number. PM formation process takes only few milliseconds and is highly dependent upon air–fuel ratio and combustion chamber pressure–temperature.[1] Under the influence of these three factors, fuel molecules break into PM forming precursor molecules (pyrolyzed compounds) after the pyrolytic reactions.[19,20] These precursor molecules undergo nucleation process and form nuclei, generally less than 3 nm in size. In surface growth, which is followed after nuclei formation, hydrogen molecules are striped off from the nuclei forming spherules with higher C/H ratio.

These spherules, varying between 20 and 50 nm, agglomerate and are the building blocks for agglomerated particles.[16] Spherules vary in size, however, their variation is limited. It helps them in combining and making relatively bigger particles. Combination may be in the form of a long chain or sometimes the first spherule joins to the last spherule in the chain and form a closed spherical agglomerated particle. It should be noted that the agglomerated particles have much larger surface area than its equivalent spherical size, having same density. This increases the tendency of gas to particle phase conversion by condensation of organic compounds present in the exhaust stream on to the surface of agglomerated particles. The fifth and last step is oxidation. It is easier to explain these PM formation steps in this linear straight way but in reality the two stage of the PM formation may actually occur simultaneously at two different locations of the combustion chamber.

3. Remediation Options for PM Emissions

Particulate emission is one of the major problems in Indian subcontinent and many other countries, mainly due to excessive PM2.5 particles (smaller than 2.5 μm in size), which is far exceeding WHO limits and is also

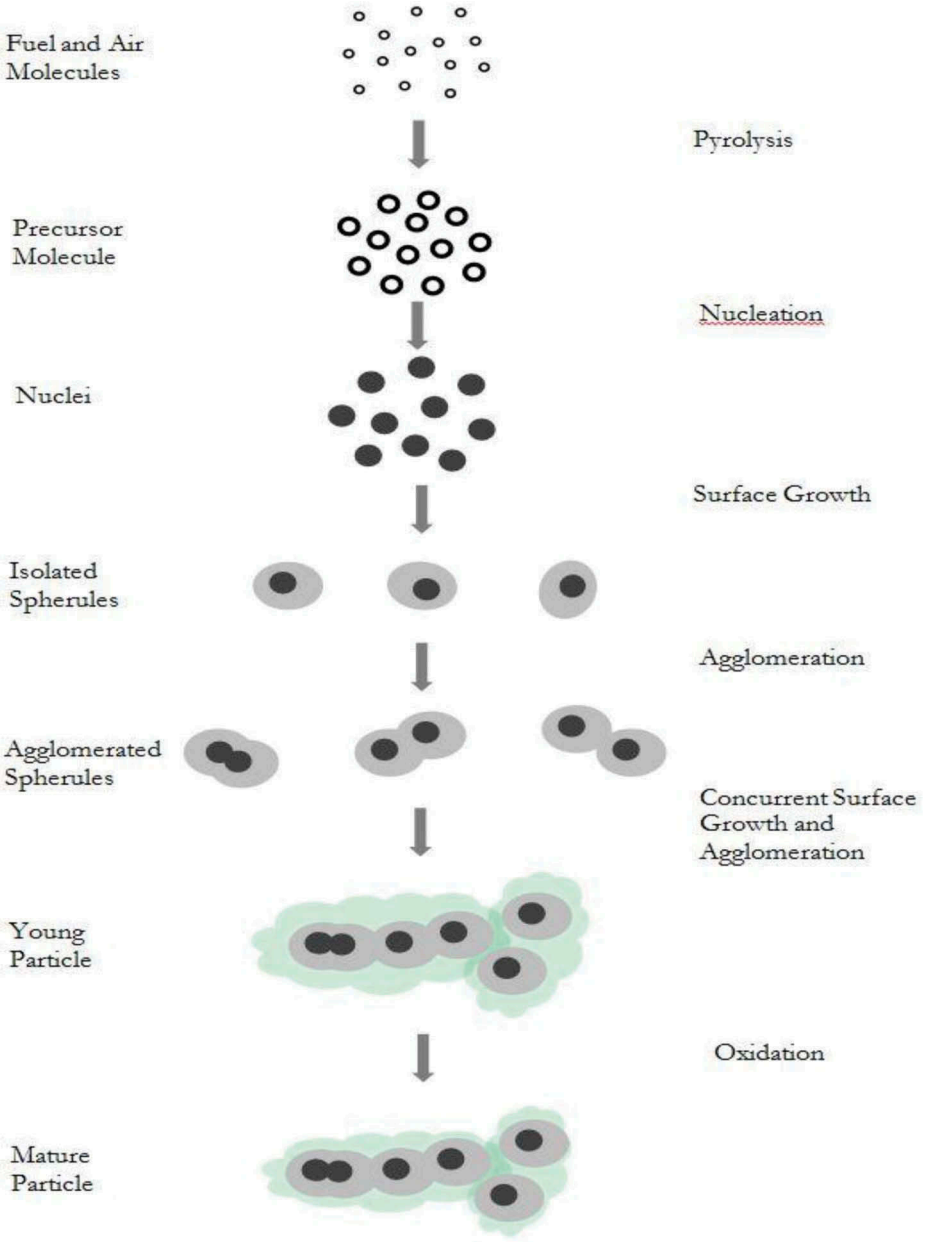

Figure 5. Schematic view of PM formation adopted from particulate emissions from vehicles (reproduced with permission from Ref. [16]).

considered as a major criteria pollutant by other regulatory agencies.[21] PM2.5 was classified as class I carcinogen by International Agency for Research on Cancer in 2013, which suggest its harmful impacts to human health both due to its smaller size and chemical composition.

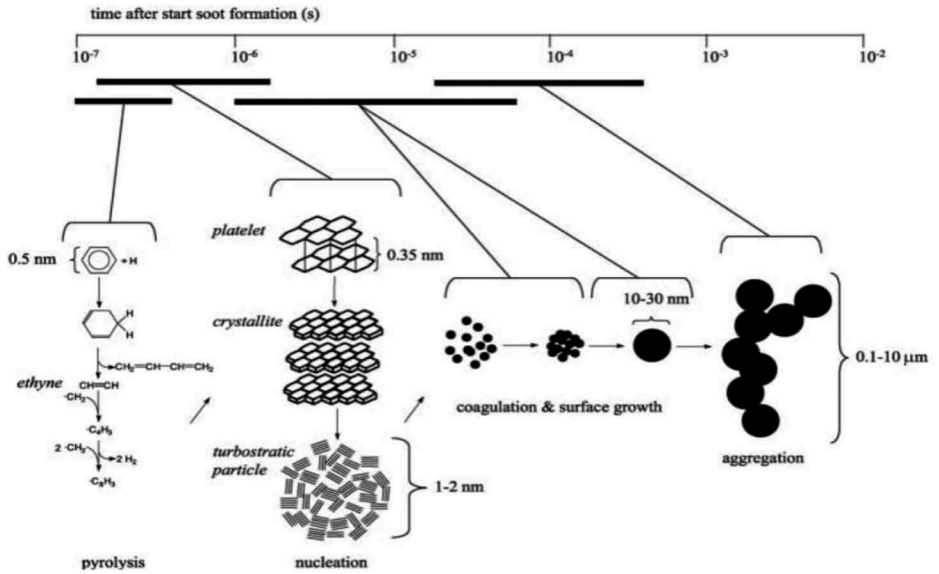

Figure 6. Schematic mechanism of the formation of PM particles (reproduced with permission from Ref. [19]).[19]

In Gangetic planes of India, during winters at low temperatures, particulates are trapped at lower altitudes due to reduced natural buoyancy and lack of efficient ventilation thus leading to dense fog episodes in the area.[22] It clearly demands for stringent emission control norms in the cities of Gangetic Basin to improve air quality in accordance to National index. Table 1 presents typical emission standards established by emission control agencies in various nations.[23]

Remediation of these serious air pollution episodes involves controlling and mitigating PM emissions including that from diesel engines as they are among the prominent sources. Special attention toward engineering design aspects of diesel engines, also involving operational parameters such as injection parameters, spray impingement, exhaust gas recirculation, etc. are being considered as the first step in PM emission remediation.[24–28] Conventional diesel engines utilize a fuel spray injection angle of ~150°. Tests were performed with dimethyl ether fuel on a direct-injection CI engine fueled at lower injection angles of 60° and 70°. Results revealed that an increase in fuel inlet pressure provides better air/fuel mixture with fine droplet dispersion, thus, affording low levels of PM emissions at all injection timings. Normally, a trade-off exists between particulates and NO_x concentrations in a typical conventional CI engine. In a study, low angle injectors with multiple injections achieved lower NO_x and PM emission levels.[29] Injection pressures and exhaust gas recirculation were tested on premixed charge compression ignition diesel engine using a single-cylinder test engine

Table 1. Emission standards for diesel engines (2014 onward) (reproduced with permission from Ref. [23]).[23]

Nations	Engine types	Units	CO	HC + NO_x	NO_x	PM
European Union and Russia	Cars and light trucks	g/km	0.50	0.17	0.08	0.005
	Heavy-duty truck and bus engines	g/kW h	1.5	0.53	0.4	0.01
	Non-road engines (>130 kW)	g/kW h	5.0	4.7	3.3	0.025
USA and Canada	Cars and light trucks	g/km	2.61	0.099	–	0.0018
	Heavy-duty truck and bus engines	g/kW h	20.77	–	0.0268	0.0134
	Non-road engines (>130 kW)	g/kW h	3.5	0.86	0.67	0.03
Japan	Cars and light trucks	g/km	0.63	0.174	0.15	0.005
	Heavy-duty truck and bus engines	g/kW h	2.22	0.57	0.4	0.01
	Non-road engines (>130 kW)	g/kW h	3.5	0.19	0.4	0.02
China	Cars and light trucks	g/km	0.5	0.23	0.18	0.0045
	Heavy-duty truck and bus engines	g/kW h	4.0	2.55	2.0	0.03
	Non-road engines (>130 kW)	g/kW h	3.5	7.0	6.0	0.2
India	Cars and light trucks	g/km	0.5	0.23	0.180	0.0045
	Heavy-duty truck and bus engines	g/kW h	4.0	2.55	2.0	0.03
	Non-road engines (>130 kW)	g/kW h	3.5	4.0	2.7	0.2
South Korea	Cars and light trucks	g/km	0.5	0.03	0.02	0.01
	Heavy-duty truck and bus engines	g/kW h	4.0	0.62	0.46	0.01
	Non-road engines (>130 kW)	g/kW h	3.5	0.19	0.40	0.02
Brazil	Cars and light trucks	g/km	1.3	0.13	0.08	0.025
	Heavy-duty truck and bus engines	g/kW h	4.0	2.55	2.0	0.03
	Non-road engines (>130 kW)	g/kW h	3.5	4.0	2.8	0.2

and an optically accessible engine. Tests revealed that higher injection pressure and exhaust gas recirculation led to lower hydrocarbon (HC), NO_x, and PM emissions compared to conventional diesel combustion.[30] These studies show optimistic visions to improve engine designs and operational parameters for controlled emission characteristics of diesel engines.[23]

Another perspective control and remediation strategy is based on aftertreatment of diesel exhaust. Here, catalyst is used to eliminate PM and other pollutants from diesel exhaust, hence providing huge research inputs and opportunities in the field of exhaust catalytic removal of diesel PM emissions.[31,32] These aftertreatment strategies are based on the use of DOCs (diesel oxidation catalysts), diesel particulate filters (DPFs), and POCs (partial oxidation catalysts). A typical diesel after exhaust treatment assembly is shown in Figure 7.

3.1. *DOCs*

DOCs are a foremost contributor to diesel exhaust emission control. It is an open monolith non-filter system that utilizes a catalytic reaction process to oxidize pollutants in diesel exhaust stream, thereby turning them into less

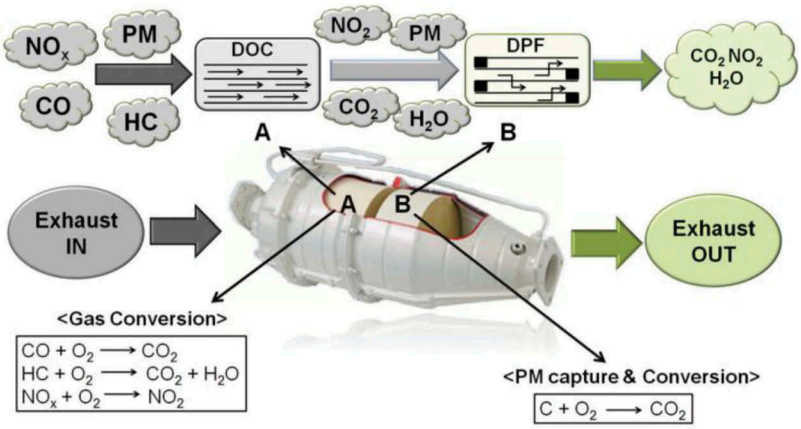

Figure 7. Schematic of DOC and DPF assembly in catalytic convertor.

harmful components (Figure 7).[33] DOC is generally constituted by assembly of following components: substrate (catalyst support), alumina washcoat (about 20–40 μm thick), and impregnated catalyst followed by canning. Cordierite honeycomb monolith and corrugated metallic types of structures are most commonly used substrates.[34] Pt/Pd (5/2) is commercially the most popular oxidation catalyst used in DOCs.[35,36] Owing to its name, DOC utilizes oxygen, which is surplus in diesel exhaust, to promote oxidation of several diesel exhaust components. Carbon monoxide (CO), gas phase HCs, and organic fraction of diesel particulates (soluble organic fraction [SOF]) can be neutralized via oxidation when passed over oxidation catalyst in DOC.

Additionally, several aldehydes and polyaromatic HCs derived from HC via partial oxidation during engine combustion can also be oxidized along with a reduction or elimination of the odor of diesel exhaust.[37,38] These processes can be described by the following chemical reactions:

$$C_nH_{2m} + [n + m/2]O_2 \rightarrow n\,CO_2 + m\,H_2O \quad \text{(R1)}$$

$$CO + 1/2\,O_2 \rightarrow CO_2 \quad \text{(R2)}$$

Reaction 1 represents two processes: oxidation of gas phase HC as well as SOF compounds. The oxidation of CO to CO_2 is described by reaction 2. Carbon dioxide and water vapor are harmless and therefore obvious emission benefit is associated with the above reactions. However, due to oxidation capabilities of catalysts, sulfur dioxide (SO_2) in diesel exhaust is oxidized to sulfur trioxide (SO_3). SO_3 then combines with water vapors in the exhaust stream to form sulfuric acid as shown by the following reactions.

$$2\,SO_2 + O_2 \rightarrow 2\,SO_3 \quad \text{(R3)}$$

$$SO_3 + H_2O \rightarrow H_2SO_4 \quad \text{(R4)}$$

As the exhaust temperature decreases in the way to exit through tailpipe, the gaseous sulfuric acid combines with water to form liquid particles composed of hydrated sulfuric acid called sulfate particles.[39] These particles contribute to increasing in total PM emissions from diesel engines. So, high sulfur diesel becomes prohibitive for catalyst applications.[40] Another important reaction in DOC applications is oxidation of NO to NO_2 (reaction 5).

In the open atmosphere after some time, reaction 5 reaches its thermodynamic equilibrium regardless of original NO_x composition. However, oxidation of NO is of immense concern in the most surface applications (tailpipe emissions from automobiles), as well as in engines working in mines far from open atmosphere. Nitrogen dioxide can efficiently oxidize carbon particles of PM emissions (reactions 6 and 7) and hence commonly used for regeneration of DPFs. Therefore, designing DOCs with high NO_2 production can support the operation of DOC/DPF systems.[41,42] These catalysts used in DOCs have the ability to adsorb oxygen due to presence of active catalytic sites, which act through following three stages: (1) bonding of oxygen to catalytically active site; (2) diffusion of reactants, such as CO, NO_x, and HCs, to active sites; (3) reaction with bonded (activated) oxygen at active sites, and (4) desorption of reaction products, such as CO_2 and water vapor, from the catalytic site and diffusion to the bulk of the exhaust gas.

$$NO + 1/2\,O_2 \rightarrow NO_2 \quad \text{(R5)}$$

$$C(s) + NO_2 \rightarrow CO + NO \quad \text{(R6)}$$

$$CO + NO_2 \rightarrow CO_2 + NO \quad \text{(R7)}$$

3.2. *DPFs*

Diesel PM emissions are accompanied by CO, NO_x, unburnt HCs in gas streams with the high concentration of O_2, CO_2, and H_2O. The emission temperature is typically below 500–550°C. These conditions are well suitable for oxidation of CO and HC but not for NO_x and PMs.[43] Hence, DPFs are used to trap PM from the exhaust stream. DPFs prevent diesel PM emissions to the atmosphere by physically capturing them; hence, showing impressive filtration efficiencies, in excess of 90%, as well as good mechanical and thermal durability. These filters are also monolith-based honeycomb structures which are partially blocked at each entry and exit ends providing entrapment for PMs (Figure 7). The porous walls of the filters allow gas to flow through capturing PMs depending upon the porosity of material used in DPFs.[44] DPFs may have limited effect in controlling the non-solid fraction of PM emissions – SOF and sulfate particles. Hence, these systems may be advanced by addition of functional components targeting the SOF – typically oxidation catalysts, while sulfate particulates may be minimized or avoided by use of ultra-low sulfur fuels.[45]

DPFs accumulate a large amount of soot due to a low density of diesel PMs (~0.1 g/cm^3) and old generation heavy-duty engines can generate more than a few liters of soot per day. Removal of these particulates, also called filter regeneration, is necessary as filter clogging results in high exhaust gas pressure drop in the filter that negatively affects the engine operation. Filter regeneration can be done either periodically, after a predetermined quantity of PM has been accumulated, or continuously, during regular operation of the filter. The filters where exhaust stream itself provides the temperature required for particulate oxidation at sufficient rate are called passive filters or continuous regenerating traps (CRTs) (Figure 8). These filters are incorporated with some active catalyst which lowers the PM oxidation temperature to a level that can be harvested from the exhaust gases during continuous operation of the engine.[46,47] The catalyst can promote oxidation of carbon through either oxygen mechanism - catalytic oxidation of carbon by oxygen, or nitrogen dioxide mechanism-catalytic oxidation of NO to NO_2, followed by the oxidation of carbon by nitrogen dioxide as shown in Eqs. (5–7).

Alternatively, there are filters that need active strategies for increasing the filter temperature. These active strategies aim at increasing the exhaust temperature by either late cycle injection of additional fuel quantities which is an in-cylinder engine management method or injection and combustion of fuel in the exhaust gas. Electrical heating is also used in many vehicle configurations. Such heaters can be placed either upstream of the filter substrate or incorporated into the filters or else electrically conductive media (such as metal fleece) can be used which can act as both the filter and the heater.[48] The third category utilizes the combination of passive and active regeneration. The diesel filter regeneration strategies are concisely shown in Figure 9.

3.3. *Partial flow filters*

Also known as POCs or flow-through filters, these devices perform both ways by collection and storage of PM providing time to let its catalytic oxidation and remediation to less harmful gaseous products. It allows the exhaust gases a free flow-through passage and maintains its storage capacity[49] (Figure 10). Hence, partial flow filters (PFFs) have similarity to both DOCs and DPFs. Nitrogen dioxide generated from upstream DOC reacts with a stored PM and reacts catalytically with a PM to accomplish regeneration of these devices. PFFs allow the gaseous products to pass through without regeneration even at its maximum storage capacity, affecting negatively only the conversion efficiency of PM. These devices had PM control efficiencies in between DOCs and DPFs and regarded as the new flow-through filter technologies to control PM

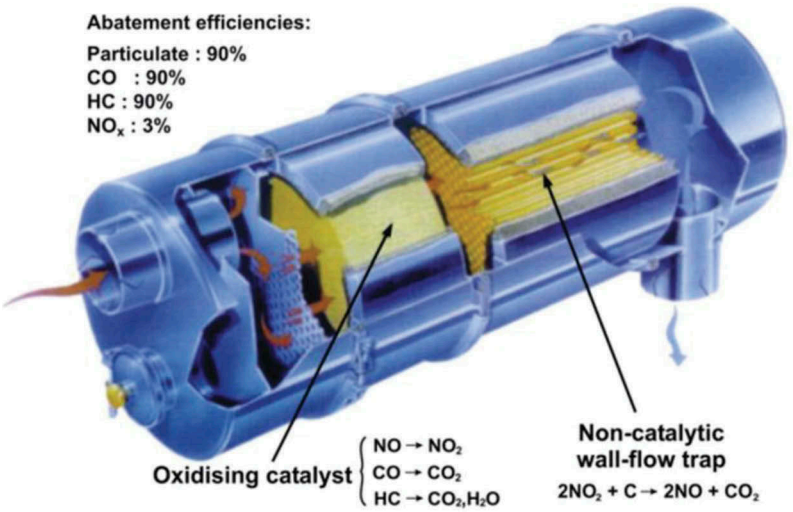

Figure 8. The continuously regenerable trap system by Johnson Matthey (reproduced with permission from Ref. [46]).

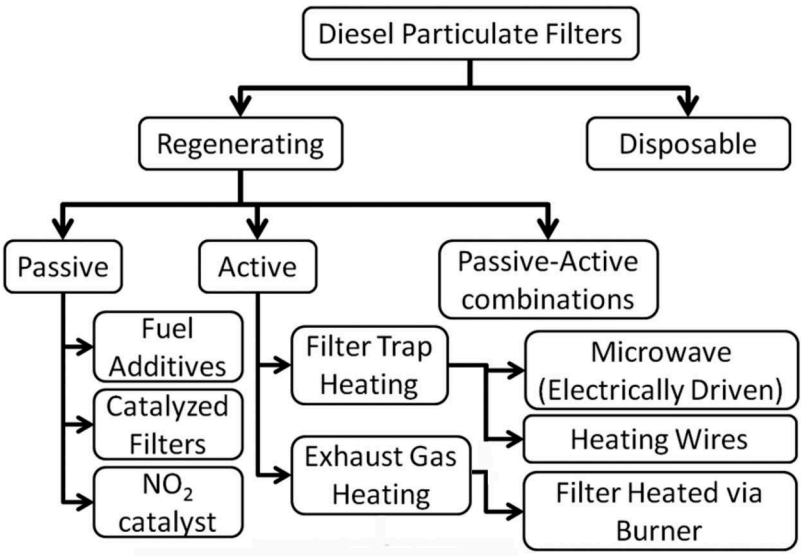

Figure 9. Possible routes for a controlled regeneration of diesel particulate filters.

emission. Traditional PFF substrates embrace metal fleece, ceramic or metallic foams, and wiremesh.[51]

In this review, we will focus on diesel particulate composition and its formation, catalysts for the oxidation of diesel particulate: Noble, non-noble metal-based catalysts, and perovskite-based catalysts in DOC and DPF applications for effective and sustained control of diesel PM emissions.

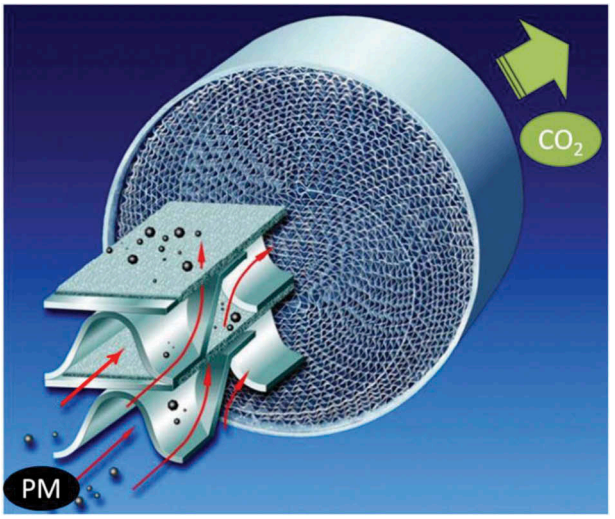

Figure 10. Metallic flow-through filter made up of corrugated metal foil and layers of porous metal fleece (reproduced with permission from Ref. [50]).[50]

4. Basic principles of PM oxidation

4.1. *Un-catalyzed PM oxidation reactions with oxygen/air*

Morphologically, PM particles are agglomerates of spherule type carbon particles with size varied from few microns to millimeters.[12] These agglomerates behave as porous particles with effectiveness factor[52] invariably unity for oxidation with O_2 owing to free diffusion of oxidant between spherules. During combustion of these spherules, oxidation occurs both at their external as well as the internal surface. This was observed by Ishiguro et al.[53] by simultaneous observation of particle size under transmission electron microscope (TEM) and specific surface area of PM. They reported the reduction of particle size could not sufficiently explain enormous increase in surface area of PM. This indicated that the pores were created within spherules during combustion with O_2. In similar experimentation, Jung et al.[54] reported that the shrinkage rate of spherules was consistent of combustion on the only exterior surface (activation energy: E_a = 148 kJ/mol). Meanwhile, investigating on ultra-low sulfur diesel (ULSD) and biodiesel soot, observations of Strzelec et al.,[55] suggested penetration of O_2 into spherules and combustion from inside the pores. They also observed a significant increase in surface area of soot, which was more than anticipated from shrinking spherules that burn only on their exteriors. This suggested enlargement of internal pores during oxidative combustion of these spherules.

The mechanism of oxidation at PM surface involves two steps, in which, at first step, the O-atom is transferred from the gas phase to form a solid complex at solid carbon surface. Then, at a second step, the complex decomposes to form carbon monoxide releasing a carbon atom from the surface.

PM oxidation by O_2 is mainly advantageous for the regeneration of particulate filters due to high concentrations of O_2 (around 10%) in diesel engine exhaust.[44] The reaction scheme[56,57] (without catalyst) involves free carbon sites C_f, chemisorbed localized molecular oxygen $C(O_2)$, chemisorbed mobile molecular oxygen $C(O_2)_m$, chemisorbed localized atoms of oxygen C(O), and chemisorbed mobile atoms of oxygen $C(O)_m$:

$$C_f + O_2 \rightarrow C(O_2) \text{ or } C(O_2)_m \tag{R8}$$

$$\begin{aligned} C(O_2)_m &\rightarrow C(O) + C(O)_m \text{ or/and } C(O_2)_m \\ &\rightarrow C(O)_m + C(O)_m \text{ or/and } C(O_2)_m \rightarrow C(O) + C(O) \end{aligned} \tag{R9}$$

$$C(O) \rightarrow CO \text{ and } C(O)_m \rightarrow CO \tag{R10}$$

$$C(O)_m + C(O)_m \rightarrow C_f + CO_2 \tag{R11}$$

$$C(O)_m + C(O) \rightarrow C_f + CO_2 \tag{R12}$$

$$CO + C(O)_m \rightarrow C_f + CO_2 \tag{R13}$$

$$CO + C(O) \rightarrow C_f + CO_2 \tag{R14}$$

$$O_2 + 2\,C(O) \rightarrow 2\,CO_2 \tag{R15}$$

Advanced DPF systems necessitate high filtration capacity and high regeneration capabilities of these filters.

This demands a thorough understanding of kinetic parameters of PM oxidation with respect to diverse engine operating conditions. As for different operating conditions, the concentrations of emission components vary. Considering that PM is composed of ~90 wt% of carbon, its oxidation with O_2 may be presumed to proceed by well-known thermodynamic pathway as follows:

$$C + O_2 \rightarrow CO_2 \qquad \Delta H^{o}_{298K} = -394 \text{kJ mol}^{-1} \tag{R16}$$

$$C + {}^{1}/_{2}O_2 \rightarrow CO \quad \Delta H^{o}_{298K} = -110\,\text{kJ mol}^{-1} \tag{R17}$$

Reactions R8–R15 mechanistically show that C_f sites are continuously consumed and renewed during complete oxidation of carbon. The order of reaction along with rate coefficient and apparent activation energy together expresses the effect various reaction parameters, such as temperature and oxidant concentration, on the overall PM oxidation rate. These parameters are taken to altogether represent multiple of elementary reactions (reactions R8–R15) occurring on the carbon surface. The overall order of reaction has been mostly observed to be in the range of 0.5–1.[58] Rate of a reaction (r) has traditionally been expressed as an exponent on the reaction gas partial pressure P_{ox} or concentration7:

$$r = A \exp\left(-{}^{E}/_{RT}\right) P^{n}_{ox} \tag{1}$$

$$k = A \exp\left(-E/RT\right) \qquad s^{-1} \tag{2}$$

where k is the rate coefficient, A is a pre-exponential factor, E is the activation energy, R is the Gas constant, T is temperature, and n is the order of reaction. However, a wide number of reports[59–62] suggested the order of reaction to be 0.5 for a wide variety of carbons. The fractional order of ~0.5 has been attributed to different adsorption sites on carbons (PM). These adsorption sites show broad distributions of activation energies for reactions R8–R15 because of $C(O)$ functionalities on the PM show a wide range of structural and kinetic parameters.[57,63]

Neeft et al.[64] studied the kinetics of the un-catalyzed oxidation of a Printex-U (a carbon black, produced from the combustion of natural gas used as model soot, 90.5–92.2 wt% C, 8.1–8.4 wt% O, 0.52–0.70 wt% H, 0.17–0.22 wt% N, and 0–0.4 wt% S) and a diesel soot on a packed bed tubular reactor. Twenty milligram soot was used in the reactor with O_2 (10 vol%) in Ar at a flow rate of 500 mL/min (s.t.p.) and 455–520°C temperature range. On a carbon mass-specific basis, the general rate expression used by these authors for the global kinetics of carbon oxidation can be written as

$$r = kS_a \exp\left(-E_A/RT\right) P_{O2}^n \tag{3}$$

where r is the reaction rate in mass of carbon reacted/unit mass of carbon present/unit time, k is the rate constant of the Arrhenius form, E_A is the activation energy in energy/mol, R is the universal gas constant in mol/energy/K, T is absolute temperature in K, P_{O_2} is the partial pressure of oxygen, and n is the reaction order in oxygen. Here, the parameter $\underline{S}_a$ represents the surface area/unit mass carbon available for reaction. As Neeft et al.[64] pointed out, the surface area can vary with conversion and is sometimes assumed to vary according to a power law relationship of the form:

$$S_a = S_{a0}(1 - \zeta)^{\alpha} \tag{4}$$

where S_{a0} is the surface area at no conversion, α is an empirical exponent, and ζ is the fractional carbon mass conversion. When particles burn in the so-called shrinking sphere mode (where burning occurs only at the surface, and the solid carbon density remains constant), the total surface area of the remaining carbon varies to the 2/3 power of the unconverted carbon fraction. When S_a is considered on a mass-specific basis (area/mass of solid carbon remaining), α has a value of 1/3 for particles burn in shrinking sphere mode (the mass-specific area grows as the particles get smaller). With this model, they found order of reaction in oxygen concentration 0.85–0.94 (Printex-U) and 0.76–0.80 (diesel soot) and a corresponding activation energy of 168 kJ/mol for the oxidation of Printex U. Yezerets et al.[65] studied the oxidation rates by O_2 of two ULSD soot (sample A: generated by engine at repetitive

low-load cycles; sample B: generated by engine at low-load steady-state mode) dispersed in a packed bed of fused silica chips (40–60 mesh). The unpretreated PM was studied with 50 mg of the sample in temperature programmed oxidation process (330–610°C) with total gas flow rate - 400 mL/min (s.t.p.) – and gas composition - 10 vol% O_2, balance He. They found the activation energy of 126 kJ/mol for sample A and 146 kJ/mol for sample B. In another study, Yezerets et al.[66] studied oxidation rate by O_2 of Printex U (model soot) and diesel soot dispersed in a packed bed of quartz sand. Here, short bursts (step-response technique) of oxygen were introduced into the bed, providing time for dissipation of heat of combustion. For diesel soot, the order of reaction with respect to O_2 was determined to be 0.61 ± 0.03 and apparent activation energy was 137 ± 9 kJ/mol. While in Printex U, the observed order of reaction was 0.71 ± 0.03, and the apparent activation energy was 132 ± 5 kJ/mol. Using a kinetic model similar to Neeft et al.[64] and experimental method similar to Yezerets et al.,[66] Strzelec et al.[55] report measurements of the oxygen reactivity of diesel engine particulates generated from 100% conventional diesel (designated here as ULSD), blend of ULSD with 20 vol% biodiesel (designated as B20), and pure biodiesel (designated as B100). Particulate samples were collected from a modern light-duty diesel engine and then devolatilized at 650°C under argon. The microreactor was operated in both temperature programmed oxidation (TPO) mode and isothermal pulsed oxidation (IPO) mode. The oxidation behavior of the samples was studied by TPO, and the isothermal oxidation rates at different degrees of carbon burnout were measured by IPO mode. Oxidation of devolatilized diesel particulate produced with biodiesel, conventional diesel fuel, and an intermediate blend of these fuels was studied by using pulsed differential oxidation. Arrhenius dependence on temperature at fixed levels of carbon conversion was observed for these samples. Further, the fuel source and degree of burnout (shown in Table 2) affected the apparent activation energy. However, the normalized (with *in situ* measured Brunauer–Emmett–Teller [BET] surface areas) oxidation rates of particulates exhibited same Arrhenius relationship at all stages of burnout and the effective activation energy (E_A) was 113 ± 6 kJ/mol.

Wang-Hansen et al.[67] evaluated the kinetics of O_2-based oxidation of carbonaceous matter (Printex-U) using temperature-programmed oxidation and isothermal oxygen step-response experiments in a continuous gas-flow

Table 2. Arrhenius activation energies estimated from the mass-specific oxidation rate measurements at three different carbon conversion levels (reproduced with permission from Ref. [55]).

Particulate	E_A 20% burnout (kJ/mol)	E_A 40% burnout (kJ/mol)	E_A 60% burnout (kJ/mol)
ULSD	109 (±5)	129 (±7)	171 (±5)
B20	112 (±4)	135 (±5)	175 (±5)
B100	133 (±7)	160 (±3)	178 (±4)

reactor with 8 vol% O_2 (N_2 as balance), at 558–607°C, and a total gas flow of 1500 mL/min (Normal Temperature and Pressure [NT]P). In a traditional approach, Wang-Hansen et al.[67] estimated global kinetic parameters using a power-law model with the general form:

$$r = k\, f(\alpha)\, C_{O_2}^{n_{O_2}} \tag{5}$$

where r represents the reaction rate, k is the Arrhenius rate constant $Ae^{-Ea/(RT)}$ where A is the pre-exponential factor, E_a the activation energy, R the gas constant, T the temperature. Moreover, C_{O_2} and n_{O_2} are the concentration and reaction order for oxygen, respectively. The function $f(\alpha)$ represents the conversion model describing the evolution of reactive carbon atoms with progressing oxidation. For the conversion model, an empirical power-law expression was used:

$$f(\alpha) = n_{C,initial}(1-\varepsilon)^{n_c} \tag{6}$$

where $n_{C,initial}$ is the amount of carbon at the start of the experiment, ε is the mole fraction of oxidized carbon (carbon conversion), and n_C is the global reaction order with respect to carbon. Low (<10%) and high (>90%) conversion degrees were not considered to avoid the fraction of highly reactive carbon species and experimental uncertainties associated with measurements of low concentrations, respectively. Linear regression of a complete set of data from isothermal step-response experiments was used to estimate the four global kinetic parameters (A, E_a, n_C, and n_{O_2}). Figure 11 shows the carbon conversion dependence of these parameters. The reactor order with respect to carbon showed the highest dependence on the carbon conversion. Comparatively, minor dependence on the carbon conversion was observed for A, E_a, and n_{O_2}. The overall activation energy decreases from 140 to 122 kJ/mol, which was similar to the observations by Kalogirou et al.[68] This decrease in activation energy was explained by Neeft[69] by considering the presence of large amounts of electrophilic atoms, i.e., surface oxygen complexes (SOCs), at high conversion degrees that weaken the carbon–carbon bond strength in the graphitic structure.

In another report, Wang-Hansen et al.[70] demonstrated two different methods to estimate the kinetics of O_2-based oxidation of carbonaceous matter (Printex-U) in a continuous gas flow reactor with 8 vol% O_2 (N_2 as balance) at 605–662°C and space velocity of ~12,000 h^{-1}. The two methods engaged the kinetic analysis of the rate changes during the progress of oxidation: either by the fractional change of atoms available for reaction (traditional approach) or by changes in the activation energy (unconventional approach). In traditional approach (Eq. (5)), considering the common ideal models reviewed by Khawam and Flanagan,[71] they used the optimal combination of models, i.e. a third-order Avrami–Erofeyev model (Eq. (7)) and a first-order reaction model (Eq. (8)). In unconventional approach,

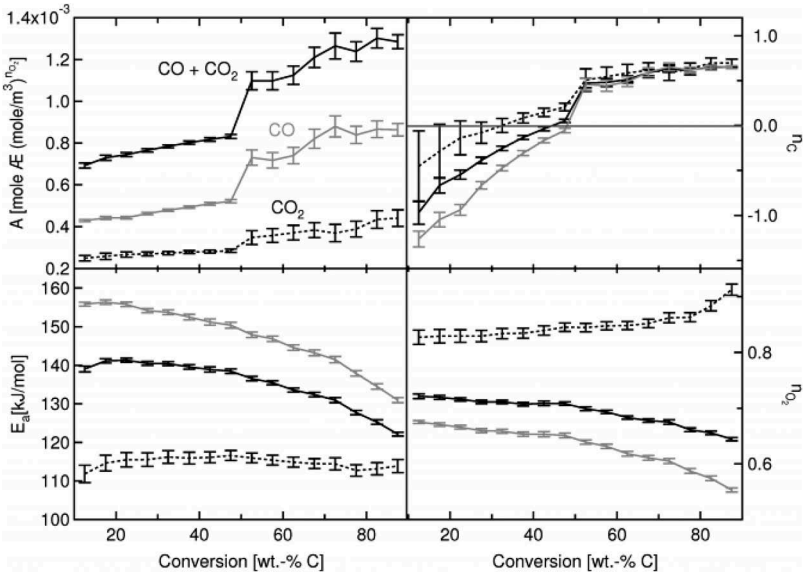

Figure 11. Dependence on degree of conversion for A, E_a, n_C, and n_{O_2}. The parameter values were obtained by linear regression (least squares) over 5 wt% sub-conversion intervals, using nine isothermal experiments at three levels of oxygen and three temperatures per oxygen level. The error bars mark the 95% confidence regions (reproduced with permission from Ref. [67]).

dispersive kinetics[71] was used based on the existence of reaction sites with different activation energies depending on reaction time, conversion, or spatial location.

These variations of activation energy were modeled by a Maxwell–Boltzmann distribution describing variations in activation energy using a final semi-empirical model equation (Eq. (9)).[72]The constants β_1 and β_2 were used to calculate rate constant k directly using the relation $k = \beta_1 \cdot \beta_2$ where β_1 representing the reciprocal of a first-order rate constant and β_2 a second-order rate constant[73] and the activation energy was obtained from the slope of the Arrhenius plot.

$$f(a) = 3(1-\alpha)[-1n(1-\alpha)]^{2/3} \tag{7}$$

$$f(\alpha) = (1-\alpha) \tag{8}$$

$$\alpha = \exp\{(-\beta_1/t)\lfloor \exp(\beta t^2) - 1 \rfloor\} \tag{9}$$

Activation energy estimated from Eq. (7) was 137.0 ± 4.3 kJ/mol, from Eq. (8) was 156.9 ± 8.2 kJ/mol, and from Eq. (9) was 141 kJ/mol. Similar values of activated energy as predicted by these kinetic models are in agreement with other literature[74–79] reporting values in the range from 125 to 168 kJ/mol. Tighe et al.[80] studied the rates of oxidation of two soots, produced from burning either ULSD or

biodiesel in an engine, which were measured at 450–550°C, with oxygen concentrations of 2.7–24.4 vol%. The soot was first preheated in argon at 700°C to remove any adsorbed volatile matter. The kinetic model which they successfully applied to soot oxidation reaction was based on the consideration that the particles burn internally inside the pores as well as externally. In this pseudo-homogeneous model, a volumetric rate constant, k_V, may be defined as Eq. (10) which on integration yielded Eq. (11):

$$\frac{dN_C}{dt} = -k_V C_{O2}^n N_C \tag{10}$$

$$\ln(1 - X_C) = -k_V C_{O2}^n t \tag{11}$$

where N_C represents moles of carbon remaining, X_C is carbon conversion, n is the order of reaction, and C_{O_2} is a concentration of oxygen at time t. Plots of $(1 - X_C)$ versus time (Figure 12(a,b) illustrated the considerable effect of temperature on the rate of oxidation by decreasing the time taken for 50% soot conversion from 2432 s at 450°C to 140 s at 550°C (for 5.4 vol% O_2). Also, there was significant effect of increasing $[O_2]$ almost tenfold from 2.7 to 24.4 vol% (at 525°C) such that time is taken for 50% soot conversion decreased from 328 to 98 s, i.e. by a factor of 3.3; thus it appears that the order of reaction with respect to O_2 was ~0.5. These plots corresponded to first-order exponential decays. Linear plots of $\ln(1 - X_C)$ against time in Figure 12(c,d) confirmed this. Thus, the overall rates in this study[80] were half-order with respect to O_2, with an apparent activation energy of 145 ± 8 kJ/mol.

4.2. *Un-catalyzed PM oxidation reactions with NO_2*

Mitigation of diesel PM emission led to the development of novel particulate trap system that reduces the emission of these PM particles into the free atmosphere. However, regeneration of these traps on a continual basis has been challenging and hence, a topic of progressive research. These efforts focused on the development of regeneration methods which efficiently oxidizes and gasifies PM deposits in the filter or catalyst structures. However, the direct oxidation of these PM particulates needs high temperatures (about 600°C). The diesel exhaust temperature varies in the range of 200–500°C, which fall short for direct PM oxidation with O_2. Also, high-temperature regeneration is inconvenient and inefficient by directly injecting fuel into the exhaust stream.[81] This provides an exploitable opportunity of low-temperature PM oxidation with nitrogen dioxide as NO_2 is known to be more reactive than the other oxidizing species (O_2, H_2O, and CO_2)

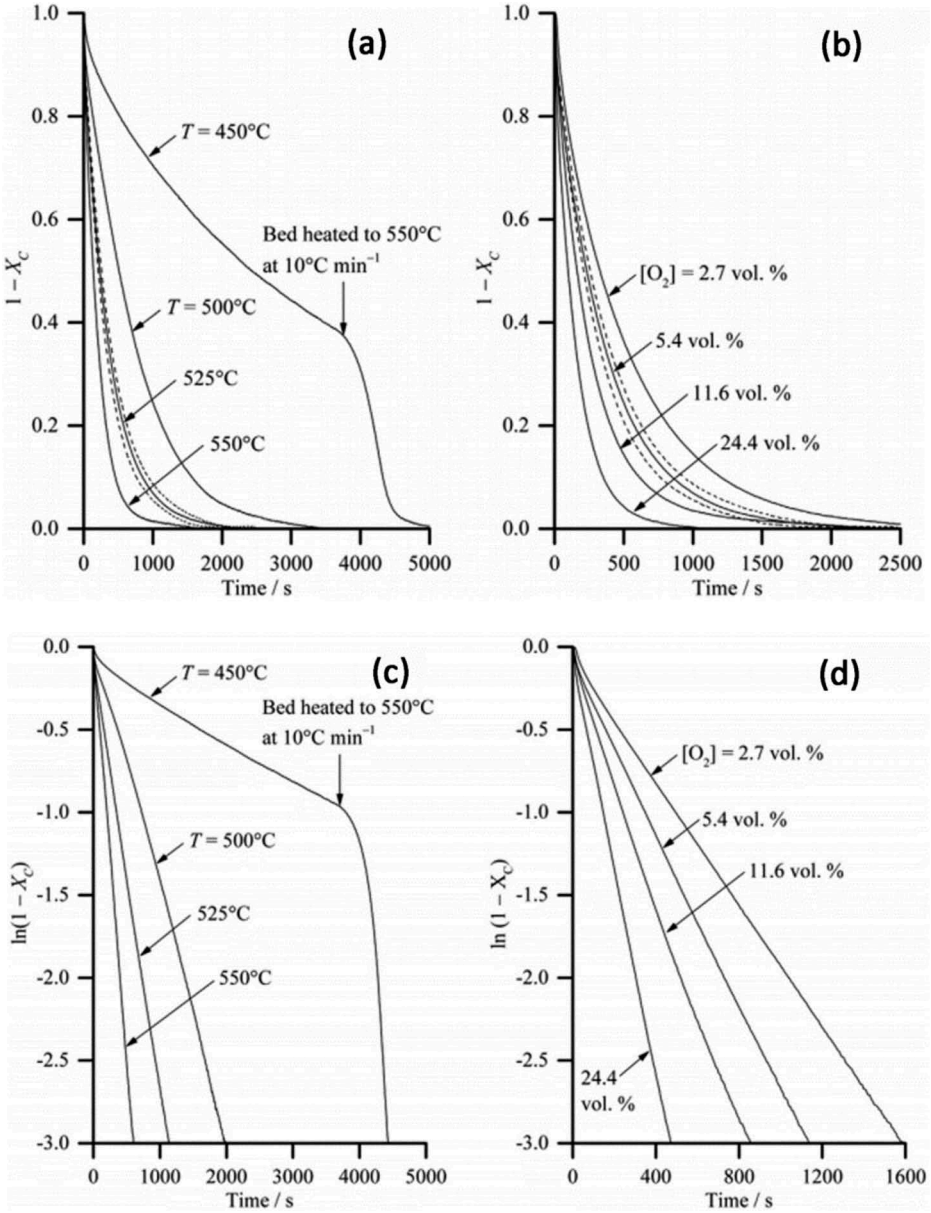

Figure 12. Plots of $(1 - X_C)$ against t for ULSD soot at (a) different T from 450 to 550°C, $[O_2]$ = 5.4 vol% and (b) different $[O_2]$ in the range 2.7–24.4 vol%, T = 525°C. *The area within the dotted lines on either side of the curve for 525°C shows the limits of measurements for five repeat experiments*. Plots of $\ln(1 - X_C)$ against t for ULSD from the measurements of X_C shown in in (c) Fig. a and (b) Fig. b. Reproduced with permission from Ref. [80].

at low temperature.[82] NO_2, after production by oxidation of NO in catalytic upstream monolithic converter, is present in sufficient concentration in exhaust gases to oxidize PM via

$$C + 2NO_2 \rightarrow CO_2 + 2NO \qquad \Delta H = -279\,kJ\,mol^{-1} \tag{R16}$$

$$C + NO_2 \rightarrow CO + NO \qquad \Delta H = -53\,kJ\,mol^{-1} \tag{R17}$$

$$C - H + 2.5\,NO_2 \rightarrow CO + 2.5\,NO + 0.5H_2O \qquad \Delta H = -784\,kJ\,mol^{-1} \tag{R18}$$

Reaction R18 indicated oxidation of SOF. The technology of continuous regeneration of monolithic wall-flow filters by NO_2 generated in an upstream oxidation catalyst was developed by Cooper and Thoss,[82] and it has been commercialized as the "Continuously regenerating trap (CRT)" system.[83] The mechanism of PM oxidation with NO_2[84–86] has been illustrated by multiple parallel and sequential (quasi-)elementary steps. Adsorption of NO_2 on carbon followed by surface reactions leads to formation of different surface functional groups (SFG), including so-called SOCs[87] viz. carbonyls, quinines, ethers, phenols, lactones, carboxylic acids, and anhydrides. Zawadzki et al.,[88] Lure and Mikhno[89], Ehrburger et al.,[90] and Muckenhuber et al.[91] postulate the formation of N-containing SFG {C(ONO)}, which they identified by diffuse reflectance infrared Fourier transform spectroscopy and temperature-programmed desorption (TPD) experiments. Muckenhuber et al.[91] also postulated elementary reaction mechanism for CO_2 production:

$$C* + NO_2 \rightarrow C(ONO)\{C* \text{ indicates Solid Carbon}\} \tag{R19}$$

$$C(ONO) \rightarrow C(O) + NO\,\{C(O) \text{ indicates SOCs}\} \tag{R20}$$

$$C(O) + C(ONO) \rightarrow [C(O-ONO)]^{\dagger} \rightarrow CO_2 + NO \tag{R21}$$

$$C(O) \rightarrow C* + CO \tag{R22}$$

NO_2, after adsorption on solid carbon, reacts to form N-containing SFG (reaction R19), which decomposes to NO and O-containing SOC (Reaction R20). N-containing SFG and O-containing SOC associated to form a transition state (†),[89,92, 93] which consequently decomposes to form CO_2. CO may be formed by adsorbed oxygen (O-containing SOC) via reaction R22, although Jeguirim et al.[93] suggest that nearly all the CO and CO_2come via the $[C(O–ONO)]^{\dagger}$ transition state.

Jacquot et al.[92] studied the rate of carbon black oxidation with NO_2 at temperatures 300–450°C and also investigated the effect of oxygen or/and water as co-feed in fixed bed reactor.

A study covering detailed parameters was performed to understand the effect of temperature and concentrations of oxidants. Based on global kinetic law and reactions below (R22–R25), a mono-dimensional model[93,94] (Eqs. (12–14)) was developed to generate intrinsic kinetic parameters of oxidation of carbon with NO_2.

$$C + 2NO_2 \rightarrow CO_2 + 2NO \quad \text{(R22)}$$

$$C + NO_2 \rightarrow CO + NO \quad \text{(R23)}$$

$$C + {}^1\!/_2 O_2 + NO_2(+NO_2) \rightarrow CO_2(+NO_2) + NO \quad \text{(R24)}$$

$$C + {}^1\!/_2 O_2(+NO_2) \rightarrow CO(+NO_2) \quad \text{(R25)}$$

$$\frac{1}{\delta m}\frac{d(\delta m)}{dt} = k_{CO_2} P_{NO_2}^{\alpha} + k_{CO} P_{NO_2}^{\beta} \quad (12)$$

$$\frac{1}{\delta m}\frac{d(\delta m)}{dt} = k_{CO_2} P_{NO_2}^{\alpha} + k_{CO} P_{NO_2}^{\beta} + k_{O_2CO_2} P_{NO_2}^{\delta} x_{O_2}^{\gamma} + k_{O_2CO} P_{NO_2}^{\xi} x_{O_2}^{\gamma} \quad (13)$$

$$\frac{1}{\delta m}\frac{d(\delta m)}{dt} = k_{CO_2} P_{NO_2}^{\alpha}\left(1 + a\, x_{H_2O}^{\varphi}\right) + k_{CO} P_{NO_2}^{\beta}\left(1 + b\, x_{H_2O}^{\mu}\right) + \left(k_{O_2CO_2} P_{NO_2}^{\delta} x_{O_2}^{\gamma} + k_{O_2CO} P_{NO_2}^{\xi} x_{O_2}^{\gamma}\right)\left(1 + c\, x_{H_2O}^{\theta}\right) \quad (14)$$

where k_{CO_2} and k_{CO} are reaction rate constants for reaction R22 and R23; $k_{O_2CO_2}$ and k_{O_2CO} are reaction rate constants for reactions R24 and R25. α and β are reaction orders with respect to NO_2 for reaction R22 and R23. δ and ξ are reaction orders with respect to NO_2 for reaction R24 and R25. γ is the order of reaction with respect to O_2. φ, μ and, θ are reaction orders with respect to water, and *a, b, c* are arbitrary constants. They observed a linear increase in the rate of carbon consumption with a corresponding increase in temperature from 300 to 450°C, NO_2 concentration from 246 to 879 ppm, O_2 concentration from 5 to 20 vol%. They noted that, at this temperature range, no oxidation of carbon occurred with O_2 and H_2O without the presence of NO_2. They observed activation energy of 45.5 kJ/mol with respect to CO_2 formation and 59.4 kJ/mol with respect to CO. The order of reaction α, β, δ, and ξ were found to be close to unity with corresponding values 1.13, 1.05, 1.07, and 1.0, respectively. Such results were also observed by Lure and Mikhno,[89] they found first-order rate dependence on NO_2 (0.38%–4.5%) with no O_2 or H_2O and Arrhenius activation energy of 50 kJ/mol in the temperature range 180–350°C. Based on temperature, pressure, and gas phase concentration measurement data from dynamometer experiments, Kandylas et al.[95] developed a full PM deposition and oxidation model. They reported activation energy of 40 kJ/mol and first-order oxidation rate dependence on NO_2. Along with Jacquot et al.,[92] Ehrburger et al.[90] also pointed out that the rate of carbon gasification by NO_2 is significantly enhanced in the presence of O_2. Jeguirim et al.[96] investigated uncatalyzed oxidation of carbon black Vulcan 6 suitable as a model soot with direct and cooperative oxidation with NO_2 and NO_2 + O_2, respectively, in presence of 5 vol% H_2O. They also used a global kinetic model similar to Eq. (13) to analyze the kinetic parameters. They found a reaction order of 0.6 and activation energy (E_{Dir}) of 26.7 kJ/mol for direct oxidation and reaction of unity and activation energy (E_{Coop}) of 47.8 kJ/mol for cooperative oxidation.

E_{Dir} lower than 50 kJ/mol as reported by Lure and Mikhno[89] indicated the catalytic effect of water on oxidation of soot with NO_2, as also supported by Jacquot et al.[92]

Tighe et al.[97] studied the oxidation of soots from ULSD and B90 (90 vol% biodiesel in ULSD) with only NO_2 (880 ppm in Ar). Assuming two reaction mechanisms: (1) oxidation occurring homogeneously throughout the soot particles and (2) oxidation only on exterior surface of shrinking nonporous PM particles, they deduced two kinetic models. Mechanism 1 was depicted using a pseudo-homogeneous model (Eqs. (15 and 16)) and mechanism 2 was depicted using shrinking core model (Eqs. (16 and 17)). For derivations of these expressions, readers can read the original article.[97]

(1) Pseudo-homogeneous model:

$$\ln(1 - X_C) = -\frac{k_s C_{NO2}^n S_{p,0}}{\rho_M (1 - \varepsilon_{p,0})} t \tag{15}$$

$$\ln(1 - X_C) = -k_V C_{NO2}^n t \quad \text{where,} \quad k_V = -\frac{k_s S_{p,0}}{\rho_M (1 - \varepsilon_{p,0})} \tag{16}$$

(2) Shrinking core model:

$$1 - (1 - X_C)^{1/3} = \frac{2 k_s C_{NO2}^n}{\rho_M d_{p,0}} t \tag{17}$$

$$1 - (1 - X_C)^{1/3} = k_{V,lm} C_{NO2}^n t \quad \text{where,} \quad k_{V,lm} = \frac{2 k_s}{\rho_M d_{p,0}} \tag{18}$$

where X_C is the carbon molar mass conversion, k_s rate constant based on surface area of particles, C_{NO_2} is the concentration of NO_2, $S_{p,0}$ is the reacting surface area per unit volume, ρ_M is the molar density of PM, $\varepsilon_{p,0}$ is the porosity parameter, and $d_{p,0}$ is the distribution probability of particle size. Figure 13a shows a plot of $\ln(1 - X_C)$ against time, which indicated that pseudo-homogeneous model is followed at high temperatures (>400°C) and is linear for a huge range of carbon conversions X_C. At low temperatures (<400°C), the plots are linear only up to $X_C = 0.65$, i.e. particles burn homogeneously up to 65 wt% conversion and then it deviates from the assumed condition of homogeneous burning. However, plots of $\{1\text{-}(1 - X_C)^{1/3}\}$ against time (Figure 13b) show some linearity over the wide range of X_C. However, both the plots were not perfectly linear over the wide range of X_C indicating a change in particle burning process with increased carbon conversion where both mechanisms 1 and 2 may contribute together.[97] In this study, the reaction order was calculated to be unity for both ULSD and B90 soot and the activation energy

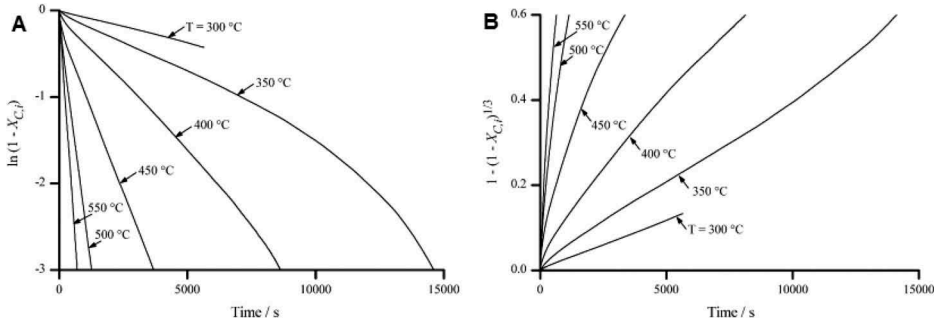

Figure 13. (a) Plot of $\ln(1 - X_{C,i})$ against time for ULSD soot and (b) plot of $\{1-(1 - X_{C,i})^{1/3}\}$ against time for ULSD soot. (There were similar plots for B90) (Reproduced with permission from Ref. [97]).[97]

was found to be 72 ± 18 and 70 ± 18 kJ/mol. Zouaoui et al.[98] investigated the oxidation of carbon black as a model diesel soot under modern diesel engine emission conditions: O_2 (0%–10%), NO_2 (0–400 ppm), H_2O (0%–10%), and 300–600°C in fixed bed reactor. They observed that carbon was mainly oxidized by NO_2 at 300-450°C and by O_2 at 450-600°C and water had a catalytic effect on these reactions. They used global kinetic model (pseudo-homogeneous) similar to as shown in Eqs. (12-14). Kinetic constant for each identified reaction (viz., soot + NO_2, soot + NO_2 + H_2O, soot + O_2, soot + O_2 + H_2O, soot + NO_2 + O_2, and soot + NO_2 + O_2 + H_2O) was evaluated. The activated energies, calculated separately for CO and CO_2 as products, for these reactions as observed by them, are shown in Table 3.

5. Catalysts for the oxidation of diesel particulate

Diesel PM emissions are a serious environmental problem and hence are subjected to strict emission control norms. Therefore, research and development activities are progressively centered on aftertreatment technologies for diesel exhaust emission. This generates uninterrupted motivation to new ideas in the field of diesel particulate filtration and oxidation catalysts. For this, the automobile catalysts at acceptably low cost need to be compact, thermo-chemically stable, capable to work at larger volumetric flow rates (high intrinsic activity) providing high

Table 3. Kinetic parameters for soot oxidation by NO_2 and O_2 (reproduced with permission from Ref. [98]).[98]

Reactions	Reaction order w.r.t. oxidant	A_{CO} Pre-exponential factor (s^{-1})	A_{co_2} Pre-exponential factor (s^{-1})	$E_{A,CO}$ Activation energy (kJ/mol)	E_{A,CO_2} Activation energy (kJ/mol)
Soot + NO_2	1	2.44×10^3	6.22×10^3	66.4	39.1
Soot + O_2	1	3.71×10^7	9.27×10^4	169.2	126.7
Soot + NO_2 + O_2	1	5.04×10^3	1.79×10^4	67.2	69.8

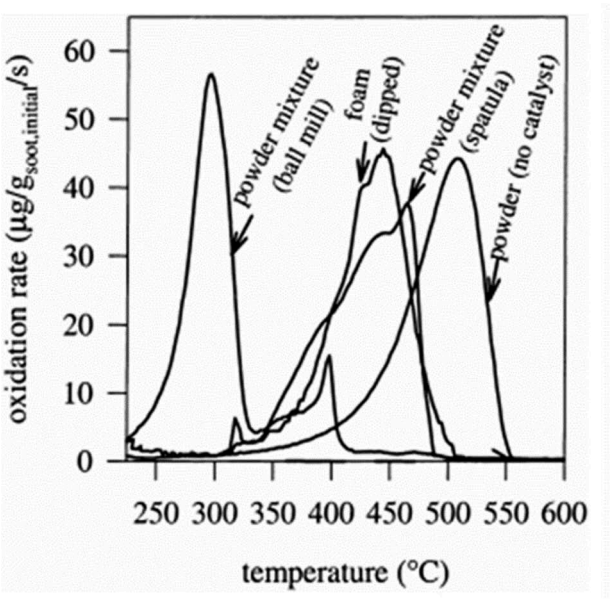

Figure 14. Rate of the catalytic oxidation of synthetic soot as function of temperature (reproduced with permission from Ref. [100]).[100]

filtration efficiency, and low back pressure.[99] The key requirement for PM oxidation is catalyst–PM contact. The loose contact mode, mimicked by mixing of a catalyst with a spatula ($Cs_2SO_4{\cdot}V_2O_5$ powder) and soot, simulates best the contact in DPF environment,[100] whereas tight contact mode (ball milled mixture of soot and $Cs_2SO_4{\cdot}V_2O_5$ powder catalyst) showed higher oxidation reaction rates closer to some fuel borne diesel PM oxidation catalysts (Figure 14).[100,101] Combustion of carbon, although being age-old practice, is still subjected to extensive research to understand the scientific phenomena involved. The theory of oxidation of solid carbon with an oxidation catalyst that is widely accepted is a deep oxidation reaction which occurs at the three-phase boundary (catalyst, solid carbon, and gaseous oxidant) involving heat and mass transfer effects. Here, the gaseous oxidants, like O_2, NO_2, or H_2O, must diffuse to the catalytic surface to form reaction intermediates, which rearrange and desorb to escape into the gas phase (Figure 15).[7]

Most of the diesel engine operations render an exhaust gas temperatures of less than 300°C, which is too low for the un-catalyzed PM oxidation with O_2/air (occurring at 450–600°C) or with NO_2 + O_2/air (300–450°C) as reviewed in the previous section. Catalyzed PM oxidation is expected to decrease the oxidation temperature to a significant level allowing PM oxidation at available exhaust temperatures and thereby increasing efficiency and fuel economy. Here, in the following sections, we will review various noble, non-noble, and perovskite-based catalysts studied and used for diesel particulate (PM) oxidation reactions.

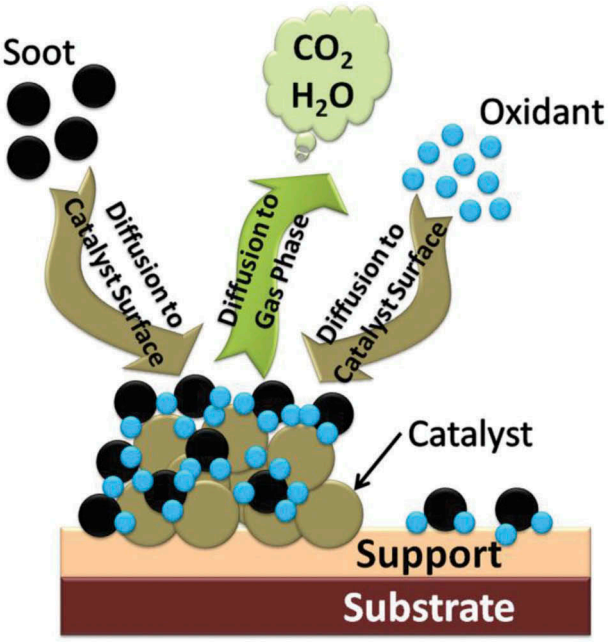

Figure 15. Schematic representation of diesel pm oxidation mechanism.

5.1. *Noble metal-based catalysts*

Pt, supported over metal oxides, is widely and commercially used as soot oxidation catalyst. Noble metals, Pt and Pd supported over high surface area supports, have also been patented as oxidation catalysts owing to their higher specific activity and better resistance to sulfur poisoning.[102,103] Pt is shown to be highly active even in lower loading (<1%).[104] Such a high activity at lower loading in a reaction (soot oxidation), where intimate soot–catalyst contact is required to promote the reaction, has been explained by taking into account the "spill-over effect" which provides the activation mechanism.[105,106] In spill-over mechanism (Figure 16), molecular oxygen is adsorbed on Pt surface followed by dissociation to activated atomic oxygen that is spilled or exchanged with lattice oxygen of support (e.g., γ-alumina[107]) around Pt crystallites.[108]

Neri et al.[104] studied the effect of Pt loading (0.1–5 wt%) on γ-Al_2O_3 in TPO apparatus and the oxidation was carried out in the range 25–900°C in flowing air (50 mL/min). They observed an oxidation temperature to shift from 650°C (with γ-Al_2O_3 as a catalyst) to <500°C (with Pt(5 wt%)/γ-Al_2O_3 as a catalyst). The effect of different supports and reactant gas with PGM was also briefly investigated. Uchisawa et al. further explored the effect of different metal oxides supports incorporated with Pt-particles. They found that despite the better dispersion of Pt-particles on Al_2O_3 and ZrO_2 supports compared to SiO_2 supports, catalytic activity was the exactly reverse. The Pt-particles on SiO_2 showed the significant improvement in catalytic PM

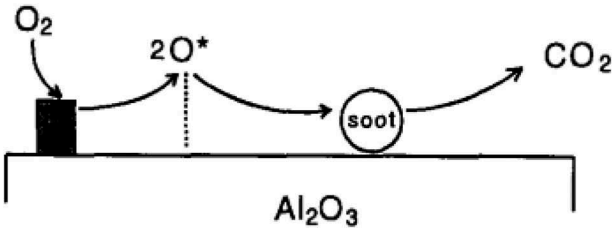

Figure 16. Mechanism of oxygen spillover during soot combustion over Pt/γ–A1$_2$O$_3$ (reproduced with permission from Ref. [104]).[104]

oxidation activity. The dispersion of Pt-particles on different supports does not play any role in gas–solid phase reaction. The Pt/SiO_2 shows the improved catalytic soot oxidation in the flow of NO + O_2 + SO_2 + H_2O and N_2 than other supported Pt-loaded catalysts.[109] Uchisawa et al. further explored the effect on carbon oxidation reaction of different non-basic supports loaded with Pt-particles. Dispersed Pt-particles on different supports (Ta_2O_5, Nb_2O_5, WO_3, SnO_2, SiO_2, TiO_2, Al_2O_3, and ZrO_2) were synthesized by wet impregnation method and evaluated for the catalytic activity for soot oxidation. In the presence of model diesel exhaust, Pt/Ta_2O_5 was the most active against carbon. They assume that the high activity of catalyst was due to the presence of non-basic supports, which do not show any affinity for SO_3 and prevent the poisoning of the catalyst.[110] Pt/MO_x (MO_x = Ta_2O_5, WO_3, Nb_2O_5, SnO_2, SiO_2, CeO_2, MoO_3, V_2O_5) loaded on SiC granular (0.15–0.25 mm) obtained by crushing the commercially available filter (Ibiden Co) were further explored in the presence of model diesel exhaust. Pt/TiO_2/SiC shows the best activity among all the tested catalysts and also stable nature against SO_3 poisoning.[111] Uchisawa et al. also investigated the effect of sulfur content of the exhaust gas for supports on which Pt-particles loaded for catalytic soot oxidation activity. As the sulfur content increased, it shows the positive influence on soot oxidation reaction. They found the promotional effect of 15 ppm SO_2 on catalytic soot oxidation activity; however, the SO_2 concentration less than 1.5 ppm did not show any improvement. The same effect of increased sulfur content was also observed in engine test.[112] Liu et al. synthesized the series of SiO_2-supported V_2O_5 or MoO_3 and Pt-particles which were investigated for the soot oxidation activity. They found that composite of mixed oxides with Pt-particles on SiO_2 performed much better than alone Pt–SiO_2. The synergistic effects of the composite were explained, as Pt converts the NO to NO_2 in the presence of O_2 in the first step and further MoO_3 and V_2O_5 oxidized the carbon in the presence of NO_2.[113] Studies on synergistic effects of Pt–K–Ba on Al_2O_3 support were also reported. It was found that Pt–K/Al_2O_3 was active against soot, however, it shows the poor stability compared to Pt–Ba/Al_2O_3.[114] Castoldi et al. also investigated the effect of Pt–Ba/Al_2O_3 for simultaneous

removal of soot and NO_x and compared with Pt/Al_2O_3. $Pt–Ba/Al_2O_3$ showed the catalytic activity for both soot oxidation and NO_x removal, however, Pt/Al_2O_3 was incapable of the simultaneous removal of soot and NO_x.[115] The effects of alkali and alkaline earth metal (K and Ba) for soot oxidation were briefly explored by Matarrese et al. $Pt–Al_2O_3$, $K–Al_2O_3$, $Pt–K/Al_2O_3$, and $Pt–Ba/Al_2O_3$ were investigated for soot oxidation in loose and full contact conditions. The activity of $Pt–K/Al_2O_3$ was observed best in loose contact condition compared to other tested catalysts. However, the $Ba–Pt/Al_2O_3$ and $K–Pt/Al_2O_3$ showed the same catalytic activity in full contact condition. It is expected that in the case of Ba, inferior activity was observed in loose contact condition. However, in full contact condition, the activity was same as K-containing catalyst. This was expected due to the surface mobility moiety which is responsible for the contact between the soot and catalyst. They also found that in the presence of noble metal, NO promotes the soot oxidation due to the conversion of NO to NO_2 which further oxidizes the soot. The effect of NO also observed in the case of alkali and alkaline earth metals. The NO reacts with Ba and K resulting in the formation of Ba/K nitrate/nitrate complex which further forms the NO_x and oxidizes the soot.[116] Matarrese et al. further investigated the catalyst $Pt–K/Al_2O_3$ for the soot and NO_x storage and reduction at a constant temperature with the lean-rich condition. They found that presence of soot reduced the NO_x storage capacity of LNP catalysts during DPNR operations.[117] Pt–Ba and Pt–K NSR catalysts were also investigated by Pieta et al. for simultaneous soot and NO_x reduction under cyclic lean-rich conditions. The activity of Pt–K was better for soot oxidation than Pt–Ba in the presence of oxygen. However, the presence of NO shows the improvement by shifting the soot oxidation temperature by 50 K to lower temperature range. They also revealed that NO_x storage capacity of catalyst depends on Pt–alkali cooperation. However, both Pt–Ba and Pt–K showed the similar trend for NO_x storage capacity. They also found that the presence of soot hindered the NO_x storage property of catalyst.[118]

The comprehensive study of Ba–K/Pt also leads to the increased interest in the study of other alkali metals. Shuang et al. studied the effect of Mg precursor of $Pt–Mg/Al_2O_3$ catalyst on soot oxidation and utilization of NO_x for oxidation of soot. The $Pt–Mg/Al_2O_3$ catalyst was prepared by impregnation method using $Mg(NO_3)_2$ and $Mg(CH_3COO)_2$ precursors. The effect of Mg precursors on the particle size of Pt-particles was explained. They found that the size of Pt-particles increased as compared to MgO in the case of acetate precursor. The size of Pt-particle was same as in the case of Pt/Al_2O_3 as shown in the schematic (Figure 17). The catalyst synthesized by acetate precursor shows the better catalytic activity than nitrate precursor. They also found that size of Pt-particles does not play any important role in the absence of NO, whereas active site available on the surface of Pt-particles

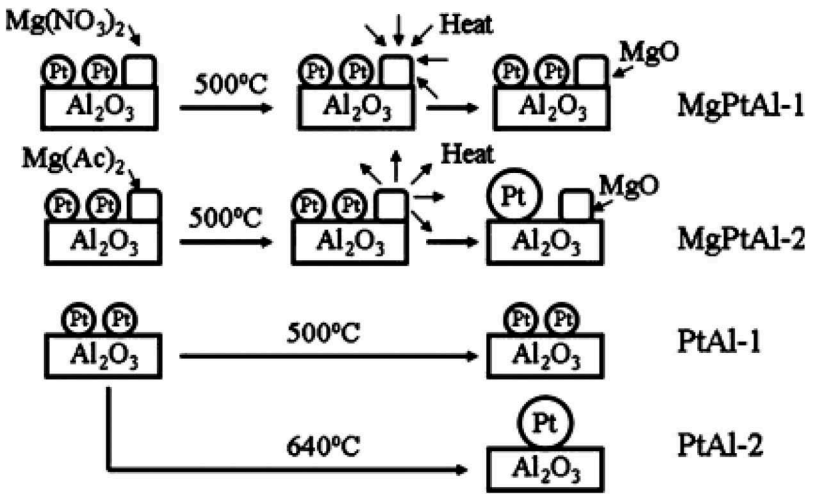

Figure 17. Schematic for growth of Pt-particle on different catalyst during calcination (reproduced with permission from Ref. [119]).[119]

is important for soot oxidation (Figure 17).[119] Engelhard reported Pt-group metals supported on different supports and developed the trap for soot oxidation. The Pt- and Rh-groups were loaded in the different ratios ([Pt: Rh] 1:1–5:1) on alkaline earth metal oxides. The developed catalyzed filter consists of 5–150 g/ft^3 with Rh/Pt 1:5 weight ratio and 30–1500 g ft^{-3} alkali mixed oxide. They reported that Pd could successfully reduce the SO_2, however, Rh improves the soot oxidation temperature.[120] Table 4 shows the brief state of the art for Noble-Metal-based soot oxidation catalysts.

5.2. *Mixed oxide-based catalysts*

Extensive use of PGM in catalytic applications was restricted due to the increasing gap between demand and supply. High cost and limited resources result in the urge for replacing of PGM with the low-cost catalyst options. Extensive research has been going on to replace the PGM, and as a result of this, several mixed oxide-based compositions were investigated for catalytic soot oxidation. Alkali metals, alkaline metals, and transition metals were explored as mixed oxide compositions for catalytic applications and found to show variable catalytic activity toward the reduction of diesel exhaust emissions.

Ahlstrom et al. investigated the synergistic effect of Cu and V by synthesizing V_2O_5–CuO on γ-alumina support. They found that the Cu–V synergistically decreased the soot oxidation temperature. They also investigated the loading effect of Pt-particle on HC and carbon oxidation.[123] Copper is more specifically established as a good oxidizing catalyst for carbon. However, a small concentration of promoter-like potassium significantly improves the catalytic soot oxidation activity. Mixed oxides Cu/K/M/Cl where M is V, Mo, and Nb were briefly

Table 4. Noble-Metal-based catalysts for soot oxidation.

Catalysts	Synthesis method	Experimental conditions	Important findings	Reference
Pt-supported metal oxides (Ta_2O_5, Nb_2O_5, WO_3, SnO_2, SiO_2, TiO_2, Al_2O_3, and ZrO_2)	Incipient-wetness method	TPR Feed: 1000 ppm NO 100 ppm SO_2, 7% H_2O, 10% O_2 in N_2 Flow rate: 0.5 dm^3/min (STP) Heating rate: 10°C/min loose contact	Pt–Ta_2O_5 is the most active catalyst for soot oxidation	[110]
Pt/MO_x/SiC Pt/MO_x (MO_x = TiO_2, ZrO_2, $Al2O_3$, Ta_2O_5, WO_3, Nb_2O_5, SnO_2, SiO_2, CeO_2, MoO_3, V_2O_5)	Incipient-wetness method	TPR Feed: 1000 ppm NO, 100 ppm SO_2, 7% H_2O, and 10% O_2 balanced with N_2 Flow rate: 0.5 dm^3/min (STP) (SV = 48,000/h) Heating rate: 10°C/min; loose contact	Pt–TiO_2/SiC shows the best catalytic activity for soot oxidation	[111]
Pt–MoO_3/SiO_2 Pt–V_2O_5/SiO_2	Impregnating method	TPR Feed: 1000 ppm NO or NO_2 100 ppm SO_2, 10% O_2, 7% H_2O in N_2 (compositions simulating those of diesel exhaust gas) Flow rate: 500 mL/min Heating rate 10°C/min; loose contact	MoO_3–Pt/SiO_2 shows the best catalytic activity with T_i, T_p, T_f at 311, 484, and 528°C, respectively	[113]
MnO_x–CeO_2–Al_2O_3 1% Pt/Al_2O_3 0.5Pt/MnO_x–CeO_2–Al_2O_3	Citric acid-aided sol–gel method Impregnating	TPO Feed: 1000 ppm NO/10% O_2/N_2 or 10% O_2/N_2 Flow rate: 500 mL/min Heating rate 10°C/min; loose contact	0.5 Pt/MnO_x–CeO_2–Al_2O_3 shows the best activity with T_{50} at 442°C	[121]
Pt/Al_2O_3 (PtAl-1) Pt–Mg/Al_2O_3 catalyst MgPtAl-1 (precursor used: $Mg(NO_3)_2$) MgPtAl-2 (precursor used: $2Mg(CH_3COO)_2$)	Impregnating	TPO Feed: 1000 ppm NO/10% O_2/N_2 Flow rate: 500 mL/min Heating rate 10°C/min Loose contact	MgPtAl-2 showing the best activity T_{50} at 415°C	[119]
3DOM $MnxCe_{1-x}O_\delta$ 3DOM $MnxCe_{1-x}O_\delta$ and 3 wt % Pt/$Mn_{0.5}Ce_{0.5}O_\delta$	PMMACCT method	TPO Feed: 10% O_2 and 0.2% NO balanced with Ar Flow rate: 50 mL/min Heating rate: 2°C/min; loose contact	3DOM Pt/$Mn_{0.5}Ce_{0.5}O_\delta$ shows the best catalytic activity with T_{10}, T_{50}, and T_{90} at 290, 343, and 373°C	[122]

CCT: Colloidal crystal template.

investigated for catalytic gasification of carbon. Watabe et al. for the first time synthesized and evaluated Cu/K/M/Cl and found the catalytically active catalyst with improvement in soot oxidation activity.[124] Further Cimbella et al. studied the Cu/K/M/Cl where M is Cr, Mn, V, and Ni. They found that Cu–K–V–Cl showed the improvement in soot oxidation and decreased the activity to 330°C, which decreased the activation energy to 56 from 178 kJ/mol and suggested the involvement of redox mechanism.[125] The effect of potassium on TiO_2-supported Cu catalyst was studied on the series of K–Cu catalyst by Yuan et al.[126] Further, Laversin et al. selected the same Cu–K mixed oxide on ZrO_2 support and revealed that the presence of K on ZrO_2 support helps to convert the monoclinic phase of ZrO_2. Cu promoted by K on ZrO_2 support results in improved soot oxidation activity by improving the contact between the soot and catalyst.[127] The activity of Cl-containing Cu/K/Mo-supported and -unsupported catalysts for soot oxidation activity was investigated. The high activity for ZrO_2-supported Cu/K/Mo/Cl was found, and this is explained by proving the mobility of the catalyst, which increased the contact of soot and catalyst.[128,129] Badani et al. also investigated Cu/K/V/Cl mixed oxides and found that mixed oxides show the improved catalytic activity than binary compounds. They also proved that though catalyst shows the improved activity, stability was very low as it got evaporated at high temperature.[130]

Several reports on cobalt-based mixed oxides for gasification of soot was reported. Querini et al. investigated the 12% Co on MgO support impregnated with 1.5% K as promoter and calcined at different temperature range (300–700°C). They found that the calcination temperature of catalyst shows the direct relation with the catalytic activity. The catalyst calcined at 300 and 400°C shows much better performance compared to the catalyst calcined at a higher temperature. They also proved that the activity is related to cobalt reducibility.[131] Miro et al. also investigated the Co–K composition for catalytic soot oxidation reaction for 12% Co and 4.5% K on different supports like MgO and CeO_2. They found very interesting results, in the case of MgO support Co acts as a source for oxygen availability, however, in the case of CeO_2 support oxygen supplied for the reaction is from the CeO_2 supports. K/CeO_2 and $Co–K/CeO_2$ show the very good catalytic activity below 400°C for soot oxidation as compared to MgO supports. They also found that $Co–K/CeO_2$ shows the simultaneous catalytic activity for the removal of NO and soot. The initial temperature was very low 250°C, and T_{max} was observed at 350°C in TPO curve. This improved catalytic activity was expected due to the formation of NO_2, which is a good oxidizing agent for carbon.[132] Further, the same work was extended by Pisarello et al. by synthesizing Co-, K-, and/or Ba-based catalysts on different supports, which includes MgO, CeO_2, and La_2O_3, and investigated for soot and NO_x removal. They found that K/La_2O_3 and K/CeO_2 showed better soot oxidation activity, however, an addition of Co in K/La_2O_3 and K/CeO_2 shows the good

performance for simultaneous removal of soot and nitric oxide. They also investigated the effect of Ba and found the Ba, K/CeO_2, and Ba/CeO_2 as very effective for trap regeneration by absorbing NO_x.[133] Ba, K, and Co/CeO_2 were further investigated in the presence of simulated diesel exhaust to confirm their activity and thermo-chemical stability. They also investigated the effect of different cobalt precursors on activity and stability. They explained the effect of gas stream of CO_2, H_2O, O_2, and NO on catalysts prepared by using different precursors.[134] Co–B–K on alumina ceramic substrate support was also investigated for soot oxidation. They also found that the presence of KNO_3 is responsible for the lower ignition temperature.[135] Dhakad et al. synthesized mixed oxides of Co_3O_4–CeO_2 by coprecipitation method and evaluated for catalytic soot oxidation reactions. They observed that 20 mole% of Co_3O_4 in CeO_2 shows the improvement in soot oxidation activity due to the enhancement in redox property. However, further increase of ceria percentage results in lower soot oxidation activity due to the formation of isolated ceria phase.[136] Dhakad et al. also investigated the alumina-supported Co–Mo–K-based mixed oxides. They proved the synergistic effect of Mo–Co–K in soot oxidation activity.[137]

Ceria shows the exceptionally good catalytic activity for soot oxidation. Several studies were reported to investigate the role of ceria in soot oxidation reaction. The catalytic activity for soot oxidation in the presence of NO_x/O_2 of ceria was compared with different supports like TiO_2 and ZrO_2. It was observed that TiO_2 and ZrO_2 were inactive, however, CeO_2 supports show the catalytic activity for soot oxidation due to the redox property of ceria. Ceria shows the better oxidation capacity in the presence of NO. As NO undergoes the oxidation reaction and converted to NO_2, however, further part of NO_2 was utilized for soot oxidation reaction, whereas some parts of NO_2 was stored on ceria.[138] Ceria was also found to be very efficient for soot oxidation activity due to oxygen buffering capacity. Several dedicated studies for the role of ceria in soot oxidation mention the oxygen involved in soot oxidation reaction is not in molecular form. They also investigated the mechanism involved in soot oxidation. The calcination temperature of the catalyst plays the crucial role in soot oxidation reaction. The ceria calcined at higher temperature shows the much better efficiency for soot oxidation reaction. They found that higher calcination temperature helps to generate the superoxide and peroxide species which actually take part in soot oxidation reaction. Peroxide ion on reaction with soot results in the formation of oxygen vacancy, which enhances the surface diffusion. However, molecular oxygen enters into the crystalline structure of catalyst and results into oxygen vacancy, which is also needed for the complete oxidation of soot.[139,140]

Metal oxides supported on ceria were also studied to investigate the effects on soot oxidation. Muroyama et al. synthesized the CeO_2 and MO_x–CeO_2 mixed oxides by coprecipitation and citric acid complex methods. Addition

of transition metal oxide improved the contact between catalyst and soot by increasing the reducing property, which decreased the soot oxidation temperature. Copper-based mixed oxides show the better catalytic soot oxidation activity compared to other transition metal mixed oxides.[141] Fu et al. mentioned the effect of preparation method on the catalytic activity of catalyst. $Cu_{0.005}Ce_{0.95}$ mixed oxide catalysts were prepared by coprecipitation and citric acid methods. The difference in physicochemical properties influenced the catalytic activity. The Cu–Ce mixed oxides prepared by citric acid method shows the improvement in catalytic activity due to the presence of $Cu_{0.005}{}^{+2}Ce_{0.95}{}^{+4}$which improves the redox property and oxygen storage capacity.[142] Potassium-promoted CuO–CeO was investigated for NO_x-assisted soot oxidation reaction.[143] Contact between the soot and catalyst is very important parameter, which is essential to improve the soot oxidation activity. $CuO–CeO_2$ was synthesized by colloidal crystal template method to obtain the three-dimensional macroporous structured catalyst. It is anticipated that three-dimensionally ordered macroporous (3DOM) structure increased the redox property and surface area which improves the soot oxidation activity by improving the contact between catalyst and soot. The $CuO–CeO_2$ proven stable as it doesn't collapse even after cyclic performance and activity remains constant.[144] Doping of alumina in the ceria lattice results in increasing the interaction of Al–Ce, improves the thermal stability, and increases the catalytic soot oxidation activity.[145] Wu et al. shows the improvement of soot oxidation activity by impregnating the $MnO_x–CeO_2$-on Al_2O_3 support. They inferred that insertion of Al_2O_3 in $MnO_x–CeO_2$ improves the textural stability and increased the MnO_x dispersion, which further enhanced the catalytic activity by synergistic effect.[146] Same catalysts were further investigated by Lin et al. $MnO_x–CeO_2–Al_2O_3$ oxides were prepared by sol–gel method and studied for the thermal stability by aging the catalyst at 800°C for 20 h. The catalyst shows the stability after aging and very small shifting of soot oxidation temperature to higher side was reported (17°C for T_{max}) while the catalyst was found to be very stable.[147]

Further several studies on mixed oxides of ceria were reported for enhanced catalytic activity as compared to only ceria catalyst. Ceria doped with variable concentrations of zirconia was synthesized and investigated for soot oxidation activity. Addition of zirconia shows the improvement in soot oxidation activity. Zirconia doping in cerium mixed oxide increased the oxygen storage capacity and made easy availability of oxygen which was further assisted with NO_x to improve the soot oxidation.[148–150] Synthesis method and morphology also affect the catalytic activity of soot oxidation for Ce–Zr mixed oxide.[150–152] Several other investigations on different metal loadings on ceria–zirconia mixed oxide were reported. Effect of Yttrium loading on physicochemical properties and catalytic activity of ceria and ceria–zirconia mixed oxide has been studied. It was observed that Y^{3+}

increased the oxygen vacancy on the surface and influenced the catalytic soot oxidation activity.[153] Weng et al. further modified the ceria–zirconia catalyst by impregnating the potassium. The potassium impregnation increased the NO_x absorption and oxygen storage capacity, which helps in the improvement of soot oxidation activity.[154]

Recently, our group studied Sr-based mixed oxides and evaluated these catalysts for the soot oxidation in the presence of air. The $SrCrO_4$ mixed oxides were synthesized by solution combustion method and Pt- (5 wt% loading) impregnated on $SrCrO_4$ by weight impregnation method. $SrCrO_4$ and Pt–$SrCrO_4$ were evaluated for soot oxidation and found that Pt-loading shows the almost same catalytic soot oxidation activity as bare $SrCrO_4$ mixed oxide. The $SrCrO_4$ was also tested for long-term performance and stability toward the SO_2, -moisture and real soot environment. The $SrCrO_4$ shows the virtually same catalytic activity and structure as the fresh catalyst.[155] Table 5 shows the brief state of the art for mixed oxide-based catalysts for soot oxidation.

5.3. *Perovskite-based catalysts*

Perovskites are the popular and most studied class of catalysts for different catalytic reactions. The first time, in the early 1970s, perovskites were studied for automobile application as an oxidation catalyst and NO reduction. Extraordinary properties of perovskites like high thermal stability and room for tuning the catalytic properties made the perovskites serious alternative to PGM catalysts.[160–162]

In the case of ABO_3, compositions A and B are cations, and O is an anion. A is the bigger cation (r_a ~0.90 A°), which mostly covers lanthanides (Ln series), alkali and alkaline earth metal (Ca, Ba, Na, K, Sr, etc.), whereas B is the smaller cation (r_b ~0.51 A°), which covers most of the metallic elements of the periodic table, i.e. 3*d*, 4*d*, and 5*d*. In the simple cubic system, A-ion can form the 12 coordinate bonds placed at the center of the cube, and B-ion can form 6 coordinate bonds placed at the corners of the cube. O-ion is placed at the center of the faces which can make the perovskite structure counterbalanced by its charge. A_2BO_4 can also be represented by ABO_3. AO where both layers are placed one above the other and form the ordered structure is also called as layered perovskite or perovskite-type mixed oxide. Figure 18 shows the basic structure for ABO_3 and A_2BO_4. However, all the perovskites should be in the range of $0.75 < t > 1$, where t is the tolerance factor with the formula $t = r_a + r_o/\{\prod 2\ (r_b + r_o)\}$.[163,164] High structure stability permits both A- and B-site substitution by a wide range of elements with variable radius and valency. However, the degree of substitution must be a range that it should not result in a destruction of a perovskite structure. General representation for both site substitution is $AA'BB'O_{3-\delta}$. Substitution plays a crucial role to enhance the catalytic activity. Although A-site substitution is not directly related to the catalytic activity, it is evidenced for improving the structural stability. However,

Table 5. Mixed oxide-based catalysts for diesel soot oxidation.

Catalyst compositions	Synthesis method	Experimental conditions	Important findings	Reference
Cu–K–V–Cl $CsVO_3$ + KCl KVO3 + KCl KVO_3 + KCl + K_2SO_4	Impregnation of the alumina support	TPO Feed: 12% O_2 balanced with He Flow rate: 4 cm^3/min Heating rate 10°C/min Tight contact	KVO_3 + KCl + K_2SO_4 is the best catalyst. Shows the T_i and T_{max} at 390 and 472°C	[130]
Mesoporous beta (MBeta) Hierarchically porous beta (HBeta) Cu–HBeta, Mn–HBeta, and CuMn–HBeta Al-MCM-41	Hydrothermal system	TPR Feed: 500 ppm NO, 10% O_2 and balance N_2 Flow rate: 200 mL/min Heating rate 10°C/min Loose contact	CuMn–HBeta shows the best catalytic soot oxidation activity with T_{10}, T_{50}, and T_{90} at 180, 260, and 300°C, respectively	[156]
$Ce_{0.9}Zr_{0.1}O_2$–NP $Ce_{0.8}Zr_{0.2}O_2$–NP $Ce_{0.7}Zr_{0.3}O_2$–NP 50-$Ce_{0.9}Zr_{0.1}O_2$–NP/FAU $Ce_{0.9}Zr_{0.1}O_2$–M $Ce_{0.9}Zr_{0.1}O_2$–SCS	Hydrothermal procedure	TG Feed: 10% O_2 in N_2 Flow rate: 100 cm^3/min Heating rate 5 °C/min Loose contact	$Ce_{0.9}Zr_{0.1}O_2$–NP shows the best catalytic activity with T_{10}, T_{50}, and T_{90} at 427, 491, and 540°C, respectively	[152]
Ag/ZrO_2 catalysts containing 0.5–20 wt% Ag	Incipient wetness method	TPO Feed: 10% O_2 and 10% H_2O with N_2 as a balance gas Flow rate: 300 mL/min Heating rate 10 K/min Loose contact	5 wt% Ag loading showing the best activity T_{50} at 583 K	[157]
CeO_2-CP1-F CeO_2-CP2-F CeO_2-CP3-F CeO_2-CP4-F	Modified co-precipitation method	TGA Feed: 5% O_2 or 500 ppm NO/5% O_2 balanced with Ar Flow rate: 200 mL/min Heating rate 10°C/min Loose contact	CeO_2-CP4-A showing the best activity with T_p at 445°C in presence of 500 ppm NO/5% O_2 balanced with Ar	[158]
CeO_2-SCS CeO_2-NP $Ce_{0.9}Pr_{0.1}O_2$-SCS $Ce_{0.9}Pr_{0.1}O_2$-NP $Ce_{0.9}Zr_{0.1}O_2$-SCS $Ce_{0.9}Zr_{0.1}O_2$-NP $Ce_{0.8}Zr_{0.1}Pr_{0.1}O_2$-SCS $Ce_{0.8}Zr_{0.1}Pr_{0.1}O_2$-NP	Hydrothermal synthesis	TGA Feed: 10 vol% O_2 in N_2 Flow rate: 100 mL/min. Heating rate 5°C/min Tight contact	$Ce_{0.8}Zr_{0.1}Pr_{0.1}O_2$-NP shows the best catalytic activity with T_{10}, T_{50}, and T_{90} at 382, 419, and 453°C, respectively	[159]

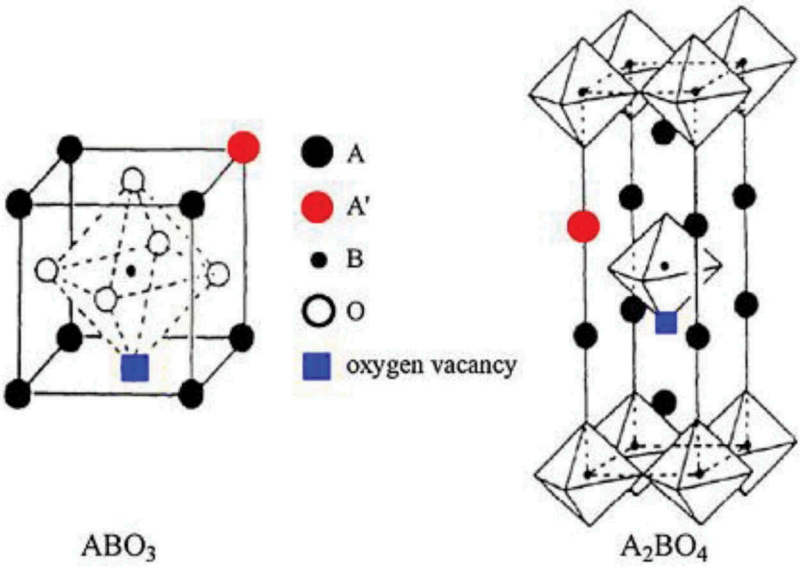

Figure 18. Ideal models of perovskite-type oxides with ABO_3 and A_2BO_4 structures. The red circle represents foreign element substituted an A-site cation; oxygen vacancy is represented by the blue square. Note: In the case of A_2BO_4, structure oxygen symbol was not mentioned for simplification (reproduced with permission from Ref. [163]).[163]

B-site substitution usually increases the oxidation rate. Substitution at lower valance A-site creates the structural defects and increased anionic and cationic vacancies, which indirectly increases the oxidation state of B-site to make electroneutral compound. This increased B-site vacancy results in the enhancement of redox property, which increases the rate of oxidation reaction by increasing the available oxygen. Increased oxygen quantity makes the more and more lattice oxygen available, which favors the low-temperature oxidation reaction and enhances the catalytic oxidation reaction.[163,165–167] Factors like ionic conductivity, lattice oxygen mobility, and oxygen sorption and desorption behavior of perovskites are the key parameters for perovskites to enhance the catalytic oxidation reactions. High temperature allows the release of oxygen from perovskite structure. Depending on temperatures, perovskites release two different kinds of oxygen (1) α-oxygen (2) β-oxygen. At low temperature, superficial weakly chemisorbed oxygen is released. Bonding of α-oxygen is very weak with the perovskite structure and usually can desorb in the temperature range of 300–600°C. However, at high-temperature, interfacial oxygen is released. β-Oxygen is strongly bonded with a perovskite structure, representing the bulk properties of such catalysts. It is usually released above 600°C.[167,168]

Solid state synthesis method was the earliest method used to achieve the perovskite phase. However, high temperature and long duration of calcination results in sintered material with low surface area and therefore reduced catalytic activity.[169] Several different methods were used like coprecipitation method,[170,171] citrate sol–

gel method,[172,173] combustion synthesis method,[174,175] reactive grinding method,[176] incipient wetness method, impregnation method, etc. to overcome the limitations of solid state synthesis. Recently, more efficient synthesis methods like microwave synthesis,[177] hydrothermal synthesis method[178] and solvothermal synthesis method,[178,179] hard templating method,[180] and colloidal templating methods[181] are used to achieve the improvement in surface area and also successfully synthesizing perovskites in nanoforms.

Improved perovskite synthesis techniques improve the surface area along with other physio-chemical properties. Easy synthesis also attracts to scale up catalyst preparations for the industrial scale. The ease of tuning the catalytic property by substituting A- and B-sites and promoting with a very small amount of PGM can increase the catalytic activity of perovskites substantially. Since last three decades, many such perovskite compositions have been investigated for soot oxidation reaction.

5.3.1. *Lanthanum-based perovskite catalysts*

Lanthanum-based perovskites are the most studied perovskite catalysts for several catalytic applications. Several $LaBO_3$ (B = transition metal) pure and A- and B-site-substituted perovskites have been reported for soot oxidation reaction. These catalytic reactions described in the literature were carried out in different experimental environments. Literature revealed that soot oxidation reactions are favorable in the presence of NO with O_2 compared to O_2/air alone.

5.3.1.1. *Lanthanum chromate.* Fino et al. extensively studied the lanthanum-based perovskites. They synthesized high surface area $LaBO_3$ (B = Mn, Fe, Cr) by combustion synthesis method. They also studied series of A- and B-site-substituted perovskites ($LaMn_{1-x}O_3$, $La_{1-x}A_xMnO_3$, $LaMn_{1-x}B_xO_3$, $LaCr_{1-x}O_3$, $LaCr_{1-x}B_xO_3$, and $LaFe_{1-x}O_3$ [with different x values; B = Mg, V, Cr, Mn, Fe; A = K, Rb, Ca, Sr]). Chromate-based perovskites were found to be the best for soot oxidation. The order of soot oxidation activity was found to be $LaMnO_3 < LaFeO_3 < LaCr_{0.9}O_3$ with the maximum soot oxidation temperature at 480°C.[182] Irfan et al. also revealed the La–Cr–O perovskites for catalytic combustion of soot.[183] Further, Fino et al. studied the A-site substitution effect by substitution with K. $La_{0.9}K_{0.1}Cr_{0.9}O_{3-\delta}$ improved the soot oxidation temperature. A-site substitution increases the availability of superficial α-oxygen and improves the soot oxidation temperature further.[174] The best performing catalyst $La_{0.9}K_{0.1}Cr_{0.9}O_{3-\delta}$ is further loaded with 1% Pt, which shows the significantly enhanced soot combustion activity. About 1% Pt loaded on $La_{0.9}K_{0.1}Cr_{0.9}O_{3-\delta}$ was selected for particulate trap coating, and engine test was performed with good catalytic activity.[184] Russo et al. also studied the alkali metal (Li, Na, Rb, K) substituted lanthanum chromate and successfully synthesized by using combustion synthesis method. They found that the Li substitution at A-site increased the availability of α-oxygen and lowered the soot combustion temperature to 408°C.[185] Alkali-substituted lanthanum chromate

Table 6. Lanthanum chromate-based catalysts for soot oxidation.

Catalysts	Synthesis method	Experimental conditions	Important finding	Reference
$LaMn_{1-x}O_3$, $La_{1-x}A_xMnO_3$, $LaMn_{1-x}B_xO_3$, $LaCr_{1-x}O_3$, $LaCr_{1-x}B_xO_3$, and $LaFe_{1-x}O_3$ with different x values B = Mg, V, Cr, Mn, Fe A = K, Rb, Ca, Sr	Combustion synthesis	TPO Feed: air Flow rate: 500 mL/min Heating rate 5°C/min Tight contact	$LaCr_{0.9}O_3$ is the best catalyst with T_m at 480°C	[182]
$LaMnO_3$, $LaFeO_3$, $LaCrO_3$, $LaCr_{0.9}O_{3-\delta}$, $La_{0.9}K_{0.1}Cr_{0.9}O_{3-\delta}$	Combustion synthesis	TPO Feed: air Flow rate: 100 mL/min Heating rate: 5°C/min Tight contact	$La_{0.9}K_{0.1}Cr_{0.9}O_{3-\delta}$ is the best catalyst with T_m at 455°C	[174]
$La_{0.9}CrO_3$, $La_{0.8}CrO_3$, $La_{0.9}Na_{0.1}CrO_3$, $La_{0.9}K_{0.1}CrO3$, $La_{0.9}Rb_{0.1}CrO_3$, $La_{0.8}Cr_{0.9}Li_{0.1}O_3$	Combustion synthesis	TPO Feed: air and 1000 ppmv NO Flow rate: 100 mL/min Heating rate: 5°C/min Tight contact	$La_{0.8}Cr_{0.9}Li_{0.1}O_3$ best catalyst shows the activity T_m at 408°C.	[185]
$LaCrO_3$ $La_{0.8}Li_{0.1}Cr_{0.9}O_3$, $La_{0.8}Li_{0.2}Cr_{0.8}O_3$ $La_{0.8}Li_{0.3}Cr0.7O_3$	Combustion synthesis	TPO Feed: Air and 1000 ppmv NO Flow rate: 100 mL/min Heating rate: 5°C/min Tight contact	$La_{0.8}Li_{0.2}Cr_{0.8}O_3$ shows the T_i below 350°C	[187]

further tested for potential stability in the presence of SO_2 and moisture at 400 and 600°C for several hours. Li-substituted lanthanum chromate was observed to show the exceptionally high stability even after several aging treatments and showed almost the same catalytic activity as the fresh sample.[186] Fino et al. further improved the catalytic activity of Li-substituted lanthanum chromate by varying the amount of Li from 0.1 to 0.3 in molar ratio. They found that 0.2 mole of Li shows the soot oxidation activity well below the 300°C. Best performing catalyst, $La_{0.8}Li_{0.2}Cr_{0.8}O_3$, was selected for the engine performance test by coating on a particulate trap.[187] $La_{0.8}Li_{0.2}Cr_{0.8}O_3$ perovskite was synthesized by high-throughput procedure and tested for soot oxidation activity.[188] Table 6 shows the lanthanum chromate catalysts for soot oxidation.

5.3.1.2. *Lanthanum magnetite.* $LaBO_3$ (B = Mn, Fe, Cr) type catalysts were synthesized and evaluated for catalytic soot oxidation. The activity of the perovskites was found to be exactly reverse for methane oxidation. $LaMnO_3$ has been showed less activity for soot oxidation.[182,174] Several attempts were made to improve the catalytic soot oxidation activity for lanthanum magnetite. A structural modification like the synthesis of fibrous $LaMnO_3$ showed the significantly improved soot trapping capacity and soot combustion activity.[189] Wang et al. improved the catalytic soot oxidation through A-site substitution by alkali metal (Li, K, Na, Rb). K-substituted lanthanum magnetite found to be very active for soot oxidation. Further, they also varied the amount of K to check the best catalytic activity at a particular concentration of K-substitution.[190,191] Li et al.

also reported the improvement in catalytic activity by K-substitution at A-site. They also coated the K-substituted perovskites on honeycomb by sol–gel-assisted dip coating method.[192] As mentioned before, the contact of soot and catalyst plays a critical role. That was further proved by synthesizing high surface area $La_{0.8}K_{0.2}MnO_3$ perovskites through the malic acid-aided process. Same synthesis protocol was applied to develop $La_{0.8}K_{0.2}MnO_3$-coated ceramic foam filters for practical application.[193] Further state of art K-substituted lanthanum magnetite was substituted with Cu ($La_{0.8}K_{0.2}Cu_{0.05}Mn_{0.95}O_3$) and studied for simultaneous removal of NO_x and oxidation of soot.[194] Fujimoto et al. improved the soot oxidation activity by substituting the lanthanum magnetite with Sr at A-site.[195] Silver-substituted perovskite catalysts with composition $(La_{1-x}Ag_x)Mn_{0.9}Co_{0.1}O_3$ were prepared which disclosed the role of silver in improvement of soot oxidation activity.[196] B-site-substituted perovskites like Ni-doped $LaMnO_3$ were reported for soot combustion.[197] Zhang et al. further synthesized the 3DOM $LaMn_{1-x}Fe_xO_3$ ($x = 0, 0.05, 0.1, 0.15$) with different pore sizes. The structural changes affect the catalytic soot oxidation activity. They found that the increased pore volume shows the enhanced soot oxidation activity.[198] Table 7 shows the brief state of the art for lanthanum magnetite type catalysts reported for soot oxidation reaction.

5.3.1.3 ***Lanthanum cobaltite.*** Teraoka et al. studied the $LaBO_3$ (B = Co, Mn, Fe) for simultaneous removal of NO_x and soot. Although substitution of A- and B-sites was responsible for enhancing catalytic activity, they found that A-site-substituted with alkali metal-based catalysts show improved catalytic activity than the other. In particular, K substituted at A-site of lanthanum cobaltite perovskites was more active for catalytic soot and NO_x removal as compared to other substitutions.[199] For improvement of catalytic activity through K-substitution of $LaCoO_3$, several studies have been reported. The structural modification also shows the improved soot oxidation activity. $La_{0.9}K_{0.1}CoO_3$ fibers were synthesized with 7.1 m^2/g, BET surface area with average diameter 600 nm which shows improvement in soot oxidation activity.[200] 3DOM $La_{1-x}K_xCoO_3$ ($x = 0–0.3$) was synthesized consisting pore sizes 240–260 nm with wall thickness of 35–45 nm. K-substituted catalyst with 3DOM shows the superior performance than nanocatalyst for soot oxidation compared to Pt catalyst.[201] Further doping of Si in the K-substituted catalyst (5.89 wt% Si–$La_{0.8}K_{0.2}CoO_3$) accelerates the soot oxidation activity by forming well-ordered structure and increased surface oxygen availability.[202] Ceria-supported K-substituted catalyst ($[La_{0.9}K_{0.1}CoO_3]_x$/nmCeO_2) shows further improvement in soot oxidation temperature.[203] Table 8 represents the activity of K-substituted and Fe-substituted catalyst for simultaneous removal of soot and NO_x. They support the state of the art of K-substituted catalysts by comparing the activity with B-site-substituted compositions with Fe. They found and proved that the increased K-substitution shows the increment in catalytic activity, whereas Fe-substitution shows the reverse trend.[204]

Table 7. Lanthanum magnetite-based catalysts for soot oxidation.

Catalysts	Synthesis method	Experimental conditions	Important findings	Reference
$La_{1-x}M_xMnO_3$ (M = Li, Na, K, Rb, x = 0, 0.10, 0.25)	Citric acid-ligated method	TPR Feed: 5% O_2 and 2000 ppm NO Loose contact	$La_{0.75}K_{0.25}MnO_3$ best catalyst shows the soot oxidation activity T_i and T_m at 285 and 348°C	[190]
$La_{1-x}K_xMnO_3$, $LaMnO_3$, $La_{0.95}K_{0.05}MnO_3$, $La_{0.90}K_{0.10}MnO_3$, $La_{0.85}K_{0.15}MnO_3$, $La_{0.80}K_{0.20}MnO_3$, $La_{0.75}K_{0.25}MnO_3$, $La_{0.70}K_{0.30}MnO_3$, $La_{0.65}K_{0.35}MnO_3$	Citric acid-ligated method	TPR Feed: 5% O_2 and 2000 ppm NO Loose contact	$La_{0.75}K_{0.25}MnO_3$ best catalyst shows the soot oxidation activity T_i and T_m at 285 and 348°C	[191]
$LaMnO_3$, $La_{0.8}K_{0.2}MnO_3$, $La_{0.8}K_{0.2}Co_{0.5}Mn_{0.5}O_3$	Citrate–gel process DOC Coating: sol–gel assisted dip-coating	TG Feed: air Flow rate: 50 mL/min Heating rate: 5°C/min Tight contact	$La_{0.8}K_{0.2}MnO_3$ shows the best catalytic activity with T_{50} at 414°C	[190]
$La_{0.8}K_{0.2}MnO_3$	Malic acid-aided process ceramic foam filters (CFF; 38 mm diameter, 50 mm length) Dip coating method Loading: 5 wt%	TG Feed: 21% O_2 and 79% N_2 Flow rate: 100 mL/min Heating rate: 10°C/min Tight loose contact	$La_{0.8}K_{0.2}MnO_3$ calcined at 550°C shows the T_{max} at 384°C	[193]
$(La_{1-x}Ag_x)Mn_{0.9}Co_{0.1}O_3$ (x = 0.0, 0.1, 0.2, 0.3)	Citrate method	TG Feed: 12%O_2/He Flow rate: 180 mL/min Heating rate: 10°C/min Tight contact	$La_{0.7}Ag_{0.3}Mn_{0.9}Co_{0.1}O_3$ is the best catalyst shows the T_m at 371°C	[196]
$LaMnO_3$ $LaMn_{0.7}Ni_{0.3}O_3$	Citric acid sol–gel method	TG Feed: 1000 ppm NO/10% O_2/N_2 or 10% O_2/N_2 Flow rate: 500 mL/min Heating rate: 20°C/min Tight/loose contact	$LaMn_{0.7}Ni_{0.3}O_3$ shows the best activity T_m at 372°C	[197]
3DOM$LaMn_{1-x}Fe_xO_3$,$LaMn_{0.95}Fe_{0.05}O_3$ $LaMn_{0.90}Fe_{0.10}O_3$,$LaMn_{0.85}Fe_{0.15}O_3$	Colloidal crystal template method	TPO Feed: 5% O_2 and 0.2% NO balanced with Ar Flow rate: 50 mL/min Heating rate: 2°C/min Loose contact	$LaMn_{0.85}Fe_{0.15}O_3$ (pore diameter 599) shows the T_m at 392°C	[198]

Table 8. Catalytic activity reported for simultaneous removal of NO_x and soot by perovskite type catalysts (reproduced with permission from Ref. [204]).[204]

Sample	T_{ig} (°C)	T_m (°C)	X_{NO}	S_{CO_2}
$LaCoO_3$	316	406	31.7	90.1
$La_{0.9}K_{0.1}CoO_3$	304	401	35.1	93.3
$La_{0.8}K_{0.2}CoO_3$	292	397	38.9	95.7
$La_{0.7}K_{0.3}CoO_3$	286	389	41	94.4
$La_{0.6}K_{0.4}CoO_3$	283	382	41.6	96.2
$La_{0.5}K_{0.5}CoO_3$	288	391	40.2	94.6
$LaCo_{0.9}Fe_{0.1}O_3$	309	409	32.8	93.7
$LaCo_{0.8}Fe_{0.2}O_3$	315	405	33.5	94.2
$LaCo_{0.7}Fe_{0.3}O_3$	323	417	33.1	94.6
$LaCo_{0.6}Fe_{0.4}O_3$	320	412	32.4	95.9
$LaCo_{0.5}Fe_{0.5}O_3$	317	416	32.5	95.1
Co_3O_4	308	414	31.6	92.7
No catalyst	408	565	10.9	80.8

As K-substituted $LaCoO_3$ showed better performance; still, several modifications were made to enhance the catalytic activity. K-substitute $LaCoO_3$ at A-site was further modified to improve the catalytic activity by substituting B-site with Fe, Ni, Cu, and Pd. Structural modifications and B-site substitution with different elements and concentration can together result in synergistic effects and help in enhancing catalytic soot oxidation activity.[205–206,207] Further, Russo et al. also studied the effect of different alkali metal substitution in $LaCoO_3$ along with most studied K-substitution for catalytic soot oxidation reaction. They synthesized alkali metal like K-, Na-, and Rb- substituted at A-site of $LaCoO_3$ perovskites. They found that Rb-substituted perovskites showed good catalytic soot oxidation activity even in the absence of NO. All the soot oxidation experiments were performed in the presence of air, while they also found that catalysts were showing high ad unaltered activity even after several aging processes. They assume that this may be due to the conversion of $La_{0.9}Rb_{0.1}CoO_3$ to $La_{0.9}Rb_{0.1}CoO_{2.5}$ during catalytic soot oxidation reaction.[208] Hong et al. disclosed the activity of $LaCoO_3$ and substitution at A-site by Cs, Sr, and Ba for simultaneous removal of NO_x and soot. They found that A-site substitution by Cs showed decent improvement in soot oxidation and NO reduction temperature compared to other, by creating oxygen defects.[210] Zhang et al. compared A-site substitution with Sr and Cs lanthanum cobalted and found that Sr-substituted perovskites showed better catalytic soot oxidation activity. Order of activity was found as follows: $La_{0.8}Ce_{0.2}CoO_3 > La_{0.9}Ce_{0.1}CoO_3 > La_{0.9}Sr_{0.1}CoO_3 > La_{0.8}Sr_{0.2}CoO_3 \approx LaCoO_3$. They also revealed the role of surface oxygen of perovskite in soot oxidation activity.[211] However, the activity of a catalyst was not as good as K-substituted perovskites. Table 9 shows the brief state of art for lanthanum cobaltite based catalysts.

Table 9. Lanthanum cobaltite-based catalysts for soot oxidation.

Catalysts	Synthesis method	Experimental conditions	Important findings	Reference
$La_{0.9}K_{0.1}CoO_3$ fibers	Sol–gel process combined with electrospinning procedure	TG Feed: air Flow rate: 100 mL/min Heating rate: 10°C/min Loose contact	T_{50} for fibers decreased from 583 to 432°C compared to non-catalyzed carbon	[200]
(3DOM) $La_{1-x}K_xCoO_3$ (x = 0–0.3)	CMCCT	TPO Feed: 5% O_2 and 0.2% NO balanced with Ar Flow rate: 50 mL/min Heating rate: 2°C/min Loose contact	$La_{0.9}K_{0.1}CoO_3$ is the best catalyst shows the T_{50} at 378°C	[201]
(3DOM) silicon-doped $La_{0.8}K_{0.2}CoO_3$		TPO Feed: 500 ppm NO, 5 vol% O_2, and the balanced N_2 Flow rate: 50 mL/min Heating rate: 2°C/min Loose contact	(3DOM) silicon-doped $La_{0.8}K_{0.2}CoO_3$ shows the soot oxidation activity T_{10}, T_{50}, T_{90} at 332, 396, 454°C and S^m_{CO2} at 98.3%	[202]
$(La_{0.9}K_{0.1}CoO_3)_x/nmCeO_2$ (x = 1, 4, 10, 20, 50, 100)	Autocombustion method assisted by rotating evaporation	TPO 5% O_2 and 0.2% NO balanced with He Flow rate: 50 mL/min Heating rate: 2°C/min Loose contact	$(La_{0.9}K_{0.1}CoO_3)_{20}/nmCeO_2$ catalyst is the best catalyst shows the T_m at 354°C	[203]
$La_{1-x}K_xCoO_3$, $LaCo_{1y}Fe_yO_3$ (x = 0.1–0.5)	Citric acid method	TPO Feed: 800 ppm NO, 10 vol% of O_2 was employed with He Flow rate: 200 mL/min Heating rate: 2°C/min Loose contact	$La_{0.6}K_{0.4}CoO_3$ shows the best catalyst shows the T_i and T_m at 283 and 382°C	[204]

(*Continued*)

Table 9. (Continued).

Catalysts	Synthesis method	Experimental conditions	Important findings	Reference
$La_{1-x}K_xCo_{1-y}Fe_yO_3$ (x = 0, 0.1, y = 0, 0.1)	Combined method of organic ligation and solution combustion	TPO Feed: 800 ppm NO, 10 vol% of O_2 was employed with He Flow rate: 200 mL/min Heating rate: 2°C/min Contact: mixed with a spatula, and then this mixture were soaked in 3 mL ethanol and ultra-sonicated	$La_{0.9}K_{0.1}Co_{0.9}Fe_{0.1}O_3$ shows the best catalytic soot oxidation activity with T_{10}, T_{50}, T_{90} at 295, 343, 396°C	[205]
$La_{1-x}K_xCo_{1-y}Cu_yO_{3-\delta}$ (x = 0, 0.1; y = 0, 0.05, 0.1, 0.2, 0.3)	Citric acid complexation method	TG/DTA Feed: 500 ppm NO, 10 vol% O_2, and balance N_2 Flow rate: 100 mL/min Heating rate: 10°C/min Tight contact	$La_{0.9}K_{0.1}$ $Co_{0.9}Cu_{0.1}O_{3-\delta}$ is the best catalyst with catalytic soot oxidation activity for T_m at 360°C	[206]
$La_{1-x}K_xCo_{1-y}Pd_yO_{3-\delta}$ (x = 0, 0.1; y = 0, 0.05)	Citrate-based sol–gel process	TG/DTA Feed: 600 ppm NO, 10 vol% O_2 and balance N_2 Flow rate: 100 mL/min Heating rate: 5°C/min Tight contact	$La_{0.9}K_{0.1}$ $Co_{0.95}Pd_{0.05}O_{3-\delta}$ Shows the best catalytic soot oxidation activity with T_i and T_m at 219 and 360°C	[207]
$La_{0.9}CoO_3$, $La_{0.9}Na_{0.1}CoO_3$, $La_{0.9}K_{0.1}CoO_3$, $La_{0.9}Rb_{0.1}CoO_3$	Solution combustion synthesis	TPC Feed: air Flow rate: 100 mL/min Heating rate: 5°C/min Tight and loose contact	$La_{0.9}Rb_{0.1}CoO_3$ shows the best catalytic soot oxidation activity with T_i and T_p at 330 and 393 C°	[208]
$La_{1-x}(M)_xCoO_3$ (M = Ce and Sr)	Solid state method	TPC Feed: 0%, 1%, and 10% O_2/He Flow rate: 60 mL/min Heating rate: 5°C/min Tight contact	$La_{0.8}Ce_{0.2}CoO_3$ shows the best catalytic activity with T_m at 435°C	[211]

5.3.1.4. *Lanthanum Ferrites.* Lanthanum ferrite was found to be moderately active catalyst for soot oxidation reaction as compared to other lanthanum-based perovskites.[174] Several efforts were made to improve the catalytic activity of $LaFeO_3$. Different preparation methods influence the structure, physicochemical properties and catalytic activity. Taniguchi et al. synthesized $LaFeO_3$ by Self-Propagating High-Temperature method. Soot oxidation activity was studied for a different time durations of mechanical ball milling. It improved surface area from 0.89 to 170 m^2/g and also increased the soot oxidation activity.[212] However, substitution by different alkali methods has been reported to improve soot oxidation activity of $LaFeO_3$. A-site substituted with Sr depicted less improvement in catalytic activity, but it was responsible for the enhanced stability of the catalyst. Series of $La_{1-x}Sr_xFeO_3$ (x = 0–1) perovskites were synthesized by self-propagating high-temperature synthesis method and evaluated for soot oxidation activity. As substitution increased, simultaneously increased the BET surface area and showed the improvement in soot oxidation activity.[213] Sr-substituted with $La_{1-x}Sr_xFeO_3$ (x = 0–0.4) having 3DOM structure was prepared and evaluated for soot oxidation.[213] Jiménez et al. reported the effect of Ca-substitution at A-site by synthesizing series of $La_{1-x}Ca_xFeO_3$ (x = 0.1–0.4).[215] Wei et al. synthesized 3DOM $Au/LaFeO_3$ (Figure 19) with different concentrations and found

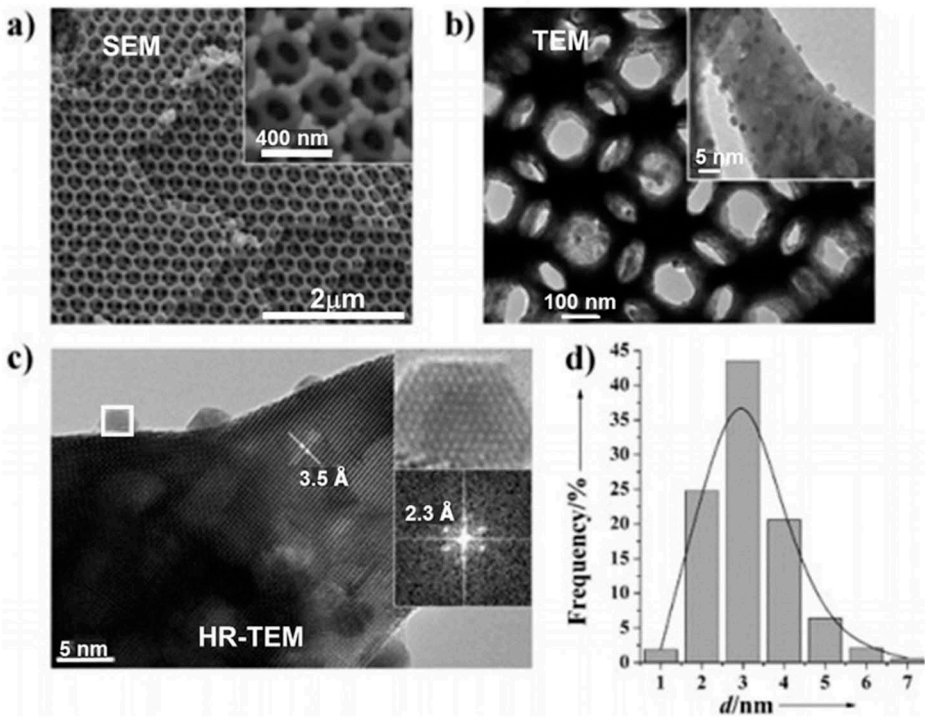

Figure 19. (a) SEM, (b) TEM, (c) HRTEM images, and (d) size distribution of Au nanoparticles of 3DOM $Au_{0.04}/LaFeO_3$. The insets in (a) and (b) show an enlarged area, and the inset in (c) shows an enlarged Au particle whose lattice fringes corresponding to the fcc (111) plane at 2.3 in a fast Fourier transform (FFT) image (reproduced with permission from Ref. [216]).[216]

Table 10. Temperatures and selectivity to CO_2 for soot combustion over different catalysts and without catalyst (loose contact condition) (reproduced with permission from Ref. [216]).[216]

Catalyst	T_i (°C)	T_m (°C)	S_{CO_2}
Pure soot	482	585	55.0
$LaFeO_3$ (particles)	378	486	80.0
$LaFeO_3$ (3DOM)	347	415	92.2
$Au_{0.005}/LaFeO_3$ (4.2 nm)	282	379	99.1
$Au_{0.01}/LaFeO_3$ (4.0 nm)	277	371	99.5
$Au_{0.02}/LaFeO_3$ (3.7 nm)	264	369	99.6
$Au_{0.04}/LaFeO_3$ (3.0 nm)	228	368	99.7
$Au_{0.06}/LaFeO_3$ (2.9 nm)	230	366	99.6
$Au_{0.08}/LaFeO_3$ (2.8 nm)	229	359	99.7
$Au_{0.08}/LaFeO_3$ (2.8 nm)	271	380	99.7
$Au_{0.04}/LaFeO_3$ (7.8 nm)	285	384	99.6
Pt/SiO_2	247	312	99.5

enhancement in catalytic soot oxidation activity (Table 10).[216] Recently, Feng et al. impregnated K and Mn simultaneously on the 3DOM $La_{0.8}Ce_{0.2}FeO_3$, which led to the formation of $K_2Mn_4O_8$ without influencing 3DOM structure. Surprisingly, it resulted in lowering T_{50} from 417 to 377°C.[217] Table 11 shows the brief state of art for lanthanum ferrite catalysts.

Table 11. Lanthanum ferrite based catalysts for soot oxidation.

Catalysts	Synthesis method	Experimental conditions	Important findings	Reference
$LaFeO_3$	Self-propagating high-temperature synthesis	TGA Feed: air Flow rate: 50 mL/min Heating rate: 3°C/min Tight contact	$LaFeO_3$ shows the T_{50} at 404°C after milling for 2 h and 6 h	[212]
(3DOM) $La_{0.8}Ce_{0.2}FeO_3$ $Mn/La_{0.8}Ce_{0.2}FeO_3$ $K–Mn/La_{0.8}Ce_{0.2}FeO_3$ $K/La_{0.8}Ce_{0.2}FeO_3$	Colloidal crystal template method	TPO Feed: 500 ppm NO and 5% O_2 balanced with N_2 Flow rate: 50 mL/min Heating rate: 2°C/min Loose contact	$K–Mn/La_{0.8}Ce_{0.2}FeO_3$ shows the best soot oxidation activity with T_{10}, T_{50}, T_{90} at 316, 377, 430°C	[217]
$La_{1-x}A_xFe_{1-y}B_yO_3$ (where A = Na, K, Rb and B = Cu)	Solution combustion synthesis	TGA Feed: 1000 ppmv NO; 10 vol% O_2, He balance Flow rate: 100 mL/min Heating rate: 5°C/min Tight contact	La–K–Cu–FeO_3 shows the best soot oxidation activity for T_m at 359°C	[218]
(3DOM) $LaCo_xFe_{1-x}O_3$ (x = 0–0.5)	CCT method	TPO Feed: 5% O_2 and 0.2% NO balanced with Ar Flow rate: 50 mL/min Heating rate: 2°C/min Loose contact	3DOM $LaCo_{0.5}Fe_{0.5}O_3$ shows the best catalytic soot oxidation activity for T_i and T_m at 256 and 397°C	[219]

CCT: Colloid crystal template.

5.3.1.5. *Other lanthanum based perovskites.* Labhsetwar et al. investigated $LaRuO_3$ perovskites in both supported and unsupported forms. They discussed the improved non-tedious synthesis method for unsupported, and alumina supported $LaRuO_3$ perovskite catalysts. They found the significant improvement in physical properties like surface area and thermal stability and high thermal stability which favors several combustion reactions.[220] A double perovskite Ln_2CuO_4 was investigated by Fino et al. with significantly improved catalytic activity thorough substitution of both A- and B-sites of perovskite. They found that V-substitution resulted in increased NO reduction and simultaneous K- and V-substitution increased the soot oxidation activity.[221] Liu et al. showed the influence of A- and B-site substitution in Ln_2CuO_4. They found that Rb substitution at A-site reduced the temperature for both soot and NO_x removal. However, they further disclosed that substitution with Na further shows improvement in the simultaneous removal of soot and NO_x.[222,223] Series of $La_{1-x}Ce_xNiO_3$ $_xCe_xNiO_3$ ($0 \leq X \leq 0.05$) were synthesized and investigated for simultaneous removal for NO_x and soot. They found that small substitution results in increased catalytic activity. Ni ions are active in soot oxidation reactions, however, less than 5% substitution surprisingly lowers ignition temperature to 300 from 450°C.[224,225] Further both A- and B-site substitution reported by Ma et al. and reported the improvement in simultaneous soot and NO_x removal. Sr substation at A-site $La_{1.8}Sr_{0.2}NiO_4$ showed ignition temperature and maximum soot oxidation temperature at 160C and 400°C.[225] Table 12 shows the brief state of art for other lanthanum based catalysts.

5.3.2. *Praseodymium based perovskite catalysts*

$PrCrO_3$ on CeO_2 were investigated for soot oxidation reactions by Fino et al. Solution combustion method was used for the preparation of $PrCrO_3$ on CeO_2. The same material was coated on the trap and tested under real conditions. They found that catalyst is extremely stable even under real engine conditions. The composition was improved by loading 1% Pt and also found the reasonably good catalytic activity. A tiny amount of noble metal can even enhance the catalytic activity and was also loaded on a prototype and tested on real engine conditions.[99,226] $PrMnO_3$ was also investigated by Megarajan et al. They synthesized Ag-substituted inside perovskite and Ag-loaded on perovskites $PrMnO_3$. They disclosed that Ag-impregnated $PrMnO_3$ showed much better catalytic soot oxidation and CO oxidation activity compared to pure $PrMnO_3$ and substituted $PrMnO_3$. They prove this by taking evidence of H_2-TPR, O_2-TPD, HR-TEM mapping, and XPS results. They found that improved catalytic activity of Ag dispersed sample was due to the presence of Ag/AgO_2 on the surface, which facilitates redox reaction.[227]

Table 12. Other Lanthanum perovskite based catalysts for soot oxidation.

Catalysts	Synthesis method	Experimental conditions	Important finding	Ref.
La_2CuO_4 ($A_{2-x}A_xB_{1-y}B_yO_{4\pm\delta}$, where *A*, A = La, K, and B, B = Cu, V)	Citrate method	TPC Feed: 1800 ppmv NO; 4 vol% O_2, He balance Space velocity: 180,000 h^{-1} Heating rate: 10°C/min Tight and loose contact	$La_{1.8}K_{0.2}Cu_{0.9}V_{0.1}O_4$ shows the best soot oxidation activity with T_{comb} at 486°C	[221]
$La_{1-x}Ce_xNiO_3$ ($0 \le X \le 0.05$)	Citric acid complexation	TPC Feed: 0.5 vol% NO and 5 vol% O_2 balanced with He Flow rate: 50 mL/min Heating rate: 1°C/min Tight contact	$La_{0.95}Ce_{0.05}NiO_3$ shows the best activity with T_i at 303°C	[224]
$La_{2-x}Rb_xCuO_{4-\lambda}$ (x = 0, 0.1, 0.2, 0.3, 0.4, 0.5)	Sol–gel auto-combustion method	TPR Feed: 5% O_2 and 0.2% NO balanced with He Flow rate: 50 mL/min Heating rate: 2°C/min Loose contact	$La_{1.6}Rb_{0.4}CuO_{4-\lambda}$ shows the best catalytic activity with T_i and T_m at 429 and 505°C	[223]
Ln_2CuO_4 (Ln = La, Pr, Nd, Sm, Gd) and $La_{2-x}Na_xCuO_4$ (x = 0, 0.1, 0.3, 0.5, 0.7, 0.9)	Sol–gel auto-combustion method	TPR Feed: 5% O_2 and 0.2% NO balanced with He Flow rate: 50 mL/min Heating rate: 2°C/min Loose contact	$La_{1.3}Na_{0.7}CuO_4$ shows the best catalytic activity with T_i and T_m at 398.4 and 463.5°C	[222]
$La_{2-x}A_xNi_{1-y}B_yO_4$ (A = Sr, Ba; B = Mn, Fe, x = 0, 0.2)	Citric acid complexation	TPR Feed: 1.0 vol% NO and 5 vol% O_2 balanced with He Flow rate: 50 mL/min Heating rate: 5°C/min Tight contact	$La_{1.8}Sr_{0.2}NiO_4$ shows the best catalytic activity with T_{ig} and T_{maxCO_2} at 160 and 400°C	[225]

CMCCT: Carboxy-modified colloidal crystal templates.

5.3.3. *Strontium and other metal-based perovskite catalysts*

$SrTiO_3$ perovskites were investigated by Bialobok et al. They synthesized the A-site substituted and impregnated with alkali metals (Li, Cs, K) perovskites. Evidence like XPS and O_2-TPD reveals that surface composition and basicity of K-substituted $SrTiO_3$ are responsible for the improved catalytic activity compared to other substituted and impregnated $SrTiO_3$.[228] However, potassium is unstable and gets evaporated at high temperature. Further similar work was expanded by Ura et al. They synthesized the K-substituted and impregnated $SrTiO_3$ by sol–gel method. This results in increased high-temperature stability and shows the good catalytic soot oxidation activity.[229] Ura et al. also investigated the effect of the various concentrations of K-substituted $SrTiO_3$ for catalytic soot oxidation reactions. They found that 0.2 is the most suitable concentration for soot oxidation reaction.[230] $SrCoO_3$ compositions were synthesized and investigated for

Table 13. Pr and Sr-based perovskites reported for the soot oxidation reaction.

Catalysts	Synthesis method	Experimental conditions	Important finding	Reference
$PrMnO_{3+\delta}$ $Pr_{0.9775}Ag_{0.0225}MnO_{3+\delta}$ 1 wt% $Ag/PrMnO_{3+\delta}$	Citrate method, impregnation method	TGA Feed: air Flow rate: 100 mL/min Heating rate: 5°C/min Tight and loose contact	$Pr_{0.9775}Ag_{0.0225}MnO_{3+\delta}$ calcined at 200°C shows the best catalytic activity for T_i and T_f at 247 and 453°C	[227]
$SrCoO_3$ $Sr_{0.8}Ce_{0.2}CoO_3$	Co-precipitation method	TGA Feed: air Heating rate: 5°C/min Loose contact	$Sr_{0.8}Ce_{0.2}CoO_3$ shows the best catalytic activity for T_i, T_{50}, and T_f at 241, 420, and 500°C	[231]
$SrTiO_3$, $Sr_{1-x}Me_xTiO_3$ (x = 0.05–0.2)	Sol–gel citric method	TGA Feed: 10% O_2 in Ar or (1500 ppm of NO + 10% O_2 in Ar) or (1500 ppm of NO_2 + 10% O_2 in Ar) Flow rate: 20 dm^3 Heating rate: 5°C/min Loose contact	$Sr_{0.8}K_{0.2}TiO_3$ shows the best catalytic activity with T_m 380°C	[229]

soot oxidation. Dhakad et al. synthesized compisitions substituted at A-site with Ce and found very high thermal stability with improved soot ignition temperature in loose contact condition for soot oxidation reactions.[231] Table 13 shows the brief state of the art for Pr and Sr based perovskite type catalysts.

5.4. *Spinels*

Spinels are the type of mixed oxides with the general formula AB_2O_4. On the ground of literature, the catalytic activity of spinels is found to be better than that individual oxides or mixed oxides. The Shangguan et al. for the first time evaluated the spinels for simultaneous reduction of NO_x and PM. They have synthesized the ACr_2O_4 (A = Cu, Mg, CO, and Mn), $CoMn_2O_4$, AFe_2O_4 (A = Cu, CO, and Ni) by the citric acid method and tested for simultaneous removal of NO_x and PM. They found that $CuFe_2O_4$ is the best performing catalyst among others in terms of lower selectivity for nitrous oxide and highest for nitrogen formation with moderate soot ignition temperature.[232] They also further modified the $CuFe_2O_4$ by doing alkali metal like Cs, K, Na, Li and also the effect of vanadium and platinum has been studied. They found that the ignition temperature decreased to 266 from 285°C as compared to undoped spinel. The proper K doping i.e. 5% results in the formation of $Cu_{0.95}K_{0.05}Fe_2O_4$ with the highest selectivity for N_2 and improved soot oxidation activity.[233] Shangguan et al. further coated the $Cu_{0.95}K_{0.05}Fe_2O_4$ catalyst on DPF and studied the removal of soot and NO_x. They found that even after coating on DPF catalyst shows the excellent catalytic activity. They confirmed that the NO and oxygen show the synergistic effect and show the significant catalytic soot

oxidation activity along with NO_x reaction activity. The very important conclusion they drawn from the experimental observations that NO_x reduction and CO_2 formation took place at the same temperature, which was the key factor for the simultaneous removal of NO_x and soot.[234] Further, Fino et al. also reported the spinel type mixed oxides for simultaneous removal of soot and NO_x. They successfully synthesized the $CoCr_2O_4$, $MnCr_2O_4$, $CoFe_2O_4$ spinels by solution combustion synthesis method achieving particle size <20 nm with a rough surface, which provides the good contact between catalyst and soot. The best performing catalyst $CoCr_2O_4$ further coated on DPF by *in-situ* combustion synthesis method to confirm the potential for real diesel engine exhaust.[235,236] $BaAl_2O_4$ composition was also reported for simultaneous removal of soot and NO_x. They found that $BaAl_2O_4$ shows the excellent soot oxidation and NO_x reduction activity. They found that nitrate formation took place due to the presence of oxygen which promotes both soot oxidation and NO_x reduction reaction.[237,238] Mg ferrite spinel catalyst also reported for the simultaneous removal of soot and NO_x. The Mg site substituted with Cs and Fe substituted with Mn show the best catalytic activity.[239] The $ZnAl_2O_4$ spinel with modification has been explored for removal of soot $_x$ from the diesel exhaust. Five percent Cu impregnated and substituted spinel have been prepared and found that impregnated spinel showed the improved catalytic activity compared to substituted and pure $ZnAl_2O_4$ spinel.[240] Table 14 shows the brief state of the art for spinels based catalysts for soot oxidation.

6. Conclusion

Diesel engines have attracted greater attention in modern society due to its robustness and efficiency along with cost-effective diesel fuel price. However, nowadays, emissions of soot from diesel exhaust have become a matter of concern due to the adverse impacts on health and the environment.

In this review, we have introduced PM emissions from diesel engines and discussed the composition and formation mechanisms of PM. Considering all the serious effects of PM, stringent emission control norms have been introduced for diesel engines, which has also led to remarkable developments of efficient and cleaner diesel engine technologies. However, complete control of diesel PM emissions cannot be obtained without efficient aftertreatment technologies, especially with aging of engine. DOC, DPF, and PFF are recognized as the best after-exhaust treatment options to deal with diesel exhaust emission-related challenges. The SOF part of soot can be oxidized along with the gaseous pollutants like CO, HC by DOC, which is non-filter open monolith system. Near-complete soot control can be achieved in DPF where soot can be efficiently trapped on the wall of DPF and oxidized above 550°C. These three most common technologies are appropriately discussed here in separate subsections. This is followed by catalytic applications for

Table 14. Spinel-based catalysts for soot oxidation.

Catalysts	Synthesis method	Experimental conditions	Important finding	Reference
$CuCr_2O_4$ $MgCr_2O_4$ $CoCr_2O_4$ $MnCr_2O_4$ $CoMn_2O_4$ $NiFe_2O_4$ $CoFe_2O_4$ $CuFe_2O_4$	Citric acid-aided (CIT) process	TPO Feed: 5% O_2 + 0.5% NO + He Flow rate: 20 cm^3/min Heating rate: 1°C/min Tight contact	$CuFe_2O_4$ is the best performing catalyst among others in terms of lower selectivity for nitrous oxide and highest for nitrogen formation with soot ignition temperature of 285°C	[232]
$Cu_{1-x}A_xFe_2O_4$ (A = Cs, K, Li, Na) X = 0.05	Citric acid-aided (CIT) process	TPO Feed: 5% O_2 + 0.5% NO + He Flow rate: 20 cm^3/min Heating rate: 1°C/min Tight contact	$Cu_{0.95}K_{0.05}Fe_2O_4$ is the best performing catalyst among others in terms of lower selectivity for nitrous oxide and highest for nitrogen formation with soot ignition at 266°C	[233]
$CoCr_2O_4$; $MnCr_2O_4$; $CoFe_2O_4$	Solution combustion synthesis method	TPR Feed: 1000 ppm NO, 10 vol% O_2, balance He Flow rate: 1.66 × 10^{-6} Nm^3/s Heating rate: 5°C/min Tight and loose contact	$CoCr_2O_4$ found to be significantly reducing the soot combustion temperature to 396°C with NO_x reduction at 385°C	[235]
$BaAl_2O_4$	The precursor solution was heated until dryness followed by calcination at 600°C for 2 h and 800°C for 6 h	TPR Feed: 1% NO, 10 vol% O_2, balance He Flow rate: 40 mL/min Heating rate: 1°C/min Tight and loose contact	$BaAl_2O_4$ shows the soot oxidation activity with Ti at 285°C	[237]
$MgFe_2O_4$	Malic acid method	TPR Feed: 4% O_2, balance He Flow rate: 100 mL/min Heating rate: 1°C/min Tight contact	$Mg_{0.7}Cs_{0.3}Fe_{1.5}Mn_{0.5}O_4$ shows the best catalytic activity with Ti at 305°C	[239]

(*Continued*)

Table 14. (Continued).

Catalysts	Synthesis method	Experimental conditions	Important finding	Reference
$ZnAl_2O_4$	Glycothermal method	TPR Feed: 5% O_2, 500 ppm NO balance He Flow rate: 500 mL/min Heating rate: 10°C/min; loose contact	5% Cu/$ZnAl_2O_4$ shows the best activity with T_{50} at 600°C	[240]
$Mn_{1-x}Ag_xCo_2O_4$	Sol–gel method	TPR Feed: 5% O_2, 0.2% NO balance He; loose contact	$Mn_{0.6}Ag_{0.4}Co_2O_4$ shows the best soot oxidation activity with T_{10}, T_{50}, and T_{90} at 250, 325, and 373°C, respectively	[241]

diesel soot oxidation. Soot oxidation reaction is thermodynamically more feasible and much faster in the presence of NO_x/air than in only air. However, by optimizing the diesel engine to produce the less soot might increase the concentration of NO_x or vice versa. This review also discusses on un-catalyzed soot oxidation with air/O_2 and NO_2 in separate subsections. The mechanistic and kinetic aspects explored by various researchers show that order and activation energy of PM oxidation vary with particle nature and composition of PM itself. Overall, PM oxidation with air shows appreciably high activation energy (120–180 kJ/mol) and hence requires high operating temperatures (>500°C) to oxidize the PM completely to CO_2 and H_2O. However, NO_2 mediated oxidation of PM has incredibly low activation energy (40–70 kJ/mol) which allows PM oxidation in the temperature range of 300–400°C.

Further, a catalyst can be applied to accelerate this oxidation process. However, contact mode between the catalyst and PM plays a significant role in catalyst activity. Tight contact mode provides the oxidation reaction rates compared to loose contact mode, whereas the real-time contact mode of catalyst and PM in a DPF environment is much similar to loose contact mode. Researchers across the world have been continuously working and upgrading the catalyst activity for this process by varying the composition and physiochemical properties of very large number of catalysts. This review therefore mainly focuses on a detailed overview on various catalyst compositions developed by researchers across the world. Noble metal-based catalysts have been most studied catalysts for PM oxidation and also found exceptional commercial success. Catalytic formulations of Pt over various supports have been widely reported and commercially used due to their high activity. An activity of Pt can be enhanced by using an alkali metal, alkaline earth metal, and other metal promoters. The higher cost and limited availability of PGM group metals have obliged researchers to search for alternative cost-effective catalysts. Mixed metal oxides were explored for their catalytic activity for PM oxidation reaction. Among the mixed metal oxides, CeO_2 is among the most studied oxide in combination with other oxides such as zirconia, alumina, etc. The mobility of oxygen and oxygen storage capacity of ceria is reported to be an important physiochemical property that proved to be beneficial for this reaction. These mixed metal oxides were capable of providing almost the same efficiency (T_{50}) as shown by Pt-based catalysts. Another class of extensively studied non-PGM-based catalysts are those Perovskite-based compositions which are also proved to be efficient catalysts due to their lattice oxygen mobility, oxygen adsorption, and desorption properties. Among perovskites, lanthanum-based perovskites are the most studied perovskites and lanthanum magnetites promoted with alkali metal showed the best efficiency in terms of lowest PM oxidation temperatures (T_m < 400°C). Spinels are another category of metal oxides explored for PM

oxidation. Doping of spinels with alkali metal introduces oxygen-deficient sites in the lattice favoring adsorption and activation of oxygen.

These catalysts can be applied for continuous generation of NO_2, which can oxidize the soot even in the presence of low NO_x. Several improvements have been still going on for designing and synthesis of a catalyst as almost all the PM control technologies depend on the catalyst for reduction of exhaust emission. Clear impact of an improved aftertreatment system based on different catalyst has been observed on soot emissions and therefore catalyst assisted soot control technolgies are very commonly applied world over. The ever-tightening PM emission norms and search for the alternates to PGM are responsible for the continued active interests in this R&D area and to support that, very large number of specially non-PGM-based catalysts are reviewed and mentioned in this review. Such new and modified catalyst compositions are still getting reported and expected to find commercial applications in future.

Acknowledgments

This work was carried out under the SERB-DST sponsored project. No. EMR/2016/006586. Ms. Rohini Khobragade acknowledges CSIR-UGC for PhD fellowship. This work is also a part of her PhD thesis under AcSIR. KRC No.: CSIR-NEERI/KRC/2018/APRIL/ERMD/3. Authors ASA-F extends appreciation to ISP programme at King Saud University through ISPP#0057.

References

[1] Benson, R. S.; Whitehouse, N. D. Internal Combustion Engines: A Detailed Introduction to the Theromodynamics of Compression-Ignition (CI) and Spark-Ignition (SI) Engines, Their Design and Development; Pergamon Press Ltd. Headington Hill Hall, Oxford OX3 OBW, England, 1979; Vol. 1.

[2] Daido, S.; Analysis of Soot Accumulation inside Diesel Engines. JSAE Rev. 2000, 21 (3),303–308. DOI: 10.1016/S0389-4304(00)00048-5.

[3] Boehman, A. L.; Song, J.; Alam, M. Impact of Biodiesel Blending on Diesel Soot and the Regeneration of Particulate Filters. Energy Fuels. 2005, 19(5),1857–1864. DOI: 10.1021/ef0500585.

[4] Candeia, R. A.; Silva, M. C. D.; Carvalho Filho, J. R.; Brasilino, M. G. A.; Bicudo, T. C.; Santos, I. M. G.; Souza, A. G. Influence of Soybean Biodiesel Content on Basic Properties of Biodiesel–Diesel Blends. Fuel. 2009, 88(4),738–743. DOI: 10.1016/j.fuel.2008.10.015.

[5] Qi, D. H.; Chen, H.; Geng, L. M.; Bian, Y. Z. Experimental Studies On The Combustion Characteristics And Performance Of A Direct Injection Engine Fueled With Biodiesel/Diesel Blends. Energy Convers. Manage. 2010, 51(12),2985–2992. DOI: 10.1016/j.enconman.2010.06.042.

[6] Roy, M. M.; Wang, W.; Bujold, J. Biodiesel Production and Comparison of Emissions of a DI Diesel Engine Fueled by Biodiesel–Diesel and Canola Oil–Diesel Blends at HighIdling Operations. Appl. Energy. 2013, 106, 198–208. DOI: 10.1016/j.apenergy.2013.01.057.

[7] Stanmore, B.; Stanmore, B.; Brilhac, J.; Gilot, P. The Oxidation of Soot: A Review ofExperiments, Mechanisms and Models. Carbon. 2001, 39(15),2247–2268. DOI:10.1016/S0008-6223(01)00109-9.
[8] Frenklach, M. Reaction Mechanism of Soot Formation in Flames. Phys. Chem. Chem. Phys. 2002, 4, 2028. DOI: 10.1039/b110045a.
[9] Xi, J.; Zhong, B.-J. Soot in Diesel Combustion Systems. Chem. Eng. Technol. 2006, 29 (6), 665–673. DOI: 10.1002/(ISSN)1521-4125.
[10] Taghavifar, H.; Khalilarya, S.; Jafarmadar, S. Three-Dimensional Energetic And Exergetic Analysis Of The Injection Orientation Of Di Diesel Engine Under Different Engine Speeds. Energy Sci. Eng. 2015, 3(4),360–370. DOI: 10.1002/ese3.2015.3.issue-4.
[11] Heywood, J. B. Internal Combustion Engine Fundamentals; McGrawHill International: New York, 1988.
[12] Niessner, R. The Many Faces of Soot: Characterization of Soot Nanoparticles Produced by Engines. Angew. Chem. Int. Ed. 2014, 53(46),12366–12379.
[13] Pueschel, R. F.; Kinne, S. A. Physical and Radiative Properties of Arctic Atmospheric Aerosols. Sci. Total Environ. 1995, 160–161, 811–824. DOI: 10.1016/0048-9697(95)04414-V.
[14] Bond, T. C.; Doherty, S. J.; Fahey, D. W.; Forster, P. M.; Berntsen, T.; DeAngelo, B. J.; Flanner, M. G.; Ghan, S.; Kärcher, B.; Koch, D.;; et al. Bounding the Role of Black Carbon in the Climate System: A Scientific Assessment. J. Geophys. Res. Atmos. 2013,118(11), 5380–5552.
[15] Report to Congress on Black Carbon, U. S. Environmental Protection Agency, EPA-450/ R-12-001, March 2012. doi:10.1094/PDIS-11-11-0999-PDN
[16] Eastwood, P. Particulate Emissions from Vehicles; John Wiley & Sons Ltd, The Atrium, Southern Gate, Chichester,West Sussex PO19 8SQ, England, 2008.
[17] Kittelson, D. B. Engines and Nanoparticles. J. Aerosol Sci. 1998, 29(5–6),575–588.DOI: 10.1016/S0021-8502(97)10037-4.
[18] Hinds, W. C. Aerosol Technology: Properties, Behavior, and Measurement of Airborne Particles; A Wiley-Interscience publication, John Wiley & Sons, River street, Hobiken, NJ 07030, 2012.
[19] Van Setten, B. A. A. L.; van Gulijk, C.; Makkee, M.; Moulijn, J. A. Molten Salts are Promising Catalysts. How to Apply in Practice? Top. Catal. 2001, 16/17(1/4), 275–278. DOI: 10.1023/A:1016644612038.
[20] Van Setten, B. A. A. L.; Makkee, M.; Moulijn, J. A. Science and Technology of CatalyticDiesel Particulate Filters. Cat. Rev. - Sci. Eng. 2001, 43(4),489–564. DOI: 10.1081/CR-120001810.
[21] Shamjad, P. M.; Tripathi, S. N.; Pathak, R.; Hallquist, M.; Arola, A.; Bergin, M. H. Contribution Of Brown Carbon To Direct Radiative Forcing Over The Indo-Gangetic Plain. Environ. Sci. Technol. 2015, 49(17),10474–10481. DOI: 10.1021/acs.est.5b03368.
[22] Chakraborty, A.; Bhattu, D.; Gupta, T.; Tripathi, S. N.; Canagaratna, M. R. Real-Time Measurements Of Ambient Aerosols In A Polluted Indian City: Sources, Characteristics, And Processing Of Organic Aerosols During Foggy And Nonfoggy Periods. J. Geophys. Res. Atmos. 2015, 120(17),9006–9019. DOI: 10.1002/2015JD023419.
[23] https://www.dieselnet.com/standards/
[24] Park, C.; Kim, S.; Kim, H.; Moriyoshi, Y. Stratified Lean Combustion Characteristics Of A Spray-Guided Combustion System In A Gasoline Direct Injection Engine. Energy. 2012, 41(1),401–407. DOI: 10.1016/j.energy.2012.02.060.

[25] Soid, S. N.; Zainal, Z. A. Spray and Combustion Characterization for Internal Combustion Engines Using Optical Measuring Techniques – A Review. Energy. 2011,36(2), 724–741. DOI: 10.1016/j.energy.2010.11.022.
[26] Brijesh, P.; Sreedhara, S. Exhaust Emissions and Its Control Methods in Compression Ignition Engines: A Review. Int. J. Of Automot. Technol. 2013, 14(2),195–206. DOI: 10.1007/s12239-013-0022-2.
[27] Abagnale, C.; Cameretti, M. C.; De Simio, L.; Gambino, M.; Iannaccone, S.; Tuccillo, R Numerical Simulation and Experimental Test of Dual Fuel Operated Diesel Engines. Appl. Therm. Eng. 2014, 65(1–2),403–417. DOI: 10.1016/j.applthermaleng.2014.01.040.
[28] Mohan, B.; Yang, W.; Chou, S. K. Development of an Accurate Cavitation Coupled Spray Model for Diesel Engine Simulation. Energy Convers. Manage. 2014, 77, 269–277.DOI: 10.1016/j.enconman.2013.09.035.
[29] Yoon, S. H.; Cha, J. P.; Lee, C. S. An Investigation Of The Effects Of Spray Angle And Injection Strategy On Dimethyl Ether (Dme) Combustion And Exhaust Emission Characteristics In A Common-Rail Diesel Engine. Fuel Process. Technol. 2010, 91 (11),1364–1372. DOI: 10.1016/j.fuproc.2010.04.017.
[30] Kiplimo, R.; Tomita, E.; Kawahara, N.; Yokobe, S. Effects of Spray Impingement, Injection Parameters, and EGR on the Combustion and Emission Characteristics of a PCCI Diesel Engine. Appl. Therm. Eng. 2012, 37, 165–175. DOI: 10.1016/j.applthermaleng.2011.11.011.
[31] Neeft, J.; Makkee, M.; Moulijn, J. Catalysts for the Oxidation of Soot from Diesel Exhaust Gases. I. An Exploratory Study. Appl. Catal. B: Enviro. 1996, 8(1),57–78. DOI: 10.1016/0926-3373(95)00057-7.
[32] Bueno-López, A. Diesel Soot Combustion Ceria Catalysts. Appl. Catal. B: Enviro.2014, 146, 1–11. DOI: 10.1016/j.apcatb.2013.02.033.
[33] Cooper, B. J.; Roth, S. A. Flow-Through Catalysts for Diesel Engine Emissions Control, Platin. Met. Rev. 1991, 35(178). 178–187. https://www.technology.matthey.com/article/35/4/178-187/
[34] Labhsetwar, N.; Biniwale, R. B.; Kumar, R.; Rayalu, S.; Devotta, S. Application Of Supported Perovskite-Type Catalysts For Vehicular Emission Control. Catal. Surv. Asia. 2006, 10(1),55–64. DOI: 10.1007/s10563-006-9005-x.
[35] Prasad, R.; Venkateswara, R. B. A Review on Diesel Soot Emission, Its Effect and Control. Bull. Chem. React. Eng. Catal. 2010, 5(2),69–86.
[36] Stratakis, G. A.; PhD Thesis: Expermimental Investigation of catalytic soot oxidation and pressure drop characteristics in wall-flow diesel particulate filters, Univerity of Thessaly, January 2004, pp. 22.
[37] Hu, S.; Herner, J. D.; Robertson, W.; Kobayashi, R.; Chang, M.-C. O.; Huang, S.; Zielinska, B.; Kado, N.; Collins, J. F.; Rieger, P.;; et al. Emissions Of Polycyclic Aromatic Hydrocarbons (Pahs) And Nitro-PAHs From Heavy-Duty Diesel Vehicles With Dpf And Scr. J. Air Waste Manage. Assoc. 2013, 63(8),984–996.
[38] Liu, Z. G.; Berg, D. R.; Swor, T. A.; Schauer, J. J. Comparative Analysis on the Effects of Diesel Particulate Filter and Selective Catalytic Reduction Systems on a Wide Spectrum of Chemical Species Emissions. Environ. Sci. Technol. 2008, 42(16),6080–6085. DOI: 10.1021/es8004046.
[39] Schneider, J.; Hock, N.; Weimer, S.; Borrmann, S.; Kirchner, U.; Vogt, R.; Scheer, V. Nucleation Particles in Diesel Exhaust: Composition Inferred from in Situ Mass Spectrometric Analysis. Environ. Sci. Technol. 2005, 39(16),6153–6161. DOI: 10.1021/es049427m.
[40] Corro, G. Sulfur Impact on Diesel Emission Control- A Review. React. Kinet. CatalLett. 2002, 75, 89. DOI: 10.1023/A:1014853602908.

[41] Müller, J.-O.; Frank, B.; Jentoft, R. E.; Schlögl, R.; Su, D. S. The Oxidation of Soot Particulate in the Presence of NO2. Catal. Today. 2012, 191(1),106–111. DOI: 10.1016/j.cattod.2012.03.010.
[42] Schejbal, M.; Štěpánek, J.; Marek, M.; Kočí, P.; Kubíček, M. Modelling of Soot Oxidation by NO2 in Various Types of Diesel Particulate Filters. Fuel. 2010, 89 (9),2365–2375. DOI: 10.1016/j.fuel.2010.04.018. 1445
[43] Hernández-Giménez, A.; Castelló, D.; Bueno-López, A. Diesel Soot Combustion Catalysts: Review of Active Phases. Chem. Pap. 2014, 68, 9. DOI: 10.2478/s11696-013-0469-7.
[44] Twigg, M. V. Progress and Future Challenges in Controlling Automotive Exhaust Gas Emissions. Appl. Catal. B: Enviro. 2007, 70(1–4),2–15. DOI: 10.1016/j.apcatb.2006.02.029.
[45] Song, J.; Alam, M.; Zello, V.; Boehman, A. L.; Bishop, B.; Walton, F. Fuel Sulfur Effect on Membrane Coated Diesel Particulate Filter. In SAE Technical Paper Series, SAE International, 2002-01-2788, 2002. doi:10.4271/2002-01-2788.
[46] Fino, D.; Specchia, V. Open Issues in Oxidative Catalysis for Diesel Particulate Abatement. Powder Technol. 2008, 180(1–2), 64–73. DOI: 10.1016/j.powtec.2007.03.021.
[47] Lizarraga, L.; Souentie, S.; Boreave, A.; George, C.; D'Anna, B.; Vernoux, P. Effect of Diesel Oxidation Catalysts on the Diesel Particulate Filter Regeneration Process. Environ. Sci. Technol. 2011, 45(24),10591–10597. DOI: 10.1021/es2026054.
[48] Kim, H. J.; Han, B.; Hong, W. S.; Shin, W. H.; Cho, G. B.; Lee, Y. K.; Kim, Y. J. Development Of Electrostatic Diesel Particulate Matter Filtration Systems Combined With A Metallic Flow-Through Filter And Electrostatic Methods. Inter. J. Automo. Technol. 2010, 11(4),447–453. DOI: 10.1007/s12239-010-0055-8.
[49] Vakkilainen, A.; Lylykangas, R. Particle Oxidation Catalyst (POC) for Diesel Vehicles. In SAE Technical Paper Series, SAE International, 2004-28-0047, 2004. doi:10.4271/2004-28-0047.
[50] Emission Control Technologies for Diesel-Powered Vehicles – Report, Manufacturers of Emission Controls Association, December 2007.http://www.meca.org/technology/technology-details?id=6&name=Particulate%20Filters
[51] http://www.meca.org/technology/technology-details?id=6&name=Particulate%20Filters
[52] Levenspiel, O;. Chemical Reaction Engineering; John Wiley & Sons: New York, 1972;pp 367–368.
[53] Ishiguro, T.; Suzuki, N.; Fujitani, Y.; Morimoto, H. Microstructural Changes of Diesel Soot during Oxidation. Combust. Flame. 1991, 85(1–2),1–6. DOI: 10.1016/0010-2180(91)90173-9.
[54] Jung, H.; Kittelson, D. B.; Zachariah, M. R. Kinetics and Visualization of Soot Oxidation Using Transmission Electron Microscopy. Combust. Flame. 2004, 136 (4),445–456. DOI: 10.1016/j.combustflame.2003.10.013.
[55] Strzelec, A.; Toops, T. J.; Daw, C. S. Oxygen Reactivity of Devolatilized Diesel Engine Particulates from Conventional and Biodiesel Fuels. Energy Fuels. 2013, 27(7),3944–3951. DOI: 10.1021/ef400440a.
[56] Marsh, H.; Kuo, K. Kinetics and Catalysis of Carbon Gasification. In Introduction to Carbon Science; Marsh, H., ., Ed.; Butterworths: London, 1989; pp 107.
[57] Haynes, B. S. A Turnover Model for Carbon Reactivity I. Development. Combust. Flame. 2001, 126(1–2),1421–1432. DOI: 10.1016/S0010-2180(01)00263-2.
[58] Hurt, R. H.; Calo, J. M. Semi-Global Intrinsic Kinetics For Char Combustion Modeling. Combust. Flame. 2001, 125(3),1138–1149. DOI: 10.1016/S0010-2180(01)00234-6.

[59] Bews, I. M.; Hayhurst, A. N.; Richardson, S. M.; Taylor, S. G. The Order, Arrhenius Parameters, and Mechanism of the Reaction between Gaseous Oxygen and Solid Carbon. Combust. Flame. 2001, 124(1–2),231–245. DOI: 10.1016/S0010-2180(00)00199-1.

[60] Hurt, R. H.; Mitchell, R. E. Unified High-Temperature Char Combustion Kinetics For A Suite Of Coals Of Various Rank. Symposium (International) on Combustion. 1992, 24 (1), 1243–1250. DOI: 10.1016/S0082-0784(06)80146-3.

[61] Mitchell, R. E.; McLean, W. J. On the Temperature and Reaction Rate of Burning Pulverized Fuels. Symposium (International) on Combustion. 1982, 19(1),1113–1122. DOI: 10.1016/S0082-0784(82)80287-7.

[62] Smith, I. W. The Combustion Rates of Coal Chars: A Review. Symposium (International) on Combustion. 1982, 19(1),1045–1065. DOI: 10.1016/S0082-0784(82)80281-6 .

[63] Hurt, R. H.; Haynes, B. S. On The Origin Of Power-Law Kinetics In Carbon Oxidation. Proc. Combust. Inst. 2005, 30(2),2161–2168. DOI: 10.1016/j.proci.2004.08.131.

[64] Neeft, J. P. A.; Nijhuis, T. X.; Smakman, E.; Makkee, M.; Moulijn, J. A. Kinetics of the oxidation of diesel soot, Fuel. 1997, 76, 1129. DOI: 10.1016/S0016-2361(97)00119-1.

[65] Yezerets, A.; Currier, N. W.; Eadler, H. A.; Suresh, A.; Madden, P. F.; Branigin, M. A. Investigation of the Oxidation Behavior of Diesel Particulate Matter. Catal. Today. 2003, 88(1–2),17–25. DOI: 10.1016/j.cattod.2003.08.003.

[66] Yezerets, A.; Currier, N. W.; Kim, D. H.; Eadler, H. A.; Epling, W. S.; Peden, C. H. F. Differential Kinetic Analysis of Diesel Particulate Matter (Soot) Oxidation by Oxygen Using a Step–Response Technique. Appl. Catal. B. Environ. 2005, 61(1–2),120–129. DOI: 10.1016/j.apcatb.2005.04.014.

[67] Wang-Hansen, C.; Kamp, C. J.; Skoglundh, M.; Andersson, B.; Carlsson, P.-A. Experimental Method For Kinetic Studies Of Gas–Solid Reactions: Oxidation Of Carbonaceous Matter. The J. Phy. Chem. C. 2011, 115(32),16098–16108. DOI:10.1021/jp204539g.

[68] Kalogirou, M.; Samaras, Z. A Thermogravimetic Kinetic Study of Uncatalyzed Diesel Soot Oxidation. J. Therm. Anal. Calorim. 2009, 98(1),215–224. DOI: 10.1007/s10973-009-0110-8.

[69] Neeft, J. P.;, Potential for reduction of diesel particulate emissions. Ph.D. thesis, Technische Universiteit Delft, 1995.

[70] Wang-Hansen, C.; Soltani, S.; Andersson, B. Kinetic Analysis Of O2- And No2-Based Oxidation Of Synthetic Soot. J. Phys. Chem. C. 2012, 117(1),522–531. DOI: 10.1021/jp307789r.

[71] Khawam, A.; Flanagan, D. R. Solid-State Kinetic Models: Basics And Mathematical Fundamentals. J. Phys. Chem. B. 2006, 110(35),17315–17328. DOI: 10.1021/jp062746a.

[72] Skrdla, P. J.; Robertson, R. T. Semiempirical Equations For Modeling Solid-State Kinetics Based On A Maxwell–Boltzmann Distribution Of Activation Energies: Applications To A Polymorphic Transformation Under Crystallization Slurry Conditions And To The Thermal Decomposition Of AgMnO4 Crystals. J. Phys. Chem.B. 2005, 109(21),10611–10619. DOI: 10.1021/jp0519870.

[73] Plonka, A.;. Dispersive Kinetics. Annual Reports Section "C" (Physical Chemistry). 2001, 97(1),91–147. DOI: 10.1039/b100666p.

[74] Messerer, A.; Niessner, R.; Pöschl, U. Comprehensive Kinetic Characterization Of The Oxidation And Gasification Of Model And Real Diesel Soot By Nitrogen Oxides And Oxygen Under Engine Exhaust Conditions: Measurement, Langmuir– Hinshelwood, And Arrhenius Parameters. Carbon. 2006, 44(2),307–324. DOI: 10.1016/j.carbon.2005.07.017.

[75] Ciambelli, P.; D'Amore, M.; Palma, V.; Vaccaro, S. Catalytic Oxidation of an Amorphous Carbon Black. Combust. Flame. 1994, 99(2),413–421. DOI: 10.1016/0010-2180(94)90148-1.
[76] Darcy, P.; Da Costa, P.; Mellottée, H.; Trichard, J.-M.; Djéga-Mariadassou, G. Kinetics Of Catalyzed And Non-Catalyzed Oxidation Of Soot From A Diesel Engine. Catal. Today. 2007, 119(1–4),252–256. DOI: 10.1016/j.cattod.2006.08.056.
[77] López-Fonseca, R.; Landa, I.; Elizundia, U.; Gutiérrez-Ortiz, M. A.; González-Velasco, J. R. A Kinetic Study of the Combustion of Porous Synthetic Soot. Chem. Eng. J. 2007,129(1–3), 41–49. DOI: 10.1016/j.cej.2006.10.029.
[78] Jaramillo, I. C.; Gaddam, C. K.; Vander Wal, R. L.; Huang, C.-H.; Levinthal, J. D.; Lighty, J. S. Soot Oxidation Kinetics under Pressurized Conditions. Combust. Flame.2014, 161(11),2951–2965. DOI: 10.1016/j.combustflame.2014.04.016.
[79] Jaramillo, I. C.; Gaddam, C. K.; Vander Wal, R. L.; Lighty, J. S. Effect of Nanostructure, Oxidative Pressure and Extent of Oxidation on Model Carbon Reactivity. Combust. Flame. 2015, 162(5),1848–1856.
[80] Tighe, C. J.; Twigg, M. V.; Hayhurst, A. N.; Dennis, J. S. The Kinetics of Oxidation of Diesel Soots and a Carbon Black (Printex U) by O2 with Reference to Changes in Both Size and Internal Structure of the Spherules during Burnout. Carbon. 2016, 107, 20–35. DOI: 10.1016/j.carbon.2016.04.075.
[81] Jung, J.; Lee, J. H.; Song, S.; Chun, K. M. Measurement of Soot Oxidation with NO2-O2 -H2O in a Flow Reactor Simulating Diesel Engine DPF. Inter. J. Automo. Technol. 2008, 9(4),423–428. DOI: 10.1007/s12239-008-0051-4.
[82] Cooper, B. J.; Thoss, J. E. The Role of NO in Diesel Particulate Emission Control. SAE Paper. 1989, 890404.
[83] Cooper, B. J.; Radnor, H. J.; Jung, W.; Thoss, J. E., Treatment of Diesel Exhaust Gases. US patent 4,902,487, 1990. doi:10.1099/00221287-136-2-327
[84] Chen, S. G.; Yang, R. T.; Kapteijn, F.; Moulijn, J. A. A New Surface Oxygen Complex on Carbon: Toward A Unified Mechanism for Carbon Gasification Reactions. Ind. Eng. Chem. Res. 1993, 32(11),2835–2840. DOI: 10.1021/ie00023a054.
[85] Moulijn, J. A.; Kapteijn, F. Towards A Unified Theory Of Reactions Of Carbon With Oxygen-Containing Molecules. Carbon. 1995, 33(8),1155–1165. DOI: 10.1016/0008-6223(95)00070-T.
[86] Li, C.; Brown, T. C. Carbon Oxidation Kinetics From Evolved Carbon Oxide Analysis During Temperature-Programmed Oxidation. Carbon. 2001, 39(5),725–732. DOI:10.1016/S0008-6223(00)00189-5.
[87] Setiabudi, A.; Makkee, M.; Moulijn, J. A. The Role of NO2 and O2 in the Accelerated Combustion of Soot in Diesel Exhaust Gases. Appl. Catal. B. Environ. 2004, 50(3),185–194. DOI: 10.1016/j.apcatb.2004.01.004.
[88] Zawadzki, J.; Wiśniewski, M.; Skowrońska, K. Heterogeneous Reactions of NO2 and NO–O2 on the Surface of Carbons. Carbon. 2003, 41(2),235–246. DOI: 10.1016/S0008-6223(02)00281-6.
[89] Lure, B.A.; Mikhno, A.V. Interaction of NO_2 with Soot, Kinetics Catal 1997, 38, 490.
[90] Ehrburger, P., Brilhac, J., Drouillot, Y., Logie, V. et al., Reactivity of Soot with Nitrogen Oxides in Exhaust Stream," SAE Technical Paper 2002-01-1683, 2002, doi:10.4271/2002-01-1683.
[91] Muckenhuber, H.; Grothe, H. The Heterogeneous Reaction between Soot and NO2 at Elevated Temperature. Carbon. 2006, 44(3),546–559. DOI: 10.1016/j.carbon.2005.08.003.
[92] Jacquot, F.; Logie, V.; Brilhac, J.; Gilot, P. Kinetics of the Oxidation of Carbon Black by NO2. Carbon. 2002, 40(3),335–343. DOI: 10.1016/S0008-6223(01)00103-8.

[93] Jeguirim, M.; Tschamber, V.; Brilhac, J. F.; Ehrburger, P. Interaction Mechanism of NO2 with Carbon Black: Effect of Surface Oxygen Complexes. J. Anal. Appl. Pyrolysis.2004, 72(1),171–181. DOI: 10.1016/j.jaap.2004.03.008.
[94] Jeguirim, M.; Tschamber, V.; Brilhac, J. F.; Ehrburger, P. Oxidation Mechanism of Carbon Black by NO2: Effect of Water Vapour. Fuel. 2005, 84(14–15), 1949–1956. DOI: 10.1016/j.fuel.2005.03.026.
[95] Kandylas, I. P.; Haralampous, O. A.; Koltsakis, G. C. Diesel Soot Oxidation with NO2: Engine Experiments and Simulations. Ind. Eng. Chem. Res. 2002, 41, 5372. DOI:10.1021/ie020379t.
[96] Jeguirim, M.; Tschamber, V.; Brilhac, J. F. Kinetics Of Catalyzed And Non-Catalyzed Soot Oxidation With Nitrogen Dioxide Under Regeneration Particle Trap Conditions. J. Chem. Technol. Biotechnol. 2009, 84(5),770–776. DOI: 10.1002/jctb.v84:5.
[97] Tighe, C. J.; Twigg, M. V.; Hayhurst, A. N.; Dennis, J. S. The Kinetics of Oxidation of Diesel Soots by NO2. Combust. Flame. 2012, 159(1),77–90. DOI: 10.1016/j.combustflame.2011.06.009.
[98] Zouaoui, N.; Labaki, M.; Jeguirim, M. Diesel Soot Oxidation by Nitrogen Dioxide, Oxygen and Water under Engine Exhaust Conditions: Kinetics Data Related to the Reaction Mechanism. C. R. Chim. 2014, 17(7–8), 672–680. DOI: 10.1016/j.crci.2013.09.004.
[99] Fino, D.; Specchia, V. Compositional and Structural Optimal Design of a Nanostructured Diesel-Soot Combustion Catalyst for a Fast-Regenerating Trap. Chem. Eng. Sci. 2004, 59(22–23),\. DOI: 10.1016/j.ces.2004.07.012.
[100] Van Setten, B. A. A. L.; Schouten, J. M.; Makkee, M.; Moulijn, J. A. Realistic Contact for Soot with an Oxidation Catalyst for Laboratory Studies. Appl. Catal. B Environ. 2000,28(3–4),253–257. DOI: 10.1016/S0926-3373(00)00182-X.
[101] Krishna, K.; Makkee, M. Pt–Ce-Soot Generated From Fuel-Borne Catalysts: Soot Oxidation Mechanism. Top. Catal. 2007, 42(1–4), 229–236. DOI: 10.1007/s11244-007-0183-1.
[102] Nitsuta, M.; Ito, M. Remover Of Particle In Exhaust Gas. Jpn. Patent. 1988, 02, 173310.
[103] Sato, M.; Terada, M. Particulate Burning Catalyst Filter. Jpn. Patent. 1986, 63, 140810.
[104] Neri, G.; Bonaccorsi, L.; Donato, A.; Milone, C.; Musolino, M. G.; Visco, A. M. Catalytic Combustion of Diesel Soot over Metal Oxide Catalysts. Appl. Catal. B Environ. 1997, 11(2),217–231. DOI: 10.1016/S0926-3373(96)00045-8.
[105] Baumgarten, E.; Schuck, A. Oxygen Spillover and Its Possible Role in Coke Burning. Appl. Catal. 1988, 37(C), 247–257. DOI: 10.1016/S0166-9834(00)80764-2.
[106] Parera, J. M.; Traffano, E. M.; Musso, J. C.; Pieck, C. L. Hydrogen And Oxygen Spillover On Pt/Al2O3 During Naphtha Reforming. In Studies in Surface Science and Catalysis, G.M. Pajonk, S. J. Teichner, and J.E. Germain (Editors), Amsterdam: Elsevier; Vol. 17, 1983; pp 101–108.
[107] Ducarme, V.; Vedrine, J. C. Study Of Surface Atom Behaviour On Pt/SiO2 And Pt/Al2O3 Catalysts By Isotopic Exchange Of Oxygen From Co2. J. Chem. Soc. Faraday Trans.1 Phys. Chem. Condens. Phases. 1978, 74, 506.
[108] Abderrahim, H.; Duprez, D. Surface Diffusion Of Oxygen In Rh/Al2O3 And Pt/Al2O3 Catalysts. Stud. Surf. Sci. Catal. 1987, 30, 359–368.
[109] Oi Uchisawa, J.; Obuchi, A.; Zhao, Z.; Kushiyama, S. Carbon Oxidation with Platinum Supported Catalysts. Appl. Catal. B. 1998, 18(3–4), L183–L187.A. DOI: 10.1016/S0926-3373(98)00046-0.
[110] Oi-Uchisawa, J.; Obuchi, A.; Enomoto, R.; Liu, S.; Nanba, T.; Kushiyama, S. Catalytic Performance of Pt Supported on Various Metal Oxides in the Oxidation of Carbon

Black. Appl. Catal. B Environ. 2000, 26(1),17–24. DOI: 10.1016/S0926-3373(99)00142-3.

[111] Oi-Uchisawa, J.; Obuchi, A.; Enomoto, R.; Xu, J.; Nanba, T.; Liu, S.; Kushiyama, S. Oxidation Of Carbon Black Over Various Pt/MOx/SiC Catalysts. Appl. Catal. B Environ. 2001, 32(4),257–268. DOI: 10.1016/S0926-3373(01)00150-3.

[112] Oi-Uchisawa, J.; Obuchi, A.; Wang, S.; Nanba, T.; Ohi, A. Catalytic Performance Of Pt/MOx Loaded Over SiC-DPF For Soot Oxidation. Appl. Catal. B Environ. 2003, 43(2),117–129. DOI: 10.1016/S0926-3373(02)00296-5.

[113] Liu, S.; Obuchi, A.; Oi-Uchisawa, J.; Nanba, T.; Kushiyama, S. Synergistic Catalysis Of Carbon Black Oxidation By Pt With MoO3 Or V2o5. Appl. Catal. B Environ. 2001, 30(3–4), 259–265. DOI: 10.1016/S0926-3373(00)00238-1.

[114] Krishna, K.; Makkee, M. Soot Oxidation over NOx Storage Catalysts: Activity And Deactivation. Catal. Today. 2006, 114(1),48–56. DOI: 10.1016/j.cattod.2006.02.009.

[115] Castoldi, L.; Matarrese, R.; Lietti, L.; Forzatti, P. Simultaneous Removal Of NOx And Soot On Pt-Ba/Al2O3 Nsr Catalysts. Appl. Catal. B Environ. 2006, 64(1–2), 25–34. DOI:10.1016/j.apcatb.2005.10.015.

[116] Matarrese, R.; Castoldi, L.; Lietti, L.; Forzatti, P. Simultaneous Removal Of NOx And Soot Over Pt–Ba/Al2O3 And Pt–K/Al2O3 Dpnr Catalysts. Top. Catal. 2009, 52(13–20),2041–2046. DOI: 10.1007/s11244-009-9400-4.

[117] Matarrese, R.; Lietti, L.; Castoldi, L.; Busca, G.; Forzatti, P. Effect Of Soot During Operation Of A Pt-K/Al2O3LNT Catalyst. Top. Catal. 2013, 56(1–8),477–482. DOI: 10.1007/s11244-013-0001-x.

[118] Pieta, I. S.; García-Diéguez, M.; Herrera, C.; Larrubia, M. A.; Alemany, L. J. In Situ Drift–Trm Study Of Simultaneous NOx And Soot Removal Over Pt–Ba And Pt–K Nsr Catalysts. J. Catal. 2010, 270(2),256–267. DOI: 10.1016/j.jcat.2010.01.003.

[119] Shuang, L.; Xiaodong, W.; Duan, W.; Rui, R. NOx-Assisted Soot Oxidation On Pt–Mg/Al2O3 Catalysts: Magnesium Precursor, Pt Particle Size, And Pt–Mg Interaction. Ind. Eng. Chem. Res. 2012, 51(5),2271–2279. DOI: 10.1021/ie202239c.

[120] Dettling, J. C.; Skomoroski, R., Catalyzed Diesel Exhaust Particulate Filter. US Patent5,100,632, Engelhard Corporation, 1992

[121] Liu, S.; Wu, X.; Weng, D.; Li, M.; Lee, H.-R. Combined Promoting Effects Of Platinum And MnOx–CeO2 Supported On Alumina On NOx-assisted Soot Oxidation: Thermal Stability And Sulfur Resistance. Chem. Eng. J. 2012, 203, 25–35. DOI: 10.1016/j.cej.2012.06.090.

[122] Yu, X.; Li, J.; Wei, Y.; Zhao, Z.; Liu, J.; Jin, B.; Duan, A.; Jiang, G. Three-Dimensionally Ordered Macroporous MnxCe1-xOδ And Pt/Mn0.5Ce0.5Oδ Catalysts: Synthesis And Catalytic Performance For Soot Oxidation. Ind. Eng. Chem. Res. 2014, 53(23),9653–9664. DOI: 10.1021/ie500666m

[123] Ahlstrom, A. F.; Odenbrand, C. U. I. Combustion of Soot Deposits from Diesel Engines on Mixed Oxides of Vanadium Pentoxide and Cupric Oxide. Appl. Catal. 1990, 60(1),157–172. DOI: 10.1016/S0166-9834(00)82179-X.

[124] Watabe, Y.; Yamada, C.; Irako, K.; Murakami, Y. Catalyst for Use in Cleaning Exhaust Gas Particulates. European Patent 0092023, 1983

[125] Ciambelli, P.; Corbo, P.; Parrella, P.; Scialò, M.; Vaccaro, S. Catalytic Oxidation of Soot from Diesel Exhaust Gases: 1. Screening of Metal Oxide Catalysts by TG-DTG-DTA Analysis. Thermochim. Acta. 1990, 162, 83–89.

[126] Yuan, S.; Mériaudeau, P.; Perrichon, V. Catalytic Combustion Of Diesel Soot Particles On Copper Catalysts Supported On TiO2. Effect Of Potassium Promoter On The Activity. Appl. Catal. B. 1994, 3(4),319–333. DOI: 10.1016/0926-3373(94)00005-0.

[127] Laversin, H.; Courcot, D.; Zhilinskaya, E.; Cousin, R.; Aboukaïs, A. Study Of Active Species Of Cu-K/ZrO2 Catalysts Involved In The Oxidation Of Soot. J. Catal. 2006, 241 (2), 456–464. DOI: 10.1016/j.jcat.2006.05.006.

[128] Mul, G.; Neeft, J.; Kapteijn, F.; Makkee, M.; Moulijn, J. Soot Oxidation Catalyzed By A Cu/K/Mo/Cl Catalyst: Evaluation Of The Chemistry And Performance Of The Catalyst. Appl. Catal. B Environ. 1995, 6(4),339–352. DOI: 10.1016/0926-3373(95)00027-5.

[129] Neeft, J. P. A.; van Pruissen, O. P.; Makkee, M.; Moulijn, J. A. Catalysts for the Oxidation of Soot from Diesel Exhaust Gases II. Contact between Soot and Catalyst under Practical Conditions. Appl. Catal. B. 1997, 12(1),21–31.

[130] Badini, C.; Saracco, G.; Serra, V.; Specchia, V. Suitability of Some Promising Soot Combustion Catalysts for Application in Diesel Exhaust Treatment. Appl. Catal. B Environ. 1998, 18(1–2),137–150. DOI: 10.1016/S0926-3373(98)00038-1.

[131] Querini, C. A.; Ulla, M. A.; Requejo, F.; Soria, J.; Sedrán, U. A.; Miró, E. E. Catalytic Combustion Of Diesel Soot Particles. Activity And Characterization Of Co/MgO And Co,K/MgO Catalysts. Appl. Catal. B. 1998, 15(1–2), 5–19.

[132] Miró, E.; Ravelli, F.; Ulla, M.; Cornaglia, L.; Querini, C. Catalytic Combustion of Diesel Soot on Co, K Supported Catalysts. Catal. Today. 1999, 53(4),631–638. DOI: 10.1016/S0920-5861(99)00151-0.

[133] Pisarello, M.; Milt, V.; Peralta, M.; Querini, C.; Miró, E. Simultaneous Removal of Soot and Nitrogen Oxides from Diesel Engine Exhausts. Catal. Today. 2002, 75(1–4),465–470. DOI: 10.1016/S0920-5861(02)00097-4.

[134] Peralta, M. A.; Zanuttini, M. S.; Querini, C. A. Activity And Stability Of BaKCo/CeO2 Catalysts For Diesel Soot Oxidation. Appl. Catal. B Environ. 2011, 110, 90–98. DOI:10.1016/j.apcatb.2011.08.030.

[135] Sui, L.; Yu, L. Diesel Soot Oxidation Catalyzed By Co-Ba-K Catalysts: Evaluation Of The Performance Of The Catalysts. Chem. Eng. J. 2008, 142(3),327–330. DOI: 10.1016/j.cej.2008.04.009.

[136] Dhakad, M.; Mitshuhashi, T.; Rayalu, S.; Doggali, P.; Bakardjiva, S.; Subrt, J.; Fino, D.; Haneda, H.; Labhsetwar, N. Co3O4–CeO2 Mixed Oxide-Based Catalytic Materials For Diesel Soot Oxidation. Catal. Today. 2008, 132(1–4),188–193. DOI: 10.1016/j.cattod.2007.12.035.

[137] Dhakad, M.; Joshi, A. G.; Rayalu, S.; Tanwar, P.; Bassin, J. K.; Kumar, R.; Lokhande, S.; Subrt, J.; Mitsuhashi, T.; Labhsetwar, N. Alumina Supported Co–K–Mo Based Catalytic Material For Diesel Soot Oxidation. Top. Catal. 2009, 52(13–20),2070–2075. DOI:10.1007/s11244-009-9403-1.

[138] Atribak, I.; Suchbasanez, I.; Buenolopez, A.; Garcia, A. Comparison Of The Catalytic Activity Of Mo2 (M=Ti, Zr, Ce) For Soot Oxidation Under NOx/O2. J. Catal. 2007, 250 [156] (1), 75–84. DOI: 10.1016/j.jcat.2007.05.015

[139] Gross, M. S.; Sánchez, B. S.; Querini, C. A. Diesel Particulate Matter Combustion With CeO2 As Catalyst. Part Ii: Kinetic And Reaction Mechanism. Chem. Eng. J. 2011, 168 (1), 413–419.

[140] Gross, M. S.; Ulla, M. A.; Querini, C. A. Diesel Particulate Matter Combustion With CeO2 As Catalyst. Part I: System Characterization And Reaction Mechanism. J. Mol. Catal. A Chem. 2012, 352, 86–94.

[141] Muroyama, H.; Hano, S.; Matsui, T.; Eguchi, K. Catalytic Soot Combustion Over CeO2-based Oxides. Catal. Today. 2010, 153(3–4),133–135. DOI: 10.1016/j.cattod.2010.02.015.

[142] Fu, M.; Yue, X.; Ye, D.; Ouyang, J.; Huang, B.; Wu, J.; Liang, H. Soot Oxidation Via CuO Doped CeO2 Catalysts Prepared Using Coprecipitation And Citrate Acid

Complex-Combustion Synthesis. Catal. Today. 2010, 153(3–4),125–132. DOI:10.1016/j.cattod.2010.03.017.
[143] Weng, D.; Li, J.; Wu, X.; Si, Z. Nox-Assisted Soot Oxidation Over K/CuCe Catalyst. J. Rare Earths. 2010, 28(4),542–546. DOI: 10.1016/S1002-0721(09)60150-2.
[144] Wang, J.; Cheng, L.; An, W.; Xu, J.; Men, Y. Boosting Soot Combustion Efficiencies Over CuO–CeO2 Catalysts With A 3dom Structure. Catal. Sci. Technol. 2016, 6 (19),7342–7350. DOI: 10.1039/C6CY01366J.
[145] Sun, S.; Chu, W.; Yang, W. Ce-Al Mixed Oxide With High Thermal Stability For Diesel Soot Combustion. Chinese J. Catal. 2009, 30(7),685–689. DOI: 10.1016/S1872-2067(08)60118-7.
[146] Wu, X.; Liu, S.; Weng, D.; Lin, F.; Ran, R. MnOx–CeO2–Al2O3 Mixed Oxides For Soot Oxidation: Activity And Thermal Stability. J. Hazard. Mater. 2011, 187(1–3),283–290. DOI: 10.1016/j.jhazmat.2011.01.068.
[147] Lin, F.; Wu, X.; Liu, S.; Weng, D.; Huang, Y. Preparation Of MnOx–CeO2–Al2O3 Mixed Oxides For NOx-assisted Soot Oxidation: Activity, Structure And Thermal Stability. Chem. Eng. J. 2013, 226(x), 105–112. DOI: 10.1016/j.cej.2013.04.006.
[148] Liang, Q.; Wu, X.; Wu, X.; Weng, D. Role Of Surface Area In Oxygen Storage Capacity Of Ceria–Zirconia As Soot Combustion Catalyst. Catal. Letters. 2007, 119(3–4),265–270. DOI: 10.1007/s10562-007-9228-0.
[149] Atribak, I.; Azambre, B.; Bueno López, A.; García-García, A. Effect Of NOx Adsorption/Desorption Over Ceria-Zirconia Catalysts On The Catalytic Combustion Of Model Soot. Appl. Catal. B Environ. 2009, 92(1–2),126–137. DOI: 10.1016/j.apcatb.2009.07.015.
[150] Atribak, I.; Buenolopez, A.; Garcia-Garcia, A. Combined Removal Of Diesel Soot Particulates And NO x Over CeO2–ZrO2 Mixed Oxides. J. Catal. 2008, 259(1),123–132. DOI: 10.1016/j.jcat.2008.07.016.
[151] Oliveira, C. F.; Garcia, F. A. C.; Araújo, D. R.; Macedo, J. L.; Dias, S. C. L.; Dias, J. A. Effects of Preparation and Structure of Cerium-Zirconium Mixed Oxides on Diesel Soot Catalytic Combustion. Appl. Catal. A Gen. 2012, 413–414, 292–300. DOI: 10.1016/j.apcata.2011.11.020.
[152] Piumetti, M.; Bensaid, S.; Russo, N.; Fino, D. Investigations into Nanostructured Ceria–Zirconia Catalysts for Soot Combustion. Appl. Catal. B Environ. 2016, 180, 271–282. DOI: 10.1016/j.apcatb.2015.06.018.
[153] Atribak, I.; Bueno-López, A.; García-García, A. Role of Yttrium Loading in the PhysicoChemical Properties and Soot Combustion Activity of Ceria and Ceria–Zirconia Catalysts. J. Mol. Catal. A Chem. 2009, 300(1–2),103–110. DOI: 10.1016/j.molcata.2008.10.043.
[154] Weng, D.; Li, J.; Wu, X.; Si, Z. Modification Of CeO2-ZrO2 Catalyst By Potassium For NOx-assisted Soot Oxidation. J. Environ. Sci. 2011, 23(1),145–150. DOI: 10.1016/S1001-0742(10)60386-5.
[155] Khobragade, R.; Einaga, H.; Jain, S.; Saravanan, G.; Labhsetwar, N. Sulfur Dioxide-Tolerant Strontium Chromate for the Catalytic Oxidation of Diesel Particulate Matter. Catal. Sci. Technol. 2018, 8(6),1712–1721.
[156] Zhou, X.; Chen, H.; Zhang, G.; Wang, J.; Xie, Z.; Hua, Z.; Zhang, L.; Shi, J. Cu/Mn Co-Loaded Hierarchically Porous Zeolite Beta: A Highly Efficient Synergetic Catalyst For Soot Oxidation. J. Mater. Chem. A. 2015, 3(18),9745–9753. DOI: 10.1039/C5TA00094G.
[157] Nanba, T.; Masukawa, S.; Abe, A.; Uchisawa, J.; Obuchi, A. Morphology Of Active Species Of Ag/ZrO2 For Low-Temperature Soot Oxidation By Oxygen. Catal. Sci. Technol. 2012, 2(9), 1961. DOI: 10.1039/c2cy00546h.

[158] Shen, Q.; Wu, M.; Wang, H.; He, C.; Hao, Z.; Wei, W.; Sun, Y. Facile Synthesis Of Catalytically Active CeO2 For Soot Combustion. Catal. Sci. Technol. 2015, 5(3),1941–1952. DOI: 10.1039/C4CY01435A.

[159] Piumetti, M.; Andana, T.; Bensaid, S.; Fino, D.; Russo, N.; Pirone, R. Ceria-Based Nanomaterials As Catalysts For Co Oxidation And Soot Combustion: Effect Of Zr-Pr Doping And Structural Properties On The Catalytic Activity. AIChE J. 2017, 63(1),216–225. DOI: 10.1002/aic.v63.1.

[160] Voorhoeve, R. J. H.; Remeika, J. P.; Freeland, P. E.; Matthias, B. T. Rare-Earth Oxides Of Manganese And Cobalt Rival Platinum For The Treatment Of Carbon Monoxide In Auto Exhaust. Science. 1972, 177(4046),353–354. DOI: 10.1126/science.177.4046.353.

[161] Voorhoeve, R. J. H.; Remeika, J. P.; Johnson, D. W. Rare-Earth Manganites: Catalysts With Low Ammonia Yield In The Reduction Of Nitrogen Oxides. Science. 1973, 180 (4081), 62–64. DOI: 10.1126/science.180.4081.62.

[162] Gallagher, P.K.; JohnsonJr., D.W.; Schrey, F. Studies of some supported perovskite oxidation catalysts, Mat. Res. Bull. 1974, 9. 1345–1352. doi: 10.1016/0025-5408(74)90057-9.

[163] Zhu, J.; Thomas, A. Perovskite-Type Mixed Oxides as Catalytic Material for NO Removal. Appl. Catal. B Environ. 2009, 92(3–4),225–233. DOI: 10.1016/j.apcatb.2009.08.008.

[164] Goldschmidt, V. M. Die Gesetze Der Krystallochemie. Naturwissenschaften. 1926, 14 (21),477–485. DOI: 10.1007/BF01507527.

[165] Zhong, Z.; Chen, K.; Ji, Y.; Yan, Q. Methane Combustion Over B-Site Partially Substituted Perovskite-Type LaFeO3 Prepared By Sol-Gel Method. Appl. Catal.A Gen. 1997, 156(1),29–41. DOI: 10.1016/S0926-860X(97)00003-3.

[166] Zhang, R.; Villanueva, A.; Alamdari, H.; Kaliaguine, S. Catalytic Reduction Of No By Propene Over LaCo1-xCuxO3 Perovskites Synthesized By Reactive Grinding. Appl. Catal. B Environ. 2006, 64(3–4),220–233. DOI: 10.1016/j.apcatb.2005.10.028.

[167] Russo, N.; Palmisano, P.; Fino, D. Pd Substitution Effects on Perovskite Catalyst Activity for Methane Emission Control. Chem. Eng. J. 2009, 154(1–3),137–141. DOI:10.1016/j.cej.2009.05.015.

[168] Patel, F.; Patel, S. Recent Trends in Catalyst Development for Diesel Engine Exhaust Emission Control. J. Environ. Res. Dev. 2012, 6(4),1047–1054.

[169] Wang, Q.; Chung, J. S.; Guo, Z. Promoted Soot Oxidation By Doped K2Ti2O5 Catalysts And No Oxidation Catalysts. Ind. Eng. Chem. Res. 2011, 50(13),8384–8388. DOI:10.1021/ie200698j.

[170] Junwu, Z.; Xiaojie, S.; Yanping, W.; Xin, W.; Xujie, Y.; Lude, L. Solution-Phase Synthesis And Characterization Of Perovskite LaCoO3 Nanocrystals Via A Co-Precipitation Route. J. Rare Earths. 2007, 25(5),601–604. DOI: 10.1016/S1002-0721(07)60570-5.

[171] Muneeswaran, M.; Jegatheesan, P.; Giridharan, N. V. Synthesis Of Nanosized BiFeO3 Powders By Co-Precipitation Method. J. Exp. Nanosci. 2013, 8(3),341–346. DOI:10.1080/17458080.2012.685954.

[172] Shabbir, G.; Qureshi, A. H.; Saeed, K. Nano-Crystalline LaFeO3 Powders Synthesized By The Citrate–Gel Method. Mater. Lett. 2006, 60(29–30),3706–3709. DOI: 10.1016/j.matlet.2006.03.093.

[173] Guo, X.; Meng, M.; Dai, F.; Li, Q.; Zhang, Z.; Jiang, Z.; Zhang, S.; Huang, Y. NOxassisted Soot Combustion Over Dually Substituted Perovskite Catalysts La1-xKxCo1-yPdyO3-δ. Appl. Catal. B Environ. 2013, 142–143(2),278–289. DOI: 10.1016/j.apcatb.2013.05.036.

[174] Fino, D.; Russo, N.; Saracco, G.; Specchia, V. The Role of Suprafacial Oxygen in Some Perovskites for the Catalytic Combustion of Soot. J. Catal. 2003, 217(2),367–375. DOI:10.1016/S0021-9517(03)00143-X.
[175] Purohit, R. D.; Tyagi, A. K.; Mathews, M. D.; Saha, S. Combustion Synthesis and Bulk Thermal Expansion Studies of Ba and Sr Thorates. J. Nucl. Mater. 2000, 280(1),51–55. DOI: 10.1016/S0022-3115(00)00026-X.
[176] Teraoka, Y.; Kanada, K.; Kagawa, S. Synthesis Of La-K-Mn-O Perovskite-Type Oxides And Their Catalytic Property For Simultaneous Removal Of {No} And Diesel Soot Particulates. Appl. Catal. B Environ. 2001, 34(1),73–78. DOI: 10.1016/S0926-3373(01)00202-8.
[177] Tang, P.; Zhang, J.; Fu, M.; Cao, F.; Lv, C. Characterization And Preparation Nanosized CeFeO3 By A Microwave Process. Integr. Ferroelectr. 2013, 146(1),99–104. DOI: 10.1080/10584587.2013.789756.
[178] Ji, K.; Dai, H.; Deng, J.; Zhang, L.; Jiang, H.; Xie, S.; Han, W. One-Pot Hydrothermal Preparation and Catalytic Performance of Porous Strontium Ferrite Hollow Spheres for the Combustion of Toluene. J. Mol. Catal. A Chem. 2013, 370, 189–196. DOI: 10.1016/j.molcata.2013.01.013.
[179] Gao, P.; Li, N.; Wang, A.; Wang, X.; Zhang, T. Perovskite LaMnO3 Hollow Nanospheres: The Synthesis And The Application In Catalytic Wet Air Oxidation Of Phenol. Mater. Lett. 2013, 92, 173–176. DOI: 10.1016/j.matlet.2012.10.091.
[180] Rumplecker, A.; Kleitz, F.; Salabas, E.-L.; Schüth, F. Hard Templating Pathways For The Synthesis Of Nanostructured Porous Co3O4. Chem. Mater. 2007, 19(3),485–496. DOI: 10.1021/cm0610635.
[181] Imhof, A.; Pine, D. J. Ordered Macroporous Materials by Emulsion Templating. Nature. 1997, 389(6654),948–951. DOI: 10.1038/40105.
[182] Fino, D.; Fino, P.; Saracco, G.; Specchia, V. Diesel Particulate Traps Regenerated by Catalytic Combustion. Korean J. Chem. Eng. 2003, 20(3),445–450. DOI: 10.1007/BF02705545.
[183] Ifrah, S.; Kaddouri, A.; Gelin, P.; Bergeret, G. On The Effect Of La–Cr–O– Phase Composition On Diesel Soot Catalytic Combustion. Catal. Commun. 2007, 8(12),2257–2262. DOI: 10.1016/j.catcom.2007.04.039.
[184] Cauda, E.; Fino, D.; Saracco, G.; Specchia, V. Nanosized Pt-Perovskite Catalyst For The Regeneration Of A Wall-Flow Filter For Soot Removal From Diesel Exhaust Gases. Top. Catal. 2004, 30/31(July 2004), 299–303. DOI: 10.1023/B:TOCA.0000029766.91816.d2.
[185] Russo, N.; Fino, D.; Saracco, G.; Specchia, V. Studies on the Redox Properties of Chromite Perovskite Catalysts for Soot Combustion. J. Catal. 2005, 229(2),459–469. DOI: 10.1016/j.jcat.2004.11.025.
[186] Mescia, D.; Cauda, E.; Russo, N.; Fino, D.; Saracco, G.; Specchia, V. Towards Practical Application of Lanthanum Chromite Catalysts for Diesel Particulate Combustion. Catal. Today. 2006, 117(1–3),369–375. DOI: 10.1016/j.cattod.2006.05.034.
[187] Fino, D.; Russo, N.; Cauda, E.; Saracco, G.; Specchia, V. La–Li–Cr Perovskite Catalysts For Diesel Particulate Combustion. Catal. Today. 2006, 114(1),31–39. DOI: 10.1016/j.cattod.2006.02.007.
[188] Iojoiu, E.; Bassou, B.; Guilhaume, N.; Farrusseng, D.; Desmartinchomel, A.;Lombaert, K.; Bianchi, D.; Mirodatos, C. High-Throughput Approach to the CatalyticCombustion of Diesel Soot. Catal. Today. 2008, 137(1),103–109. DOI: 10.1016/j.cattod.2008.02.016.
[189] Li, S.; Kato, R.; Wang, Q.; Yamanaka, T.; Takeguchi, T.; Ueda, W. Soot Trapping And Combustion On Nanofibrous Perovskite LaMnO3 Catalysts Under A Continuous Flow

Of Soot. Appl. Catal. B Environ. 2010, 93(3–4),383–386. DOI: 10.1016/j.apcatb.2009.10.012.

[190] Wang, H. The Catalytic Behavior Of La-Mn-O Nanoparticle Perovskite-Type Oxide Catalysts For The Combustion Of The Soot Particle From The Diesel Engine. Chinese Sci. Bull. 2005, 50(14),1440. DOI: 10.1360/982004-203.

[191] Wang, H.; Zhao, Z.; Xu, C.; Liu, J. Nanometric La1-xKxMnO3 Perovskite-Type Oxides –Highly Active Catalysts For The Combustion Of Diesel Soot Particle Under Loose Contact Conditions. Catal. Letters. 2005, 102(3–4),251–256. DOI: 10.1007/s10562-005-5864-4.

[192] Li, L.; Shen, X.; Wang, P.; Meng, X.; Song, F. Soot Capture And Combustion For Perovskite La–Mn–O Based Catalysts Coated On Honeycomb Ceramic In Practical Diesel Exhaust. Appl. Surf. Sci. 2011, 257(22),9519–9524. DOI: 10.1016/j.apsusc.2011.06.050.

[193] Shimokawa, H.; Kusaba, H.; Einaga, H.; Teraoka, Y. Effect Of Surface Area Of La–K–Mn–O Perovskite Catalysts On Diesel Particulate Oxidation. Catal. Today. 2008, 139 (1–2), 8–14. DOI: 10.1016/j.cattod.2008.08.003.

[194] Peng, X.; Lin, H.; Shangguan, W.; Huang, Z. A Highly Efficient And Porous Catalyst For Simultaneous Removal Of NOx And Diesel Soot. Catal. Commun. 2007, 8(2),157–161. DOI: 10.1016/j.catcom.2006.04.015.

[195] Fujimoto, J.; Masuda, K.; Hanaki, Y.; Munakata, F. Particulate Matter Oxidation On Ruddlesden–Popper-type, La1.8Sr1.2Mn2O7. J. Ceram. Soc. Jpn. 2011, 119(1385),85–87. DOI: 10.2109/jcersj2.119.85.

[196] Pecchi, G.; Dinamarca, R.; Campos, C. M.; Garcia, X.; Jimenez, R.; Fierro, J. L. G. Soot Oxidation On Silver-Substituted LaMn0.9Co0.1O3 Perovskites. Ind. Eng. Chem. Res. 2014, 53(24),10090–10096. DOI: 10.1021/ie501277x.

[197] Wu, X.; Ran, R.; Weng, D. NO2-aided Soot Oxidation On LaMn0.7Ni0.3O3 Perovkite-Type Catalyst. Catal. Letters. 2009, 131(3–4), 494–499. DOI: 10.1007/s10562-009-9917-y.

[198] Zheng, J.; Liu, J.; Zhao, Z.; Xu, J.; Duan, A.; Jiang, G. The Synthesis And Catalytic Performances Of Three-Dimensionally Ordered Macroporous Perovskite-Type LaMn1-xFexO3 Complex Oxide Catalysts With Different Pore Diameters For Diesel Soot Combustion. Catal. Today. 2012, 191(1),146–153. DOI: 10.1016/j.cattod.2011.12.013.

[199] Teraoka, Y.; Nakano, K.; Kagawa, S.; Shangguan, W. F. Simultaneous Removal Of Nitrogen Oxides And Diesel Soot Particulates Catalyzed By Perovskite-Type Oxides. Appl. Catal. B Environ. 1995, 5, L181–L185. DOI: 10.1016/0926-3373(94)00059-X.

[200] Gong, C.; Song, C.; Pei, Y.; Lv, G.; Fan, G. Synthesis Of La0.9K0.1CoO3 Fibers And The Catalytic Properties For Diesel Soot Removal. Ind. Eng. Chem. Res. 2008, 47(13),4374–4378. DOI: 10.1021/ie071599f.

[201] Xu, J.; Liu, J.; Zhao, Z.; Xu, C.; Zheng, J.; Duan, A.; Jiang, G. Easy Synthesis Of Three-Dimensionally Ordered Macroporous La1-xKxCoO3 Catalysts And Their High Activities For The Catalytic Combustion Of Soot. J. Catal. 2011, 282(1),1–12. DOI:10.1016/j.jcat.2011.03.024.

[202] Feng, N.; Chen, C.; Meng, J.; Wu, Y.; Liu, G.; Wang, L.; Wan, H.; Guan, G. Facile Synthesis Of Three-Dimensionally Ordered Macroporous Silicon-Doped La0.8K0.2CoO3 Perovskite Catalysts For Soot Combustion. Catal. Sci. Technol. 2016, 6(21),7718–7728.DOI: 10.1039/C6CY00677A.

[203] Liu, J.; Zhao, Z.; Lan, J.; Xu, C.; Duan, A.; Jiang, G.; Wang, X.; He, H. Catalytic Combustion of Soot over the Highly Active (La0.9k0.1coo3)X/Nmceo2 Catalysts. J. Phys. Chem. C. 2009, 113(39),17114–17123. DOI: 10.1021/jp9056303.

[204] Bin, F.; Song, C.; Lv, G.; Song, J.; Gong, C.; Huang, Q. La1-xKxCoO3 And LaCo1-y FeyO3 Perovskite Oxides: Preparation, Characterization, And Catalytic Performance In The Simultaneous Removal Of No X And Diesel Soot. Ind. Eng. Chem. Res. 2011, 50 (11),6660–6667. DOI: 10.1021/ie200196r.

[205] Zhang, G.; Zhao, Z.; Liu, J.; Xu, J.; Jing, Y.; Duan, A.; Jiang, G. Macroporous Perovskite-Type Complex Oxide Catalysts Of La1-xKxCo1-yFeyO3 For Diesel Soot Combustion. J. Rare Earths. 2009, 27(6),955–960. DOI: 10.1016/S1002-0721(08) 60369-5.

[206] Li, Z.; Meng, M.; Zha, Y.; Dai, F.; Hu, T.; Xie, Y.; Zhang, J. Highly Efficient Multifunctional Dually-Substituted Perovskite Catalysts La1-xKxCo1-yCuyO3-δ Used For Soot Combustion, NOx Storage And Simultaneous NOx-Soot Removal. Appl. Catal. B Environ. 2012, 121–122(x), 65–74. DOI: 10.1016/j.apcatb.2012.03.022.

[207] Li, Z.; Meng, M.; Dai, F.; Hu, T.; Xie, Y.; Zhang, J. Performance Of K And Ni Substituted La1-xKxCo1-yNiyO3-δ Perovskite Catalysts Used For Soot Combustion, NOx Storage And Simultaneous NOx-Soot Removal. Fuel. 2012, 93, 606–610. DOI: 10.1016/j.fuel.2011.10.040.

[208] Guo, X.; Meng, M.; Dai, F.; Li, Q.; Zhang, Z.; Jiang, Z.; Zhang, S.; Huang, Y. NOxAssisted Soot Combustion Over Dually Substituted Perovskite Catalysts La1-xKxCo1-y PdyO3. Appl. Catal. B. 2013, 142–143(2),278–289. DOI: 10.1016/j.apcatb.2013.05.036.

[209] Russo, N.; Furfori, S.; Fino, D.; Saracco, G.; Specchia, V. Lanthanum Cobaltite Catalysts for Diesel Soot Combustion. Appl. Catal. B Environ. 2008, 83(1–2),85–95. DOI: 10.1016/j.apcatb.2008.02.006.

[210] Hong, -S.-S.; Lee, G.-D. Simultaneous Removal of NO and Carbon Particulates over Lanthanoid Perovskite-Type Catalysts. Catal. Today. 2000, 63(2–4),397–404. DOI: 10.1016/S0920-5861(00)00484-3.

[211] Zhang, R.; Luo, N.; Chen, B.; Kaliaguine, S. Soot Combustion over Lanthanum Cobaltites and Related Oxides for Diesel Exhaust Treatment. Energy Fuels. 2010, 24 (7), 3719–3726. DOI: 10.1021/ef901279w.

[212] Taniguchi, K.; Hirano, T.; Tosho, T.; Akiyama, T. Mechanical Activation Of Self-Propagating High-Temperature-Synthesized LaFeO3 To Be Used As Catalyst For Diesel Soot Oxidation. Catal. Letters. 2009, 130(3–4),362–366. DOI: 10.1007/s10562-009-9953-7.

[213] Hirano, T.; Tosho, T.; Watanabe, T.; Akiyama, T. Self-Propagating High-Temperature Synthesis With Post-Heat Treatment Of La1-xSrxFeO3 (X=0–1) Perovskite As Catalyst For Soot Combustion. J. Alloys Compd. 2009, 470(1–2),245–249. DOI: 10.1016/j.jallcom.2008.02.038.

[214] Sadakane, M.; Asanuma, T.; Kubo, J.; Ueda, W. Facile Procedure To Prepare Three-Dimensionally Ordered Macroporous (3dom) Perovskite-Type Mixed Metal Oxides By Colloidal Crystal Templating Method. Chem. Mater. 2005, 17(13),3546–3551. DOI: 10.1021/cm050551u.

[215] Jiménez, R.; Zamora, R.; Pecchi, G.; García, X.; Gordon, A. L. Effect Of Ca-Substitution In La1-xCaxFeO3 Perovskites On The Catalytic Activity For Soot Combustion. Fuel Process. Technol. 2010, 91(5),546–549. DOI: 10.1016/j.fuproc.2009.12.017.

[216] Wei, Y.; Liu, J.; Zhao, Z.; Chen, Y.; Xu, C.; Duan, A.; Jiang, G.; He, H. Highly Active Catalysts Of Gold Nanoparticles Supported On Three-Dimensionally Ordered Macroporous LaFeO3 For Soot Oxidation. Angew. Chemie Int. Ed. 2011, 50 (10),2326–2329. DOI: 10.1002/anie.201006014.

[217] Feng, N.; Chen, C.; Meng, J.; Liu, G.; Fang, F.; Wang, L.; Wan, H.; Guan, G. K–Mn Supported On Three-Dimensionally Ordered Macroporous La0.8Ce0.2FeO3 Catalysts

For The Catalytic Combustion Of Soot. Appl. Surf. Sci. 2017, 399, 114–122. DOI:10.1016/j.apsusc.2016.12.066.

[218] Mescia, D.; Caroca, J. C.; Russo, N.; Labhsetwar, N.; Fino, D.; Saracco, G.; Specchia, V. Towards A Single Brick Solution For The Abatement Of NOx And Soot From Diesel Engine Exhausts. Catal. Today. 2008, 137(2–4),300–305. DOI: 10.1016/j.cattod.2007.11.010.

[219] Xu, J.; Liu, J.; Zhao, Z.; Zheng, J.; Zhang, G.; Duan, A.; Jiang, G. Three-Dimensionally Ordered Macroporous LaCoxFe1-xO3 Perovskite-Type Complex Oxide Catalysts For Diesel Soot Combustion. Catal. Today. 2010, 153(3–4),136–142. DOI: 10.1016/j.cattod.2010.01.063.

[220] Labhsetwar, N. K.; Watanabe, A.; Mitsuhashi, T. New Improved Syntheses Of LaRuO3 Perovskites And Their Applications In Environmental Catalysis. Appl. Catal. B Environ. 2003, 40(1),21–30. DOI: 10.1016/S0926-3373(02)00123-6.

[221] Fino, D.; Fino, P.; Saracco, G.; Specchia, V. Studies On Kinetics And Reactions Mechanism Of La2-xKxCu1-yVyO4 Layered Perovskites For The Combined Removal Of Diesel Particulate And NOx. Appl. Catal. B Environ. 2003, 43(3),243–259. DOI: 10.1016/S0926-3373(02)00311-9.

[222] Liu, J.; Zhao, Z.; Xu, C.; Duan, A. Simultaneous Removal Of NOx And Diesel Soot Over Nanometer Ln-Na-Cu-O Perovskite-Like Complex Oxide Catalysts. Appl. Catal. B Environ. 2008, 78(1–2),61–72. DOI: 10.1016/j.apcatb.2007.09.001.

[223] Liu, J.; Zhao, Z.; Xu, C.; Duan, A.; Jiang, G. The Structures, Adsorption Characteristics Of La–Rb–Cu–O Perovskite-Like Complex Oxides, And Their Catalytic Performances For The Simultaneous Removal Of Nitrogen Oxides And Diesel Soot. J. Phys. Chem. C.2008, 112(15),5930–5941. DOI: 10.1021/jp709640f.

[224] Zhao, B.; Wang, R.; Yang, X. Simultaneous Catalytic Removal Of NOx And Diesel Soot Particulates Over La1-xCexNiO3 Perovskite Oxide Catalysts. Catal. Commun. 2009, 10 (7), 1029–1033. DOI: 10.1016/j.catcom.2008.10.024.

[225] Ma, Z.; Gao, X.; Yuan, X.; Zhang, L.; Zhu, Y.; Li, Z. Simultaneous Catalytic Removal Of NOx And Diesel Soot Particulates Over La2-xAxNi1-yByO4 Perovskite-Type Oxides. Catal. Commun. 2011, 12(9),817–821. DOI: 10.1016/j.catcom.2011.01.023.

[226] Cauda, E.; Fino, D.; Saracco, G.; Specchia, V. Preparation and Regeneration of a Catalytic Diesel Particulate Filter. Chem. Eng. Sci. 2007, 62(18–20),5182–5185. DOI: 10.1016/j.ces.2006.12.048.

[227] Megarajan, S. K.; Rayalu, S.; Nishibori, M.; Teraoka, Y.; Labhsetwar, N. Effects Of Surface And Bulk Silver On PrMnO3+δ Perovskite For Co And Soot Oxidation: Experimental Evidence For The Chemical State Of Silver. ACS Catal. 2015, 5(1),301–309. DOI: 10.1021/cs500880w.

[228] Białobok, B.; Trawczyński, J.; Rzadki, T.; Miśta, W.; Zawadzki, M. Catalytic Combustion Of Soot Over Alkali Doped SrTiO3. Catal. Today. 2007, 119(1–4),278–285. DOI: 10.1016/j.cattod.2006.08.024.

[229] Ura, B.; Trawczyński, J.; Kotarba, A.; Bieniasz, W.; Illán-Gómez, M. J.; Bueno- López, A.; López-Suárez, F. E. Effect Of Potassium Addition On Catalytic Activity Of SrTiO3 Catalyst For Diesel Soot Combustion. Appl. Catal. B Environ. 2011, 101(3–4),169–175. DOI: 10.1016/j.apcatb.2010.09.018.

[230] Ura, B.; Trawczyński, J.; Zawadzki, M.; Gomez, M. J. I.; Lopez, A. B.; Suarez, F. E. L. Sr1-Xkxtio3 Catalysts for Diesel Soot Combustion. Catal. Today. 2011, 176(1),169–172. DOI: 10.1016/j.cattod.2010.11.097.

[231] Dhakad, M.; Rayalu, S. S.; Kumar, R.; Doggali, P.; Bakardjieva, S.; Subrt, J.; Mitsuhashi, T.; Haneda, H.; Labhsetwar, N. Low Cost, Ceria Promoted Perovskite Type Catalysts

for Diesel Soot Oxidation. Catal. Letters. 2008, 121(1–2),137–143.DOI: 10.1007/s10562-007-9310-7.

[232] Shangguan, W.; Teraoka, Y. Kagawa S.Simultaneous Catalytic Removal Of NOx And Diesel Soot Particulates Over Ternary Ab2o4 Spinel-Type Oxides. Appl. Catal. B. 1996, 8(2),217–227. DOI: 10.1016/0926-3373(95)00070-4.

[233] Shangguan, W.; Teraoka, Y.; Kagawa, S. Promotion Effect Of Potassium On The Catalytic Property Of CuFe2O4 For The Simultaneous Removal Of NOx And Diesel Soot Particulate. Appl. Catal. B Environ. 1998, 16, 149–154. DOI: 10.1016/S0926-3373(97)00068-4.

[234] Liu, G.; Huang, Z.; Shangguan, W.; Yan, C. Simultaneously Catalytic Removal Of NOx And Particulate Matter On Diesel Particulate Filter. Chinese Sci. Bull. 2003, 48(3),305–308. DOI: 10.1007/BF03183304.

[235] Fino, D.; Russo, N.; Saracco, G.; Specchia, V. Catalytic Removal Of NOx And Diesel Soot Over Nanostructured Spinel-Type Oxides. J. Catal. 2006, 242, 38–47. DOI:10.1016/j.jcat.2006.05.023.

[236] Fino, D.; Russo, N.; Saracco, G.; Specchia, V. Removal Of NOx And Diesel Soot Over Catalytic Traps Based On Spinel-Type Oxides. Powder Technol. 2008, 180(1–2), 74–78. DOI: 10.1016/j.powtec.2007.03.003.

[237] Li, Y.-J.; Lin, H.; Shangguan, W.-F.; Huang, Z. Properties Of BaAl2O4 In The Simultaneous Removal Of Soot And NOx. Chem. Eng. Technol. 2007, 30(10),1426–1433. DOI: 10.1002/(ISSN)1521-4125. 2040

[238] Lin, H.; Li, Y.; Shangguan, W.; Huang, Z. Soot Oxidation And NOx Reduction Over BaAl2O4 Catalyst. Combust. Flame. 2009, 156(11),2063–2070. DOI: 10.1016/jcombustflame.2009.08.006. .

[239] Lee, Y. H.; Lee, G.-D.; Park, S. S.; Hong, -S.-S. Catalytic Removal Of Carbon Particulates Over MgFe2O4 Catalysts. React. Kinet. Catal. Lett. 2005, 84(2),311–317. DOI: 10.1007/s11144-005-0224-3.

[240] Zawadzki, M.; Staszak, W.; López-Suarez, F. E.; Illan-Gomez, M. J.; Bueno-Lopez, A. Preparation, Characterisation And Catalytic Performance For Soot Oxidation Of Copper-Containing ZnAl2O4 Spinels. Appl. Catal. A Gen. 2009, 371(1–2),92–98. DOI: 10.1016/S0008-6223(01)00103-8.

[241] Liu, H.; Dai, X.; Wang, K.; Yan, Z.; Qian, L. Highly Efficient Catalysts Of Mn1-xAgxCo2O4 Spinel Oxide For Soot Combustion. Catal. Commun. 2017, 101, 134–137. DOI:10.1016/j.catcom.2017.08.007.